CO_2 REFORMING OF CH_4 OVER STRUCTURED Ni-BASED CATALYSTS

by

Aybüke Leba

B.S., Chemical Engineering, Eskişehir Osmangazi University, 2007

M.S., Chemical Engineering, Boğaziçi University, 2011

Submitted to the Institute for Graduate Studies in
Science and Engineering in partial fulfillment of
the requirements for the degree of
Doctor of Philosophy

Graduate Program in Chemical Engineering

Boğaziçi University

2017

CO_2 REFORMING OF CH_4 OVER STRUCTURED Ni-BASED CATALYSTS

APPROVED BY:

Prof. Ramazan Yıldırım (Thesis Supervisor)	……
Prof. Ahmet Erhan Aksoylu	……
Prof. Ayşe Nilgün Akın	……
Prof. Hüsnü Atakül	……
Assoc. Prof. Hasan Bedir	……

DATE OF APPROVAL: 21.09.2017

to my family

ACKNOWLEDGEMENTS

This PhD work would not have been possible without the support of many people during this period. It is an honor for me to thank them for their contributions. First of all, I would like to express my gratitude to my thesis supervisor Prof. Ramazan Yıldırım for his valuable guidance, supportive suggestions, innovative approach, motivation, and encouraging me. It was really a great privilege for me to work with him at this study.

I would also like to thank to my thesis committee members; Prof. Ahmet Erhan Aksoylu, Prof. Ayşe Nilgün Akın, Prof. Hüsnü Atakül and Assoc. Prof. Hasan Bedir for being a member of my thesis committee and devoting their valuable time to read and comment on my thesis.

Very special thanks to Prof. M. Mehmet Çamurdan for his invaluable advices and support from the beginning to the end of my education in Boğaziçi University.

I would like to also thank to Assoc. Prof. A. Kerem Uğuz who has been always supportive and hopeful to me during my PhD study.

I am very grateful to Dr. Melek Selcen Başar for sharing her knowledge, everlasting help and lovely friendship throughout my work. Dr. Bilge Uluocak and Dr. Burcu Selen Çağlayan also deserve special thanks for their help and advanced guidance in my SEM and XPS characterization studies respectively.

Special thanks to Belkız Merve Eropak, Ali Uzun, Çağla Odabaşı, Dr. A. İpek Paksoy, Cihat Öztepe for their intimate friendship, cheerfulness and endless support during my PhD years. I am also grateful to all former and current members of KB403, KB405 and KB411. It was really great pleasure for me to work with the CATREL team and all colleagues in the Department of Chemical Engineering at Boğazici University. I am very thankful for their kindness, help and warm friendship.

Heartfelt thanks goes to my friends, Püren Mutlutürk Meral, Özlem Karataş Yavuz, M. Murat Çobanoğlu, Duygu Kocaman, Çağlar Meriçer, Ceren Çelik, Nazire Kılıç Şafak, Burcu Dayanıklı Karaduman, Medine İldeş, Hasan Yavuz, Efe Atay, Ömür Karataş, who always believe in me and stand by me with their supports and friendship. I also thank to Gülşah Güray for her fresh morning broadcast in Radyo Eksen, which gives me the necessary energy to start my experiments.

Cordial thanks for Bilgi Dedeoğlu for his advanced technical assistance and support. Murat Düzgünoğlu, Melike Gürbüz, Başak Ünen, Belgin Balkan and Yakup Bal also deserve thanks for their support and help.

I would like to thank to the scientists, environmental and community volunteers and other committed workers who are inspiring and motivating me by their contributions to the benefit of society and the earth. There is no any word to express my respect and admiration for those who willingly work day and night for a better world.

My grandfather, Ali Yazar, my aunt, Nuran Çamurdan, my uncle, Yılmaz Leba, the ones who are not physically on the earth but always with me in my memory, also deserve my thankfulness for believe in me and giving me strength during my PhD years.

Finally, I would like to thank to my lovely family; my mother, Özvin Leba, my father, Tufan Leba, my brother, Aybars Leba, for their patience, ever-lasting encouragement and intimate support throughout my entire education life. In spite of living far away from them for years, they always provide me all kinds of material and spiritual support unconditionally whenever I need. Therefore, this thesis is dedicated to them in order to show my deepest gratitude.

The financial support for this research was provided by BAP through Project 15A05D3.

ABSTRACT

CO_2 REFORMING OF CH_4 OVER STRUCTURED Ni-BASED CATALYSTS

The aim of this study was to contribute to the development of an economical CDRM process requiring less amount of energy and utilizing cheaper, more active and more stable catalyst. For this purpose, the photocatalytic assistance in CDRM process over Ni-Co impregnated MgO, ZnO and TiO_2 were tested first at 0-500 °C under UV and visible light in a photocatalytic reaction system. However, no considerable CH_4 or CO_2 conversion was obtained even if TiO_2 photocatalyst was tried to be improved by the addition of dye or organolead perovskite sensitizers to increase its visible light sensitivity. The study was proceeded with the use of various structured Ni-based catalysts such as wash-coated MgO, CeO_2 or SiO_2 over monoliths, $Ni_xCo_{3-x}O_4$ nanowires and Ni-based nanorods due to their low pressure drop and high surface area. The performance tests of structured Ni-based catalysts were done at a temperature range from 600 °C to 900 °C with various gas hourly space velocities (GHSV) and CH_4/CO_2 ratios. SEM-EDX, XRD and XPS studies were also performed to understand the surface morphology of the catalysts. The results showed that 8wt.%Ni-2wt.%Co over MgO wash-coated monolith structure led to higher CH_4 and CO_2 conversions as well as closer H_2/CO product ratio to one compared to particulate MgO catalysts and CeO_2 or SiO_2 wash-coated monoliths. SEM-EDX and XPS results of 8wt.%Ni-2wt.%Co over MgO wash-coated monolith catalyst spent at 750 °C also showed considerable amount of coke formation; however, the use of 3% oxygen in the feed suppressed the coke formation significantly. The catalyst was stable for 48 h in the presence of O_2 added feed (3%) over 42000 $mlg_{cat}^{-1}h^{-1}$ at CH_4/CO_2 feed ratio of one and 750 °C. $Ni_xCo_{3-x}O_4$ nanowire structures also showed high catalytic activity at the same conditions; however, they were not stable even under the O_2 added feed. The addition of Pd to this catalyst did not improve its stability either. The performance test of Ni-based MgO nanorods and their coated form over monolith was also tested. Although they resulted lower catalytic activity than Ni-based MgO wash-coated monolith, they seemed to be more resistant to coke formation as the SEM analysis indicated.

ÖZET

Ni TEMELLİ YAPILANDIRILMIŞ KATALİZÖRLER ÜSTÜNDE CH_4'ÜN CO_2 REFORMLANMASI

Bu çalışmanın amacı, daha az enerji tüketen ve daha ucuz, aktif ve kararlı katalizör kullanana daha ekonomik bir CDRM prosesinin geliştirilmesine katkıda bulunmaktır. Bu amaçla, önce Ni-Co emdirilmiş MgO, ZnO ve TiO_2 üzerinde fotokatalitik detstekli CDRM prosesi UV ve görünür ışık altında 0-500 °C'de test edilmiştir. Ancak, ışık duyarlılığını arttırmak için TiO_2 fotokatalizörü, boya veya organolead perovskite duyarlaştırıcıların eklenmesiyle geliştirilmeye çalışılsa bile önemli bir CH_4 veya CO_2 dönüşümü elde edilmemiştir. Çalışmaya, düşük basınç ve yüksek yüzey alanı sağlamasından dolayı, MgO, CeO_2 ya da SiO_2 ile ıslak-kaplanmış monolitler, nano $Ni_xCo_{3-x}O_4$ telleri ve nano MgO çubukları gibi Ni-bazlı çeşitli yapılar üzerinde devam edilmiştir. Ni bazlı katalizörlerin performans testleri 600 °C ila 900 °C arasında bir sıcaklık aralığında, çeşitli gaz akış hızlarında (GHSV) ve CH_4 /CO_2 oranlarında incelenmiştir. Ayrıca katalizörlerin yüzey morfolojisini anlamak için SEM-EDX, XRD ve XPS analizleri de yapılmıştır. Sonuçlar, ağırlıkça %8 Ni-%2 Co içeren MgO ıslak-kaplanmış monolitin, partiküllü MgO katalizöre ve CeO_2 veya SiO_2 ile ıslak-emdirilmiş monolitlere kıyasla, daha yüksek CH_4 ve CO_2 dönüşümlerine ve bire daha yakın H_2/CO ürün oranına yol açtığını göstermiştir. SEM-EDX ve XPS sonuçları aynı zamanda 750 °C'de kullanılmış ağırlıkça %8 Ni-%2 Co içeren MgO ile ıslak-kaplanmış monolit katalizör üzerinde önemli miktarda kok oluştuğunu da göstermiştir. Ancak, besleme gazına 3% oksijen eklenmesiyle kok oluşumu önemli ölçüde bastırılmıştır. Beslemeye 3% oksijen katıldığında katalizör, 750 °C'de CH_4/CO_2 besleme oran birde ve 42000 $mlgcat^{-1}h^{-1}$ gaz akış hızında 48 saat kararlı kalmıştır. Nano $Ni_xCo_{3-x}O_4$ yapıları da aynı koşullarda yüksek katalitik aktivite göstermiş ancak O_2 eklenmiş besleme altında bile kararlı olmamışlardır. Bu katalizöre Pd ilavesi de kararlılığı artırmamıştır. Ni bazlı nano MgO yapılar ve bunların monolite kaplanmış halleri üzerinde de performans testi gerçekleştirilmiş, MgO ıslak-kaplanmış monolitten daha düşük katalitik aktivite gösterseler bile, SEM analizlerinde bu yapıların koka karşı daha dirençli olduğu görülmüştür.

TABLE OF CONTENTS

LIST OF FIGURES

LIST OF TABLES

LIST OF SYMBOLS

at	Atomic
F	Molar flow rate
T	Temperature
W	Catalyst weight
wt	Weight
x	Mole fraction
X	Conversion
Y	Yield
θ	Angle
ΔG°_{298K}	Gibb free energy
ΔH°_{298K}	Standard enthalpy of reaction

LIST OF ACRONYMS/ABBREVIATIONS

AM	Air Mass
BE	Binding Eenergy
BET	Brunauer, Emmett and Teller
CATREL	Catalysis and Reaction Engineering Laboratory
CBXN	Carboxen
CDRM	CO_2 reforming of CH_4
DME	Dimetylether
DMF	Dimethylformamide
EDX	Energy Dispersive X-Ray
GC	Gas Chromatography
GHSV	Gas Hourly Space Velocity
GTL	Gas to Liquid
ID	Inner Diameter
IWI	Incipient Wetness Impregnation
MeOH	Methanol
MFC	Mass Flow Controller
MW	Molecular Weight
NASA	National Aeronautics and Space Administration
NOCM	Non Oxidative Coupling of Methane
ODS	Oxidative Desulfurization
PNOCM	Photocatalytic Non Oxidative Coupling of Methane
POX	Partial Oxidation
RWGS	Reverse Water Gas Shift
SCDR	Steam And Carbon Dioxide Reforming
SEM	Scanning Electron Microscopy
SR	Steam Reforming
TOS	Time on Stream
UV	Ultraviolet
XPS	X-ray Photoelectron Spectroscopy (XPS).

XRD	X-Ray Diffraction

1. INTRODUCTION

The increasing energy demand of world has been a serious concern for last few decades since traditional fossil fuels (coal, natural gas, and oil) are believed to be depleted in near future. In addition, the utilization of current fossil fuels is one of the main reasons of global warming. With the increase of world population and the fast industrialization of human beings, greenhouse gases such as CO_2, CH_4 and N_2O have been increasing in the atmosphere every day. According to NASA, CO_2 level in the atmosphere has been reached its highest level of 406.6 part per million (ppm) since 1880 and current global temperature is up now 0.94 °C, which is the warmest record since 2001. It has been declared that a global temperature rise of 2 °C is a high risk for human beings; therefore, 75% decline in carbon emissions in industrial countries by 2050 is needed to prevent this temperature increase (Khan *et al*., 2014). One of the main detrimental effect of this global warming is the climate change. For the last decades, several lakes are faced to drought and the glaciers started to melt increasing the sea level which may drown cost of the several cities in near future. This change also influences the habitat of the several animals which are in danger of extinction. In our country, it has started to show itself especially in 2017 summer with the unexpected strong winds, heavy rains due to the extreme evaporation and flood in many areas that has badly influenced the daily life. Besides, the drought of clean water sources seems to be one the main problem for agriculture which is one the main resource for subsistence of our country.

As one of the solutions for this serious environmental problem, the utilization of alternative energy technologies such as renewable energy sources, nuclear energy, natural gas (shale gas or biogas) and biomass, instead of traditional fossil fuels, has been highly recommended especially in the industrialized countries to reduce the greenhouse gas levels (Gaillard *et al*., 2017; Wang *et al.*, 2017). According to the trends in global CO_2 emissions report (2016) of Netherlands Environmental Assessment Agency, China and United States as well as the Russian Federation and Japan, as the top emitters, started to decrease their CO_2 emissions by 0.7%, 2.6%, 3.4% and 2.2% respectively compare to previous year while the levels in India and European Union increased by 1.3% and 5.1%, respectively (Olivier *et al*., 2016). In addition, it has been reported that there has been 15.2% increment in the utilization

of renewable electricity sources such as wind and solar energy, and 1.3% rise in the utilization of nuclear energy. The main causes of CO_2 emissions are fossil fuel combustion with 46% and coal-fired power plants with 31% (Olivier *et al*., 2016). For these reasons, there have been great efforts in order to reduce the greenhouse gases in the atmosphere.

The catalytic reaction of carbon dioxide and methane leading a valuable synthesis gas product (mixture of H_2 and CO) through CO_2 reforming of CH_4 (CDRM) process has been suggested as one of the potential processes that can be developed for this purpose compared to other reforming methods such as steam reforming (SR) or partial oxidation (POX). In addition, CDRM can produce a syngas mixture with low H_2/CO ratio (close to one), which can be beneficial as a feedstock for the production of several chemicals such as methanol and higher molecular weight hydrocarbons through processes like Fisher-Tropsh (Cheng *et al*., 2010). Moreover, natural gas and biogas depending on their CO_2 and CH_4 concentration can be directly utilized in CDRM process.

The main drawback of CDRM is the high temperature requirement of the reaction to produced high conversion levels since it is an endothermic process. This situation tends to cause catalyst deactivation or metal sintering. In order to meet necessary demands of CDRM for the industrial commercialization, the studies on this issue, in general, focus on providing an active catalyst which can resist to deactivation or decreasing the economic cost of CDRM by low operating temperature with long-term catalytic stability.

For this purpose, several catalysts have been developed so far by various researchers. Various active metals (with additives) and effective supports having mobility of oxygen ions to react with adsorbed carbon have been used; similarly, several catalyst preparation methods were utilized to enhance the surface properties (Ay and Üner, 2015; Luisetto *et al*., 2012). The noble metals such as Ru, Pd, Pt and non-noble metals such as Ni, Co, Fe have been found to be highly active for CDRM. However, the cost of the noble metals and the rapid deactivation of the non-noble metals have been major drawbacks for their utilization in CDRM (Liu *et al*., 2010).

One of the objectives of this study was to develop a more economic CDRM process with reducing the high temperature requirement of the process through the photocatalytic

assistance; however, no significant CH_4 or CO_2 conversion was achieved. Then the development and test of various structured Ni-based catalysts were aimed so that low pressure drop and, low coke formation, optimum syngas ratio and high stability could be achieved. The thesis consists of five parts. In the first part, the photocatalytic assistance in CDRM process was evaluated over Ni-based particulate catalysts to decrease the temperature dependency of the system. In the second part, Ni-based wash coated monolithic structures were designed and tested to investigate their catalytic contribution in CDRM. In the third part, $Ni_xCo_{3-x}O_4$ nanowires were grown over monolithic structures and tested in CDRM process for the first time. In the fourth part, Ni-based catalysts over MgO nanorod structures were prepared and tested in CDRM to evaluate their catalytic performances. In the last part, some thermodynamic analysis was conducted in the presence of carbon and compared with the experimental results.

Chapter 2 involves a detailed literature survey and theoretical background as well as the advantages and obstacles of CDRM, suggested Ni-based catalysts and supports, photocatalytic systems, O_2 effect on CDRM, monolithic structures as well as nano-array structures for CDRM. Chapter 3 contains a detailed experimental work for catalyst preparation for all types of catalytic structures and reaction tests. Chapter 4 presents the results obtained in the experiments and in the thermodynamic analysis as well as the discussions of these results. Chapter 5 covers the conclusions of the present study and recommendations for the future work.

2. LITERATURE SURVEY

2.1. CO_2 Reforming of Methane (CDRM)

CDRM process (2.1) mainly depends on the exploitation of main greenhouse gases of carbon dioxide and methane as feedstock to produce gas mixture of carbon monoxide and hydrogen with is called syngas (Wu *et al*., 2013):

$$CH_4 + CO_2 \leftrightarrow 2H_2 + 2CO \qquad \Delta H^{\circ}_{298K} = 247\ \text{kJ/mol} \tag{2.1}$$

CDRM has been attractive for many researchers for last few decades since it provides many benefits not only for the environmental issues, but also for Fisher-Tropsh process by leading a H_2/CO syngas ratio close to unity (Budiman *et al.*, 2012). In order to produce syngas, there are other studied methods such as steam reforming of methane (Equation 2.2) and partial oxidation of methane reaction (Equation 2.3) (Meshkani *et al*., 2014; Wu *et al*., 2013)

$$CH_4 + H_2O \leftrightarrow 3H_2 + CO \qquad \Delta H^{\circ}_{298K} = 206\ \text{kJ/mol} \tag{2.2}$$

$$CH_4 + 1/2O_2 \leftrightarrow 2H_2 + CO \qquad \Delta H^{\circ}_{298K} = -36\ \text{kJ/mol} \tag{2.3}$$

Among these processes, steam reforming of methane (SRM) lead to highest H_2/CO syngas ratio of 3 while partial oxidation (POX) give way to 2. In order to product oxygenated compounds and other liquid hydrocarbons such as methanol through Fisher-Tropsh process which is a gas to liquid (GTL) process, in which a low H_2/CO ratio of syngas is necessary (Abdollahifar *et al*., 2014; Budiman *et al.*, 2012; Ray *et al.*, 2017; Serrano-Lotina and Daza, 2013; Serrano-Lotina and Daza, 2014; Wu *et al*., 2013). At this point, CDRM seems to be a good alternative comparing to other reforming technologies.

In addition, CDRM can make it possible to direct use of natural gas, which contains high amount of methane. The storage and transportation of natural gas has been considered as quite difficult, uneconomical and dangerous (Al-Fatesh, 2015). Therefore, the direct

conversion of natural gas into valuable chemicals seems to be more economical and safe way through CDRM process especially when it is also rich in terms of CO_2 composition. Moreover, land fill gas (45–55% CH_4, 30–40% CO_2, 10–15% N_2, 0–5% O_2) and biogas (40–70% CH_4, 30–60% CO_2) obtained from the anaerobic digestion of biomass can also be directly utilized in CDRM process (Al-Fatesh, 2015; Kohn *et al.*, 2010; Vasileiadis and Ziaka-Vasileiadou, 2004).

2.2. Obstacles in CDRM Process

Although the process has several superiorities as mentioned in previous section, there is still some obstacles in the industrial utilization of CDRM. In the first place, CDRM is a highly endothermic process and requires high temperature such as 800-900 °C to operate. (Liu *et al.*, 2010). According to the thermodynamic data analysis, it is not possible to conduct this process spontaneously below appx. 650 °C at atmospheric pressure (Jose´-Alonso *et al.*, 2013). Without catalysts, acceptable methane conversion can be obtained at above 850 °C (Abdollahifar *et al.*, 2016). Moreover, CDRM consumes more energy comparing with conventional SRM. For instance, in order to produce 1 mol of H_2, 69 and 124 kJ of energy are necessitated in SRM and CDRM processes, respectively (Corthals *et al*., 2011).

In addition, CDRM process is accompanied by several side reactions such as reverse water gas shift (RWGS) (Equation 2.4), methane cracking (Equation 2.5) and Boudourard reaction (CO disproportionation) (Equation 2.6) (Wu *et al.*, 2013). RWGS is an unwanted reaction in CDRM since it tends to break the desirable syngas ratio of 1 through the consumption of hydrogen and formation of carbon monoxide at low temperatures (Kaydouh *et al.*, 2016; Matei-Rutkovska *et al*., 2016; Serrano-Lotina and Daza, 2014) Besides, unwanted carbon is formed through the methane cracking reaction, which usually occurs at temperatures above 557-553 ˚C, and through Boudourard reaction, which usually takes place at temperatures below 700 ˚C (Budiman *et al*., 2012). This coke formation is the main constrains for CDRM development since it is usually responsible for the catalyst deactivation, the reactor bed clogging and pressure drop in CDRM process (Estephane *et al*., 2015).

$$CO_2 + H_2 \leftrightarrow CO + H_2O \qquad \Delta H^{\circ}_{298K} = -39.5\ \text{kJ/mol} \tag{2.4}$$

$$CH_4 \leftrightarrow C + 2H_2 \qquad \Delta H^{\circ}_{298K} = 75\ \text{kJ/mol} \tag{2.5}$$

$$2CO \leftrightarrow C + CO_2 \qquad \Delta H^{\circ}_{298K} = -171\ \text{kJ/mol} \tag{2.6}$$

Furthermore, catalyst deactivation can be observed due to the metal sintering of the active sites, the formation of inactive species or the oxidation of active metals during CDRM process. For instance, metal sintering, which is the erosion of catalyst active site due to phase growth, can give way to the formation of metal ensemble and may lead to weak interaction between the support and active site. Moreover, it can plug the reactor tubes (Budiman *et al*., 2012).

Besides to these drawbacks and difficulties, CDRM has been still a valuable process which should be developed considering the environmental benefits for the sake of global future. Therefore, many researchers have been focused on the ways of overcoming these obstacles by evaluating catalysts with various active metals and supports, operating conditions and new alternative reaction systems to achieve an optimum CDRM process. Budimen *et al.* (2012) has discussed the thermodynamically alternative ways to avoid carbon formation in CDRM. In their study, either excess CO_2 in the feed can be used or high operating pressure can be an option at low temperatures. In addition, if the methane composition and carbon oxidation on the catalyst surface are kinetically balanced, carbon deposition can be inhibited. The oxidation of reactive carbon to CO can be performed by some species having oxygen from CO_2 activation (Budiman *et al*., 2012; Takanabe *et al*., 2005). Serrano-Lotina and Daza (2013) has also declared that the utilization of appropriate catalysts and supports can be helpful in the control of coke formation through reaction kinetics. Moreover, high temperatures, high mass to flow ratios (W/F) or high CO_2/CH_4 ratio can be a solution. For instance, an operating condition such as temperature above 700-800 ˚C with a CO_2/CH_4 ratios higher than 1 have been usually suggested to avoid these regions (Jose´-Alonso *et al.*, 2013; Serrano-Lotina and Daza, 2013).

2.3. Ni-based Catalysts for CDRM

The studies carried out on CDRM have showed that both noble based catalysts such as Pt, Ru, Pd etc. and non-precious transition metals such as Ni, Co etc. are highly active in this process. However, noble metals have high costs, which are the main drawbacks for the industry even if they exhibit a remarkable stability (Pakhare and Spivey, 2014: Reddy *et al*., 2010). In the case of transition metals, Ni and Co based catalysts have been widely studied due to their low cost. However, Ni-based catalysts are generally lack of stability due to the tendency of coke formation and sintering problem; therefore, there is a significant restriction in industrial utilization of Ni-based catalysts (Abdollahifar *et al*., 2016; Ay and Üner, 2015; Du *et al*., 2013; Lavoie, 2014). On the other hand, Co based catalysts was believed to be better in terms of carbon deposition due to the fact that carbon deposition mechanism on Co catalyst is quite different than the one on Ni catalyst. However, catalytic activity of Co based catalysts in CDRM can be lower than the one obtained with Ni or noble catalysts (Budiman *et al.*, 2012, Luisetto *et al.*, 2012). For these reasons, today several attempts have been conducting on the resistance of Ni-based catalysts towards coke formation and the catalytic activity of Co based catalysts for the improvements.

The choice preparation method of catalysts, in general, affects the chemical and physical properties of the active metals and support. Benrabaa *et al.* (2012) have investigated the catalytic performance of $NiFeO_4$ catalysts in CDRM at various temperatures, which were prepared by 3 different preparation methods such as co-precipitation, hydrothermal and sol gel process. Among them, the catalysts prepared by sol-gel method showed higher catalytic performance compared to the others. During catalyst preparation, the dispersion of active metals is one of the key factors on the catalyst behavior in reaction tests. Frontera *et al.* (2013) have noted in their study of Ni dispersion that Ni remained coke free when it was well dispersed on the support such as silica and pure-zeolite.

The particle size of the Ni is believed to have an impact on the amount of carbon deposition (Abdollahifar *et al*., 2016). It has been declared that small particle size of Ni catalyst is beneficial due to the high surface area provided and the good resistance to coke formation (Han *et al.*, 2017) However, it was also claimed that the aggregation of small Ni nanoparticles is inevitable at high reaction temperatures such as 800 °C resulting in coke

formation and the loss of the catalytic activity (Han *et al.,* 2014). Even if the reaction temperature is low (such as 500 °C), Ni particle size could increase after the reaction (Baudouin *et al*, 2013; Han *et al*, 2017).

The active metal loading also influences the catalytic activity and carbon deposition. Some studies showed that more than 80 mol% Ni led high carbon deposition (Gao *et al.,* 2017) The study of Li *et al*. (2015) over Ni-MgO catalyst indicated that Ni loading from 2% to 10% has a positive effect on catalytic activity and stability while from 10% to 20% has a negative impact probably due to the increased particle size with the increased Ni loading. On the other hand, 2% Ni containing sample was deactivated stemming from Ni oxidation (Li *et al*., 2015).

The effect of second metal addition to Ni-based catalysts on the coke formation and catalytic performance in CDRM have been also widely studied by several researchers since the addition of second metal was believed to improve the transport of hydrogen and/or oxygen between the catalyst and the support (Ay *et al*., 2015). Some of these studies on this issue have been conducted on Ni catalysts with noble metal such as Rh, Pt, Pd and Ru as a promoter to optimize the activity of the catalysts (Liu *et al*., 2010, Oyama *et al*., 2012). Co metal was also believed to have a key role in the increase of CO_2 adsorption capacity which may eliminate the carbon deposition and by the oxidation of surface carbon to CO or CO_2 (Al-Fatesh, 2015; Estephane *et al*., 2015; Gao *et al*., 2017; Son *et al*., 2014a; Son *et al*., 2014b; Zhang *et al.,* 2008). From the economic point of view, the addition of non-noble metals such as cobalt to Ni catalyst seems to be more preferable since they are cheaper than noble metals (Abdollahifar *et al*., 2016; Li *et al*., 2015).

The improvements caused by the addition of Co metal to Ni catalyst may be also related to the alloy formation, high metal dispersion and solid formation. Gao *et al.* (2017) investigated the catalytic performance of bimetallic Ni-Co catalyst with a 4:1 molar ratio over silica support in CDRM. The addition of Co into Ni catalyst was believed to enable the controlling of Ni metal size and increase the interaction of Ni-silica support as well as inhibit the Ni sintering and oxidation through the electron transfer of Co. They also concluded that the catalytic activity of this catalyst remained the same over 30 h without any carbon deposition or metal sintering (Gao *et al*., 2017).

Luisetto *et al*. (2012) investigated the catalytic performance of monometallic Ni (7.5 wt.%), Co (7.5 wt.%) and bimetallic Co-Ni (Co 3.75 wt.%, Ni 3.75 wt.%) catalysts over CeO_2 support, which was prepared by co-precipitation method. As to their report, bimetallic catalyst showed the best catalytic activity among these catalysts with a 97% CH_4 conversion at 800 °C. In terms of H_2/CO selectivity, Co-Ni/CeO_2 also gave way to higher ratio comparing Ni/CeO_2 and Co/CeO_2. They also indicated that only 6 wt.% amorphous carbon deposition on the spent samples of Co-Ni/CeO_2 at 750 °C under 20h stream was observed in their thermal analysis (TG-DTA), while Ni/CeO_2 lost its catalytic activity during these hours with 8% decrease probably due to the amorphous and graphitic carbon (25 wt.%).

Phongaksorn *et al*. (2015) has reported that 5 wt.% Ni-5 wt.% Co/Al-Mg-O bimetallic catalyst prepared by incipient wetness impregnation method showed an outstanding reducibility and metal dispersion over support comparing 10 wt.% Ni/Al-Mg-O and 10 wt.% Co/Al-Mg-O particulate catalyst. High CO_2 adsorption capacity of bimetallic catalyst was also believed to inhibit coke formation.

The amount of Co in Ni-based catalysts has been considered as a significant parameter on the catalytic performance of the Ni-Co bimetallic catalysts since it may affect the reduction and oxidation processes over catalysts (Budimen *et al.*, 2012). Estephane *et al.* (2015) investigated the effect of Co loading in the Ni catalysts over ZSM5 with a 7 wt.% in total. They found that bimetallic catalyst (Co/Ni:2) showed the highest CH_4 and CO_2 conversion (over 60%) at 700 °C and led to the lowest carbon formation; they claimed that cobalt enabled the reverse water gas shift reaction and behaved as a synergist to nickel.

San-Jose-Alonso *et al*. (2009) has reported that 9 wt.% Co and 1-8 wt.% Ni-Co catalyst were quite active the due to methane decomposition by cobalt although they resulted in high amount of coke. They also showed better stability in long-term due to the formation of large particles, which leads non-deactivating carbon deposits. Alonso *et al*. (2013) have investigated the effect of low Co and Ni metal content over alumina supported catalysts. It was found that 1, 2.5 and 4 wt.% metal content resulted in less than 0.01% carbon at 973 K probably due to the advantage of small particles inhibiting carbon growing, compatible with the literature where larger than six nm metal particles was believed as having a tendency on

methane decomposition, thus carbon deposits. However, methane conversion of these catalysts was lower than high metal content containing catalyst (9 wt. %).

Li *et al.* (2017) found that 12wt.%Co loaded Mg-Al catalysts showed more stable catalytic activity than the same amount of Ni loaded catalyst since Co particles were not sintered showing good thermal stability stemming from the strong interaction of Co metal and Mg-Al support in this study. However, Long *et al*. (2013) declared, in their study of Mg(Al)O mixed oxide-supported Co and Ni-Co bimetallic catalysts, that Ni containing catalyst showed better catalytic activity than those do not have. Also, the best results in terms of catalytic activity and stability were obtained when Ni/Co ratio was 8/2.8/2.

The calcination temperature as well as reduction temperature was believed to influence the rate of coke formation on Ni-based catalyst (Horváth *et al.*, 2017). Ay *et al*. (2015) investigated the effect of calcination temperatures such as 700 °C and 900 °C on Ni, Co monometallic and Ni–Co bimetallic catalysts over CeO_2 support prepared by incipient wetness impregnation method in dry reforming of methane. They found that there is an opposite relationship with the increasing calcination temperature and catalytic activity; the carbon deposition was also higher over the Ni/CeO_2 and $Ni–Co/CeO_2$ calcined at 700 °C. Among these catalysts, Ni/CeO_2 and $Ni–Co/CeO_2$ catalysts have higher catalytic activity than the Co/CeO_2 catalysts in all cases.

2.4. Supports and Promoters for CDRM

Various supports such as Al_2O_3, MgO, SiO_2, La_2O_3, CeO_2 and ZrO_2 have been tested and suggested for Ni-based catalysts since type of the support has been believed to be a significant parameter as its thermal stability affects the morphology of the active metal particles. During the thermal treatment process, crystalline phase of the support can be changed and this situation may lead to a decrease in pore volume and diameter of the support. These changes in support have an impact on the metal sintering, which enhances the carbon deposition, and the interaction of the support with active metal, which should be strong (Budiman *et al.*, 2012). The preparation method of the catalysts as well as the addition of promoter can also play a key role on the catalytic performance of CDRM (Brandford and

Vannice, 1996; Du *et al*., 2013; Damyanova *et al*., 2011; Monroy *et al*., 2012; Rong-jun, *et al*., 2015; Sengupta and Deo, 2015).

Among the suggested supports, basic supports such MgO, CaO, BaO, K_2O, and Ca_2SiO_4 has been widely used in various CDRM publications (Asencios *et al.*, 2011; Monroy *et al*., 2012; Titus *et al*., 2016) since they have an ability to increase CO_2 activation and hence suppress coke formation. ZrO_2 support has also highly suggested since it has a high ionic conductivity and thermal stability, which is also important for dry reforming (Asencios *et al.*, 2011). Al_2O_3 has been widely used due to its availability, mechanical strength and high surface area (Sengupta and Deo, 2015). Also, the formation of $NiAl_2O_4$ spinel in Ni/Al_2O_4 catalyst was also believed to have a key role in the high stability of the catalyst (300 h at temperatures that ranged from 700◦C to 850◦C) (Shang *et al.*, 2017). CeO_2 has been also preferred as a support material for Ni-Co based catalyst since it has been known to have O_2 storage capacity and setting free ability to moderate carbon deposition and activate CO_2 after reduction (Luisetto *et al.*, 2012).

MgO as one of the basic supports that has a high melting point and it can form solid-solution catalyst with Ni metal leading a good stability for dry reforming of methane and high metal dispersion (Frusteri *et al*., 2001). Meshkani *et al.* (2014) has indicated that solid formation of MgO with NiO on Ni/MgO catalyst prevented the coke deposition and resulted in active and stable dry reforming of methane process. Asencios *et al.* (2011) has also investigated the $NiO/MgO/ZrO_2$ catalyst prepared by polymerization method in reforming of biogas and oxygen (CH_4: CO_2: O_2 = 1.5: 1.0: 0.25) and compare its catalytic activity with Ni/MgO and Ni/ZrO_2 catalysts. They concluded that $NiO\text{-}MgO\text{-}ZrO_2$ catalysts containing 20 wt.% Ni performed better than the sole Ni/MgO and Ni/ZrO_2 catalysts. The main reason was that the solid-solution formation may lead to increase in CH_4 and CO_2 conversions and the oxygen vacancies in ZrO_2 and MgO may pay a key role in the removal of coke formation on the surface due to the solid solution effect they formed. In terms of syngas formation, both $NiO/MgO/ZrO_2$ and Ni/MgO catalyst have caused similar H_2/CO ratios at 750 °C than other synthesized catalysts.

On the other hand, MgO was also believed to have low specific surface, which may have an impact on the catalytic CDRM over Ni-based catalysts. It has been indicated that

higher specific surface area gave way to higher initial catalytic activity since it resulted higher active metal dispersion (Zhang *et al*. 2014). In order to make an improvement on MgO surface area, several attempts such as the addition of another support like Al_2O_3 or developing MgO nanocrystals having low size such 10–12 nm have been made (Abdollahifar *et al*., 2014; Xu *et al.*, 2001). Abdollahifar *et al.* (2014) has developed Ni/Al_2O_3-MgO nanocatalyst operated by sonochemistry method having a surface area 38.93 m^2/g, which was 53.25 m^2/g before the 10 wt.% Ni addition to support. It was declared that increasing amount of active metal have a tendency to decrease the surface area, which led to low CH_4 and CO_2 adsorption site. In addition, preparation method they used led to small Ni particle size as 21.4 nm. This situation was believed to give way to high catalytic performance near to thermodynamic equilibrium conversions as well as produce a syngas ratio of 1 at 600–800 °C.

The effects of promoters such as Ce, Mg, La and Co on the catalytic performance of Ni-based catalysts have also widely studied by various researchers (Amin *et al.*, 2016; Khajenoori *et al.,* 2015). The addition of La_2O_3 was believed to stabilized the surface carbonate species which increasing the source of oxygen species and promote the carbonaceous species gasification in CDRM (Frusteri *et al*., 2001). Moreover, suggested supports can act as a promoter in some cases due to their nature like the basicity of MgO (Son *et al*., 2014; Zhang *et al*., 2016). Gandhi *et al*. (2015) has investigated the effect of various promoters such as ZrO_2, CeO_2 and MgO on the catalytic activity of Al_2O_3 supported Ni catalyst. Among these catalysts, highest conversions were obtained over 10% Ni/5% ZrO_2-Al_2O_3 and 10% Ni/5% MgO-Al_2O_3 while 10% Ni/5% CeO_2-Al_2O_3 catalyst was the most stable one. In this study, ZrO_2 was believed to inhibit coke formation and MgO as well as CeO_2 helped to Al_2O_3 with their basicity and oxygen vacancies (Gandhi and Patel, 2015). Similarly, Garcia *et al*. (2009) has evaluated the effect of MgO content on Ni-ZrO_2 catalyst for dry reforming of methane and found that addition of 5% MgO had a positive effect on the thermal stabilization of ZrO_2, the basicity of support as well as the reducibility of Ni metal. On the other hand, Sengupta and Deo (2015) has found that addition of low amount of CaO has improved the catalytic activity while MgO did not at all probably due to its strong interaction of Ni and Co phases in their synthesis conditions. Limited interaction of CaO with Ni phase was believed to lead improved activity forming additional sites to chemisorb H_2 and CO_2 at higher temperatures.

Yao *et al*. (2016) have investigated the promoting effect of Mn and Zr on Ni/SiO_2 catalyst for dry reforming of methane. They found that the addition of Mn to Ni/SiO_2 showed higher catalytic activity than Ni/SiO_2 catalyst and superior stability at a temperature range from 600 °C to 800 °C; the Mn addition led to better dispersion of Ni active metal with the formation of $NiMn_2O_4$ species, while the addition of Zr into Ni/SiO_2 have negatively affected the catalytic activity of the catalyst and gave way to an increase in the reducibility of the catalyst (Yao *et al*., 2013).

The reduction and calcination procedures of the supports are also important parameters in the reforming processes. Wang *et al*. (2009) has found that the unreduced NiO/MgO catalysts was deactivated during the reforming of methane; therefore, it should be reduced. Wang and Ruckenstein (2001) has investigated the effect of calcination temperature on Co/MgO catalyst in DRM catalytic performance. They found that there is a relation between the Co loadings and the calcination temperature to obtain a high catalytic activity. As to their findings, the catalyst should be precalcined at 500 °C or 800 °C in the case of 8-36 wt.% Co loading. If the catalyst was loaded more than 48 wt.% Co, it showed unstable behaviors even if it is calcined at 500 °C or 800 °C due to the formation of large metallic particles. In addition, various Co-containing species such as Co_3O_4, $MgCo_2O_4$, and (Co, Mg) O (solid solution of CoO and MgO were observed depending on the calcination temperature. Among these, the reduction of Co_3O_4 and $MgCo_2O_4$ was believed to let the sintering and coke formation.

Cosimo *et al*. (2014) has also investigated the calcination temperature effect (673 K, 773 K and 873 K) on the catalytic properties of MgO support. They found that the increase in calcination temperature decreased the density of strong base sites and lead to weak OH groups but increased the medium strength base sites. The rate limiting step of the base-catalyzed reaction was related to the basicity of the MgO support which was related to the calcination temperature. Namely, the calcination temperature of MgO support directly affects the density, nature and strength of surface basic sites on MgO and surface OH groups and stability leading stable structures at higher calcination temperature.

Gao *et al*. (2016) developed an active Ni/SiO_2 catalysts prepared by incipient wetness impregnation (IWI) with 85% CO_2 conversion, 80% for CH_4 conversion and low metal sintering as well as zero carbon deposition. The main reason was for this improvement that

the prior hydrogen treatment before calcination step showing small Ni particle size and increasing support metal interaction. In Ni actives metals, especially strong metal-support interactions needed since Ni metals have a tendency to be sintered at high temperatures and naturally resulted in large particles with high coke deposition. However, even if Ni particle size was controlled by the support maintaining in some cases, the size of the particles has been larger after long reactions.

2.5. Photocatalytic Assisted CDRM

2.5.1. Photocatalytic Systems

A photosystem is a chemical process that converts water and carbon dioxide to carbohydrates and oxygen by using sunlight. Similar to natural photosynthesis, photocatalysis also uses some form of photocatalysts under UV or visible light illumination to reduce or to oxidize the pollutants into innocuous compounds as in Figure 2.1, and it generally operates at room temperature and atmospheric pressure. To maintain reactions in the presence of light irradiation, the photocatalysis uses semiconductors (Equation 2.7), which are attractive materials for light-harvesting applications because of their energy band gap an available electronic states having energy range similar to that of visible light (Kiesgen de Richter *et al*., 2013; Philippopoulus and Nikolaki, 2010)

Nowadays, the photocatalysis has taken a great attention since it only depends on the behavior of photos and can be appreciable in various industries such as the self-cleaning material production or clean water treatments. There are two artificial photosynthesis methods: homogenous which mimics e transfer steps of water in natural photosynthesis, and heterogeneous system which is related to dye sensitized photochemical system in solar cells (Arifin *et al*., 2012).

$$\text{Photocatalyst} + \text{hv}^{+} \leftrightarrow \text{e}^{-} + \text{h}^{+} \qquad (2.7)$$

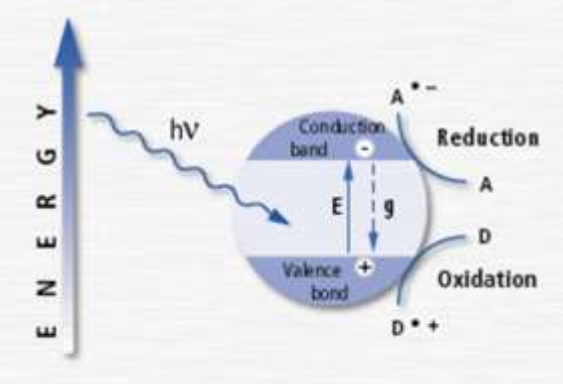

Figure 2.1. Photocatalysis on a semiconductor (Philippopoulus and Nikolaki, 2010).

There are two types of heterogeneous photocatalysts: semiconductor photocatalysts and highly dispersed photocatalysts. Semiconductor catalysts absorb the photoenergy more than its band gap energy. This type of catalysts (such as TiO_2) show large and intense absorption bands in the UV spectrum. On the other hand, highly dispersed catalyst, such as titanium dispersion on silica, exhibits narrower and less intense absorption bands (Yuliati and Yoshida, 2008).

TiO_2 is widely preferred for many photocatalytic applications due to its advanced properties such as being inexpensive, safe and stable (Handoko *et al*., 2013). However, its large band gap limits the solar radiation to only the UV spectrum, which covers only 4% solar radiation and it, is unable to adsorb visible light, which accounts for 50% of solar radiation. Liang *et al.* (2011) has additionally claimed that trying different TiO_2 formulations including mixtures of its two polymorphs, anatase and rutile is another popular pathway to explore for enhancing photocatalytic activity. Anatase typically seems to have higher photocatalytic activity than rutile, while the precise mixtures of both phases exhibit even better performance. As to the photocatalytic pathway of TiO_2, the preliminary step in TiO_2 photo catalytic oxidation is understood to be the formation of both hydroxyl radicals (·OH) and super oxide radical anions through the reactions of photo-generated electron-hole, with solutes present in the system.

The photocatalytic activities can be conducted in the present of natural sunlight or of a UV light sources such as Xe or mercury lamp. In the case of photocatalytic reduction of CO_2 into fuels by using natural sunlight, which seems to be promising to sustainably produce

energy, it is possible to use a focused device to collect the light and transmitting it to an optical fiber reactor (Anpo *et al*., 2013). However, today, it is known that the photocatalytic activities under natural sunlight seem to be inadequate since the use of the solar energy reaching earth in very low percentage (such as only 3–4%); although some researchers have been conducted gel-derived TiO_2–SiO_2 mixed oxide-based photocatalysts to reduce CO_2 with H_2O to fuels under natural sunlight by using a solar concentrator.

To improve the photo activities under natural sunlight, many metals have been also loaded on TiO_2–SiO_2 mixed oxide along with different catalyst carriers. Guan *et al*. (2003) has obtained high production rates of the main products such as H_2 (32.8 mmol/g-cat h) and HCOOH (20.7 mmol/gcat h), but very low for CH_4 (0.3 mmol/g-cat h) in the study of CO_2 with H_2O under concentrated sunlight using $K_2Ti_6O_{13}$ based photocatalysts. However, most of the photocatalytic applications in general had used a UV light source such as Xe lamp in order to get rid of this kind of problem.

2.5.2. Photocatalytic Systems for CDRM

The photocatalytic system seems to be one of the promising alternatives in order to overcome the industrial energy limit of CDRM since it is not possible to maintain a simultaneous CDRM reaction at low temperatures since reaction has high ΔG (Equation 2.8). By means of the photocatalytic energy assisted CDRM, it can be process at mild temperatures (Yuliati and Yoshida, 2008).

$$CH_4 + CO_2 \leftrightarrow 2CO + 2H_2 \qquad \Delta G_{298\,K} = 170\ \text{kJ/mol} \tag{2.8}$$

A photocatalyst should limit over potentials and increase the product selectivity through kinetic barriers of these compounds as well as being sustainable and low-carbon sources since CO_2 and CH_4 are highly stable molecules (Finn *et al*., 2012; Yuliati and Yoshida, 2008). For instance, for the reduction of CO_2 into CO or hydrocarbons, electrons in the semiconductor should have high negative chemical potential while for water oxidation, holes need more positive potential level (Li *et al*., 2014). In the case of methane, high photoenergy region is necessitated to induce it through electronic transition (Yuliati and Yoshida, 2008). Also, in order to break 1 mol C-H bond, 434 kJ energy is needed, which is

much higher than the one for C–H and C–C bonds in higher hydrocarbons such as benzene or ethane. Yuliati *et al*. (2007) could convert CH_4 into some radicals such as hydrogen or higher hydrocarbons such as ethane using photoenergy through photocatalyst at room temperature in the study photocatalytic non oxidative coupling of methane (PNOCM) (Equation 2.9).

$$2CH_4 \leftrightarrow C_2H_6 + H_2 \qquad \Delta G_{298\,K} = 68.6\ \mathrm{kJ/mol} \tag{2.9}$$

They obtained 78% ethane as main product, 9% ethane and 9% propane from PNOCM reaction over Ga_2O_3 catalysts. It was also reported that Ga_2O_3 showed improved activity comparing SiO_2-TiO_2 which are known as highly active catalysts for NOCM. In another study of Yuliati *et al.* (2008), PNOCM was performed over Ga_2O_3 and SiO_2 supported Ga_2O_3 catalyst at room temperature in a closed rector system combined with gas chromatography. Xe lamp with 220-300 nm and 300W was chosen for photo source. It was found that unsupported Ga_2O_3 resulted in high methane conversion and high ethane selectivity but the hydrogen produced was not equivalent of ethane due to consecutive coupling and coke or carbon formation. On the other hand, the catalyst with the supported Ga_2O_3 gave better result as 0.1% of selectivity.

The photocatalytic reduction of CO_2 in aqueous solution which may form several chemicals such as formaldehyde (HCHO), formic acid (HCOOH), methyl alcohol (CH_3OH), methane (CH_4), ethyl alcohol (C_2H_5OH) and ethane (C_2H_6) or CO with CH_4 or H_2 also have been widely studied by several researchers (Doherty *et al*., 2010; Teramura *et al*., 2004; Usubharatana *et al*., 2006). Various photocatalysts (semiconductors) such as tungsten trioxide (WO_3), titanium dioxide (TiO_2), zinc oxide (ZnO), cadmium sulfide (CdS), gallium phosphide (GaP), and silicon carbide (SiC) have been employed in assorted manners (separately/mixed/metal-doped forms) for this process. For instance, Tennakone *et al*. (1984-1989) performed several photocatalytic CO_2 reduction studies by photocatalysts over various supported TiO_2 materials including platinum (Pt), gold (Au), silver (Ag), cobalt (Co) etc. (Usubharatana *et al*., 2006). Dimitrijevic *et al.* (2011) has indicated that the improved efficiency of CO_2 reduction can be demonstrated over the synthesized novel titania-based nanomaterials having specific surface structures, through coupling titania to dyes, enzymes, metallic catalysts, or quantum dots. However, a better understanding of processes that occur

on the surface of TiO_2 during carbon dioxide reduction, including adsorption/desorption of CO_2 and formation of intermediate products, as well as the role of adsorbed water has been needed in order to elucidate the reaction mechanism.

In literature, there has been limited study on photocatalytic energy assisted CDRM as to photocatalytic reduction of CH_4 or CO_2 in separately. Most of the studies could be conducted under source ultraviolet (UV) light or modified TiO_2 photocatalysts (Han *et al*., 2016). The studies regarding this issue have started within the last decade and increased in last years with the advances on photocatalytic technology (László *et al*., 2016).

Shi *et al*. (2004) has studied on coupled semiconductor (CS) Cu/CdS–TiO_2/SiO_2 photocatalyst for CH_4 and CO_2 utilization and gave way to 1.47% for CH_4 and 0.74% for CO_2 conversions in which the acetone was main product with a selectivity of 92.3% under 20 mW/cm^2 UV intensity.

Yuliati *et al*. (2008) has conducted photocatalytic conversion of CH_4 and CO_2 in the presence of gallium oxide photocatalyst (β-Ga_2O_3) at room temperature in a system having a closed quartz reactor with a Xe lamp. It has been also found that only hydrogen and some hydrocarbons at room were produced. At mild temperatures of 200 °C, CO was also obtained with UV irradiation assisted system and its composition was increased to 94% at 500 °C. On another study of the photocatalytic reaction between methane and CO_2 over MgO and ZrO_2 at room temperature, it has been indicated that very low amount of H_2 has been produced comparing to the production of CO. That has been occurred due to the conversion of CO_2 into CO, where the methane converted into acetate and formate. Thus, CO is produced from the reaction between these surface formates with CO_2 under irradiation (Yuliati and Yoshida, 2008). Nishmura *et al.* (2012) has found 8306 ppmV CO product from CO_2 reforming over Cr- or Ag-doped TiO_2 film.

Mahmodi *et al*. (2013) has reported an 10% CO_2 conversion resulting acetate and formate products achieved in the study of photocatalytic conversion of CO_2 and CH_4 an immobilized ZnO semiconductor on stainless steel mesh under 250 UV light power when the experimental conditions were optimized. On the other hand, Merajin *et al*. (2013) has obtained acetic acid and formic acid as the main product from the photocatalytic reaction

between CH_4 and CO_2 over nano TiO_2 particles coated on stainless steel webnet under 125 W UV irradiation in a gas-phase batch reactor. The conversions were 26.32% for CO_2 and 31.63% for CH_4 when 45% CO_2: 45% CH_4 10% He of gaseous mixture was fed to the system.

Delavari and Amin (2016) has also produced a gas mixtures having the composition of 4.7% ethane, 4.3% acetic acid, 3.9% formic acid, 41.4% methyl acetate formic acid and 45.7% methyl formate with a maximum CO_2 conversion of 37.9% on the photocatalytic system over titania (TiO_2) nanoparticles semiconductor on stainless steel mesh under 250 W UV light power. Delavari *et al*. (2016) has also obtained 80.5% H_2 and 18.9% CO as the main products when they performed their studies over nitrogen-doped titania (TiO_2) nanotube arrays under the same light power.

Yazdanpour and Sharifnia (2013) has declared that CuPc/TiO_2 catalyst could lead 14% CO_2 and 18% CH_4 conversion under visible light while it was not possible to obtain any conversion over unmodified TiO_2 catalyst at the same conditions (Lichtfouse *et al*., 2015). Recently, Han *et al*. (2017) has developed an efficient light photocatalytic CRM by combining Pt/black TiO_2 catalyst leading H_2 and CO yields reached 71 and 158 mmol/h/gcat, with a quantum efficiency of 32.3% at 550 °C, and 129 and 370 mmol/h/gcat, with a quantum efficiency of 57.8% at 650 °C under visible light illumination by filtering UV light from AM 1.5 G sunlight in a photocatalytic assisted CDRM system.

2.6. Oxygen Assisted CDRM

CDRM process can be utilized with additional oxidant such as oxygen or steam in order to restrict coke formation steps and achieve a stable catalytic performance with valuable products. The addition of oxygen can promote the catalyst reactivation through oxidation of the formed coke and improve the reforming reaction through coke-CO_2 reaction with H_2 production (Fan *et al.,* 2011). Similarly, additionally steam feeding to the system can provide additional hydrogen and oxygen to the surface to inhibit the coke formation (Ay and Üner, 2015). In the literature, there has been also some work combining the dry reforming with other processes technologies for various aims such as with partial oxidation (oxy-CO_2 reforming), auto-thermal reforming, steam reforming or O_2 addition along with

CO_2 to regenerate the deactivated catalyst through (Assabumrungrat *et al*., 2009; Chen *et al*., 2011; Danilova *et al*., 2015; Qiu *et al*., 2012).

Chen *et al.* (2011) investigated the catalytic performance of Co-Ni bimetallic aerogel catalysts with various Co/Ni ratios in oxidative CO_2 reforming (Oxy-CO_2 reforming) since the exothermic combustion of CH_4 with O_2 (Equation 2.10) or partial oxidation (Equation 2.11) may make an internal contribution to the heat demand of endothermic CDRM reaction. Danilova *et al.* (2015) tested the nickel catalysts supported on a porous nickel ribbon with a MgO also in a combined system of steam and carbon dioxide reforming (SCDR), which is thought to be beneficial to decrease the carbon formation and to obtain a synthesis gas with a H_2/CO ratio of about 2.

Moreover, it is also possible to remove deposited coke and regenerate the deactivated catalysts in reforming or cracking processes with pure carbon dioxide (Equation 2.12), oxygen (Equation 2.13) or steam (Equation 2.14) feed under periodic operations (Promaros *et al.*, 2007). Zhang and Amiridis (1998), for instance, used either oxygen or steam to get rid of the coke over silica supported Ni catalyst in the study of hydrogen production from methane cracking process. They successfully regenerated the catalysts and obtained additional hydrogen during the steam regeneration case.

$$CH_4 + 2O_2 \leftrightarrow CO_2 + 2H_2O \qquad \Delta H^{\circ}_{298K} = -801\ \text{kJ/mol} \tag{2.10}$$

$$CH_4 + 1/2O_2 \leftrightarrow CO + 2H_2 \qquad \Delta H^{\circ}_{298K} = -36\ \text{kJ/mol} \tag{2.11}$$

$$C + CO_2 \leftrightarrow 2CO \qquad \Delta H^{\circ}_{298K} = -546\ \text{kJ/mol} \tag{2.12}$$

$$C + O_2 \leftrightarrow CO_2 \qquad \Delta H^{\circ}_{298K} = -393.5\ \text{kJ/mol} \tag{2.13}$$

$$\text{C}+H_2O \leftrightarrow CO + H_2 \qquad \Delta H^{\circ}_{298K} = +131.3\ \text{kJ/mol} \tag{2.14}$$

Assabumrungrat *et al.* (2009) also used oxygen to generate of Ni/SiO_2-MgO catalyst in dry reforming of methane under periodic and steady state operation. The catalyst was generated in the presence of both O_2 and CO_2 at 750 °C by keeping its catalytic activity for

at least 12 cracking/regeneration cycles. In steady state operation, addition of O_2 with a CO_2/O_2 ratio of 7/3 led to an increase in CH_4 conversion from 62% to 80% at 650 °C and 95% at 750 °C due to the partial consumption of methane with oxygen. However, it was noted that higher oxygen amount resulted less hydrogen formation which is an unwanted situation since it broke the synthesis gas ratio (Equation 2.15).

$$2H_2 + O_2 \leftrightarrow 2H_2O \qquad \Delta H^{\circ}_{298K} = -486.3\ \text{kJ/mol} \qquad (2.15)$$

Therefore, as to this study, periodic operation with combined partial oxidation of methane and CO_2 reforming is more preferable for the generation purpose of the catalyst. O'Connor and Ross (1998) previously conducted a similar study over Pt/ZrO_2, $Pt/Al2O_3$ and Ni/Al_2O_3 catalysts at 550-800 °C. It has been stated that both hot spots in the catalyst bed and activity loss of the catalyst were decreased in the combination of carbon dioxide reforming reaction partial oxidation reaction, which are endothermic and exothermic, respectively.

Tomishige *et al*. (2004) has investigated oxygen effect on the steam and dry reforming of methane over Pt/Al_2O_3, Ni/Al_2O_3 and commercial steam reforming Ni catalyst. It has been indicted that Ni-based catalyst can be easily oxidized in the presence of oxygen and may have an activation for the combustion not for reforming while Pt based catalysts were more resistant to O_2. This case is actually one of the widespread problems of Ni and Co based catalysts which should be taken into consideration (Li *et a*l., 2016). On the other hand, XRD analysis of 15 wt.% Ni/SiO_2 catalyst after 10 successive cracking/regeneration cycles with O_2 presence showed no changes in the shape of Ni peaks at all indicating that remained crystallite size of the Ni particles during the successive cycles and only trace amounts of the presence of nickel oxide (Aiello *et al*., 2000).

In most of these studies, additional oxygen usages tend to have play factor in the product distribution. The syngas ratio obtained from CDRM was slightly affected by the reaction of these species with carbon resulting an increase or a decline in the amount of CO or H_2 due to the fact that they were used more or less with the same amount of the reactants.

2.7. Monolithic Structures

Monolithic structure is one piece of special material having many channels inside separated by thin, vertical, parallel channels that are able to be coated by catalyst or directly be catalyst itself in the catalytic applications (Dimitrijevic *et al*., 2011). They can consist of either metal, plastic or ceramic materials. The ceramic monolith structures are a mixture of oxides such as alumina, magnesia, and silica and can be in in various forms like cordierite and mullite monoliths as in Figure 2.1; the commercial formula of these ceramics can be represented as $2MgO.2Al_2O_3.5SiO_2$ and $3Al_2O_3.2SiO_2$, respectively.

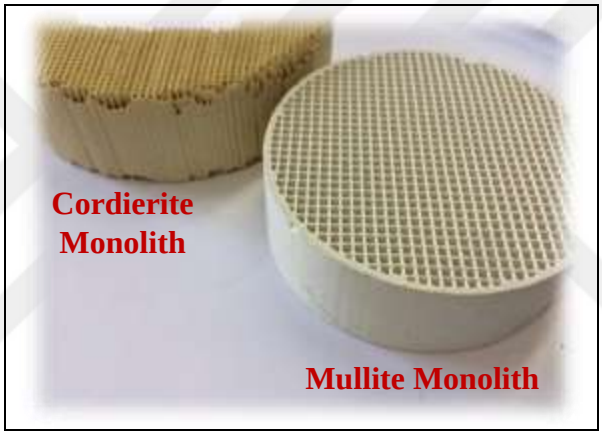

Figure 2.2. The image of mullite and cordierite monoliths.

The monoliths are used in many chemical processes; they can currently be seen in the automotive industry to clean the exhaust cleanup systems, the selective catalytic reduction of NOx in power stations exhaust gases and the catalytic combustion of volatile organic compounds since monoliths used in these applications are resistance to high temperatures and temperature shocks with the help of low thermal expansion property (Villegas *et al.*, 2007). Moreover, these structures may have also high mechanical resistance and good refractory properties (Villegas *et al*., 2007). In addition, these kind monolithic structures provide low pressure drop (thus low energy loss) as to the packed bed reactors, since they have straight parallel channels as in seen Figure 2.3 (Giroux *et al.*, 2005). This property may enable their usage especially in high gas space velocities. Furthermore, they are easier to be scaled up by just regulating the number of channels to separate the products (Ciambelli *et*

al., 2010; Giroux *et al.*, 2005; Heck *et al*., 2001; Özyönüm and Yildirim, 2016; Qiu *et al*., 2012; Villegas *et al.*, 2007).

On the other hand, these structured materials may have low BET surface area (for cordierite typically 0.7 m^2 g^{-1}) for catalytic applications as a support. Therefore, this type of structured are necessitate the coating of all surfaces with a support through wash-coating process. The procedure began with the slurry coating of support suspension over bare monoliths surfaces (Figure 2.3) and followed by drying and calcination processes. There are several factors influencing the success of the slurry coating procedure such as nature and particle size the precursor powder, nature and concentration of dispersants, loading of powder, temperature, binders etc. (Villegas *et al*., 2007).

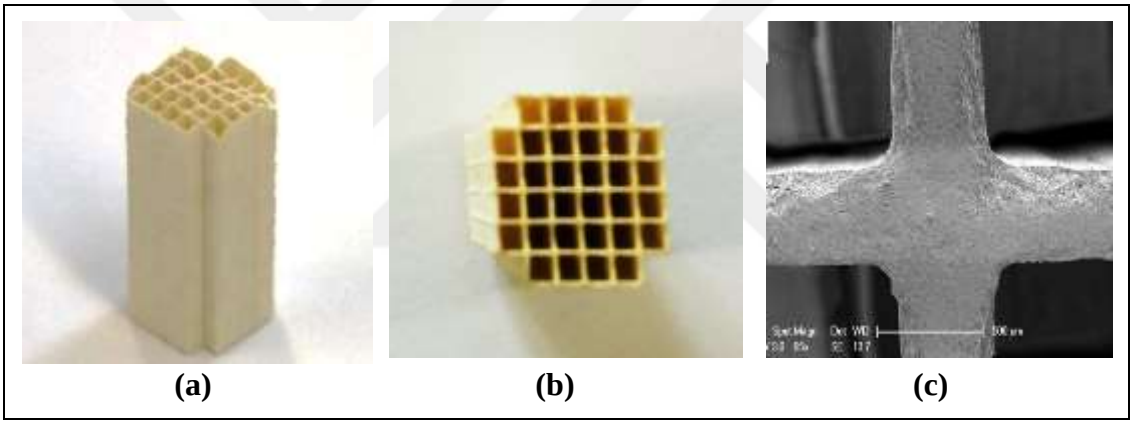

Figure 2.3. The images (a-b) and SEM image (c) of bare monoliths.

Although monolithic bed offers many advantages comparing regular packed bed reactors, in literature, most of CDRM studies have been conducted over particulate catalyst in a fixed bed reactor while there were also a few studies performed with the monoliths. As it mentioned before, carbon formation is one of the main drawbacks of CDRM especially while using Ni-based catalysts, nor only for decreasing the catalytic activity but also for having a high tendency for reactor plugging (Chen *et al*., 2012). In order to prevent this situation, monolithic beds seemed to be a good solution since it provides easy flow through its channels with low pressure drop.

Some of the examples of CDRM studies over monolithic structures can be as follows: Ni/Al_2O_3 catalyst, micro-fibrous structured Ni/Al_2O_3 catalyst, wash-coated monolithic Rh/Al_2O_3 catalyst, Ni-based monolithic catalysts over FeCrAl/SBA15, Ni supported on γ-Al_2O_3 promoted by Ru both in packed and monolithic reactors (Chen *et al*., 2012; Luisetto *et al*., 2017; Ryu *et al*., 2007; Soloviev *et al*., 2011; Wang *et al*., 2008).

In other reforming technologies such as SRM, metal type of monolithic structures to produce hydrogen are in general used to overcome heat transfer limitation in steam reforming of methane, which are good at heat conduction (Giroux *et al*., 2005). Ryu *et al.* (2007) has obtained higher methane conversion in steam reforming of methane over commercial Ni-based catalyst wash-coated on a monolith with 50 m-thick FeCralloy plates than the same volume of coarsely powdered Ni catalysts due to the enhanced heat transfer capability of metal monolith. Moreover, their study showed that monolithic catalyst worked at higher than 28000 h^{-1} GHSV without any pressure drop.

Ciambelli *et al*. (2010) performed a study on the effect of supports structure over Ni catalysts such as ceramic honeycomb and foam structures in CH_4 autothermal reforming. The structured supports are first wash-coated by CeO_2–Al_2O_3-based slurry then impregnated by nickel nitrate solution. They indicated that pre-treatment and the drying rate of the supports are important parameters for wash coat adhesion quality between the supports and catalysts. Moreover, it has been reported that precursor size of the powder, nature of the powder and dispersants, their concentration, slurry temperature and binders are other parameters for the quality of wash-coating procedure (Villegas *et al*., 2007).

Qui *et al*. (2012) has investigated the effect of Ni/Mg mole ratio of Ni–MgO/c-Al_2O_3 cordierite monolithic catalysts on dry reforming of model biomass fuel gas (H_2/CO/C_2H_4/CH_4/CO_2/N_2 = 16.0/12.1/2.5/15.1/22.0/32.3, vol.%) in a lab-scale stainless steel tubular reactor; their study resulted in high catalytic performance per unit mass of active metal obtained in monolithic catalyst (87.2% CH_4 and 54.4% CO_2 conversions with 1.17 H_2/CO ratio at 750 °C) as well as high operating stability (60 h) and low-pressure drop.

2.8. Ni-based Nano-array Structures for CDRM

Nanoparticles have drawn a great attention in heterogonous catalysis in recent years since they can be prepared in any desired size, structure, morphology and composition (Gawande *et al*., 2015). Today, numerous examples of nanocatalysts have been developed by researchers such as well-defined magnetic nanocatalysts, single-atom catalysts, core–shell and yolk–shell nanocatalysts, silica-based hybrid catalysts etc. (Gawande *et al*., 2015). They tend to have several exposed corners and edge atoms for catalysis and ability of electron transfer and amount of active sites in various ways (Chen *et al*., 2016).

Nowadays, there is a new group of advanced integrated nanocatalysts (INCs) introduced into the nano-science; they are usually in the form of globular or sphere-like morphologies; they are a multicomponent material with a nano-architecture (Gawande *et al*., 2015). This kind of new structured catalysts was thought to be directly used in the industry instead of regular coated monolithic structures which may lack of mediocre-uniformity high catalyst loading, low materials utilization, random catalytic sites, poor wash coat adhesion, short life-time, degradation tendency etc. (Guo *et al*., 2013).

The nanocatalysts used in these structured systems usually have a spinel oxide morphology consisting of AB_2O_4 composition in which A is for divalent cations in the tetrahedral sites while B means trivalent cations in the octahedral sites (Windisch Jr. *et al*, 2002). They are usually synthesized through hydrothermal method which is one of the common technique to synthesize nanostructured materials to obtain well dispersed and homogenous nanoparticles. It usually depends on a heterogonous reaction of aqueous solvents or minerals under high pressure and temperature to dissolve and recrystallize which are generally insoluble under regular conditions (Byrappa and Adschiri, 2007).

M_xCo_3-xO_4 spinel structure is one of the most popular ones in which 3d-transisitons metals such as Cu, Mn, Ni, Zn etc can be substitute into. More recently, Ren *et al.* (2016) have developed a new type of nano-array based monolithic catalysts such as $M_xCo_{3-x}O_4$ (M=Co, Ni, Zn). They obtained 100% propane conversion at temperature less than 400 °C under flow rate of 150 mL/min with 15 mg Ni doped Co_3O_4-based nano-array (Ren *et al*., 2016). They have also previously obtained 80% NO conversion at 275 °C in the study of NO

oxidation over Co_3O_4 nano-array based catalytic honeycombs which was believe to be promoted by small grain size and porous nature of nanowires (Ren *et al.,* 2013).

The mechanism consists of the uniform integration of nanoarrays like nanowires into monolithic honeycombs which can act either as support, active material or catalysts. All channels of monoliths are covered by nanowires. It has been suggested that this type of nano-structured catalyst offers some advantages such as high surface area, thermal stability, high catalyst utilization efficiency and mechanical robustness comparing with the wash-coated monolithic catalysts (Guo *et al*., 2013; Ren *et al*., 2013). Also, they can provide precise and optimum microstructure control as well as applicability in correlating materials structure with properties (Du *et al*., 2016). In addition, they have fewer height (less than 10 nm) high than wash-coated structured catalysts (40-100 nm) which affects the diffusion distance and amount of material usage (Ren *et al*., 2014)

Besides to cordierite or mulltite monolith, various material can be used a structure material such as carbon nanotubes etc. Marban *et al.* (2008) has introduced a mesoporous Co_3O_4 nanowire arrays over on a stainless steel mesh, in which the wires 500 nm has diameter, 71 m^2/g BET surface area of and a 3.4 nm pore size. They obtained a high heat exchange with low pressure drop and a remarkable stability at a temperature range from 100–175 °C. Ke *et al.* (2015) has produced Co_3O_4 nanowire arrays functionalized carbon nanotubes (fCNTs) to generate a 3D nanostructure for high-performance supercapacitor, in which there is a strong electrostatic interaction between the carboxyl groups and amine groups in fCNTs and amine-modified Co_3O_4 nanowire arrays. Jiang *et al.* (2016) has synthesized a hierarchical $Ni_{0.54}Co_{0.46}O_2$ nanowires/nanosheets on bio-mass carbon fiber cloth (CFC) by using different precipitators in hydrothermal method.

The spinel structures in literature have been widely used also without any base material to be constructed. They have already found as efficient in several studies due to their special morphology. Chang *et al.* (2012) has synthesized $NiCo_2O_4$ spinel structured which was prepared by oxalate co-precipitation method and investigated its surface morphology and crystallinity. They found that the content of Ni and Co in the spinel structured affect the particle size of the structure. Among their synthesized materials such as NiO, Co_3O_4 and $NiCo_2O_4$, $NiCo_2O_4$ has the smallest particle as 34.10 nm due to ionic replacement of Ni^{+2}

during the preparation procedure. Tao *et al*. (2015) has demonstrated a high catalytic activity in methane oxidation over $NiCo_2O_4$ catalysts from the combination of nickel cations, cobalt cations and surface lattice oxygen atoms or oxygen vacancies at the atomic scale. (Chen *et al.* (2017) has developed Pd impregnated spinel cobalt oxide (Co_3O_4), which was synthesized with various morphologies (cubical, flower-like, plate-like and rectangular-like) through hydrothermal method for CH_4 and CO oxidation reactions. Pd-impregnated Co_3O_4 catalysts exhibited enhanced activity comparing to bare Co_3O_4 catalyst in CH_4 oxidation probably due to the changed unit morphology with various interaction between Pd and Co_3O_4 unit cells. On the other hand, the CO oxidation activity over the Pd loaded Co_3O_4 forms such as rectangular-like, flower-like, plate-like was decreased whereas it was increased over the Pd-cubical Co_3O_4, which was clearly affected by O_{ads}/O_{lat} molar ratio and the specific area reaction rate of various Pd/Co_3O_4 forms.

In addition, there are other nanostructured materials such as MgO, SiO_2, CeO_2, ZnO etc. Ren *et al.* (2014) has also developed 1% Pt-ZnO nano-arrays over monoliths for CO oxidation. Their annealing tests showed that that the morphology of the arrays analyzed by XRD instrument did not changed. Also, the loss of surface area after 100 h 800◦C annealing was smaller than the form of wash-coated catalysts, which is 5% in ZnO nano-arrays and 50% in ZnO wash-coated powders. In addition, they were able to work under 50 ml/min for 10 days with good mechanical integrity with little morphology and weight loss. Zhang *et al.* (2017) has prepared a hierarchical ultrathin $Ni_{1-x}Co_xO_y$ nanoflakes MnO_2 nanowire by a hydrothermal reaction-chemical bath deposition-calcination as the electrodes for supercapacitor. Al-Hazmi *et al*. (2012) has developed a MgO nanowires through the microwave assisted hydrothermal process for the first time by using magnesium acetate and urea which can be used in nanotechnology systems and agents. Dou and Zeng (2014) developed highly active mesoporous silica nanowires implanted molybdenum oxide which has three-dimensional network structure with shallow wormhole channels and enhanced porosity for oxidative desulfurization (ODS) of model diesels (Gawande *et al*., 2015). Chen *et al.* (2016b) has produced a uniform manganese oxide nanorods and nanowires onto the cordierite honeycomb monolithic substrates by generic one-pot hydrothermal synthesis route for (CO) oxidation. Due to the cost considerations, replacement of precious noble metals is necessary.

3. EXPERIMENTAL WORK

3.1. Materials

3.1.1. Gases

The gases used in this research were purchased from Linde Group or HABAŞ. The properties of these gases such as suppliers, specifications and their usage target in this study are shown in Table 3.1.

Table 3.1. The properties of the gases used in this study.

Gas	Formula	Suppliers	Specification	Application
Argon	Ar	Linde	99.998%	GC carrier gas
Carbon dioxide	CO_2	BOS	99.995%	GC calibration, Reactant
Carbon monoxide	CO	Linde	99.998%	GC calibration
Hydrogen	H_2	BOS	99.998%	GC calibration, Reduction
Methane	CH_4	BOS	99.5%	GC calibration, Reactant
Nitrogen	N_2	HABAŞ	99.998%	Inert
Oxygen	O_2	Linde	99.998%	GC calibration, Reactant

3.1.2. Chemicals

The chemicals with high purity was used for catalyst preparation. The distilled water and the deionized water were prepared by GFL 2001/4 Distilled Water Instrument and Zeneer Power I Water Purification System respectively in Chemical Engineering Research Laboratories at Boğaziçi University. The other solid and liquid chemicals were purchased from various suppliers. Their properties such as specification, suppliers, and molecular weight are shown in Table 3.2.

Table 3.2. The properties of the chemicals used for catalyst preparation.

Chemical Name	**Formula**	**Suppliers**	**Specification**	**MW (g/ gmol)**
(cis,bis((isothiocyanato)bis(2 ,2-bipyridyl-4,4-dicarboxylato)ruthenium(II))	$C_{26}H_{16}N_6O_8RuS_2$	Aldrich	95%	705.64
Cobalt nitrate hexahydrate	$Co(NO_3)_26H_2O$	BDH	97%	291.03
Colloidal Cerium(IV) oxide	CeO_2	NanoTek, Alfa Aesar	20% aq. colloidal solution	172.12
Colloidal silica	SiO_2	Sigma-Aldrich	30 wt.% aq. solution	60.08
Diethyl ether	$(C_2H_5)_2O$	Merck	>99.5	74.12
Ethanol	C_2H_5OH		% 96	46.07
Hydrogen chloride solution	HCl	Merck	37.0 - 38.0%	36.46
Lead (II) oxide	Pbl_2	Aldrich	>99.5	461.01
Magnesium acetate hydrate	$(CH_3COO)_2Mg .4H_2O$	Merck	99.5 - 102.0%	214.46
Magnesium oxide	MgO	Sigma-Aldrich	98%	40.31
Methylamine solution	CH_5N solution	Aldrich	33 wt.% in absolute ethanol	31.06
N, N Dimethylformamide (DMF)	$HCON(CH_3)_2$	Merck	>99.8	73.09
Nickel nitrate hexahydrate	$Ni(NO_3)_26H_2O$	Merck	99%	290.81
Palladium(II) nitrate hydrate	$Pd(NO_3)_2 \cdot xH_2O$	Aldrich	-	230.41
Titanium dioxide	TiO_2 (P25)	Degusa	99.9%	79.866
Urea	$CO(NH_2)_2$	Merck	99.0 - 100.5%	60.06
Zinc oxide	ZnO	Aldrich	99.999%	81.39

3.2. Experimental Systems

The catalysts used in this study were first prepared by various catalysts preparation methods; then, they were used in particular constructed experimental systems for photocatalytic or catalytic reaction tests as well as characterized through some characterization techniques for further investigation. Therefore, experimental systems in this study can be categorized into of three groups such as catalyst preparation systems, reaction systems and catalyst characterization systems.

3.2.1. Catalyst Preparation Systems

The catalysts used in this study were prepared in different forms such as particulate, coated monolith or nanowire. Therefore, the catalyst preparation systems were quite different with each other.

The *incipient-to-wetness impregnation* method was used for the preparation of particulate catalysts. This system (Figure 3.1) includes a Retsch UR1 ultrasonic mixer providing uniform mixing, a KNF Neuberger vacuum pump, a Büchner flask for support material, a Masterflex computerized-drive peristaltic pump, a beaker for the precursor solution inside and a silicone tubing to carry this precursor solution through the peristaltic pump into support material. In this method, proper amount of support was put into the Büchner flask and mixed by Retsch UR1 ultrasonic mixer under vacuum for 30 minutes. At the meantime, proper amount of active metal/s are dissolved in deionized water. After mixing the support, active metal solution is fed to the support in flask by peristaltic pump with a proper flow rate. The slurry obtained are well mixed by ultrasonic mixer under vacuum to achieve a uniform metal distribution over support, kept for at least 90 minutes and dried in the oven at the specified temperature.

For monolith catalysts, *wash-coating method* was used as in Figure 3.2. The system contains a Retsch UR1 ultrasonic mixture, beaker and Bosh microwave oven. For air flowing, a syringe was also used. In this method, cut and cleaned monoliths are dipped into support solutions on Retsch UR1 ultrasonic mixer for 40 minutes. Every 5 minutes, monoliths are taken out from the solution and flushed by air to prevent the channel clogging.

After this coating process, monoliths are dried in Bosh microwave oven for 45 minutes with a power of 160 W. The coated and dried monolith are then weighed and the whole process are repeated until the target amount of support coating are obtained. The proper amount of active metal solution is prepared, injected drop by drop to the channels of the monolith through a syringe and dried in the oven at the specified temperature.

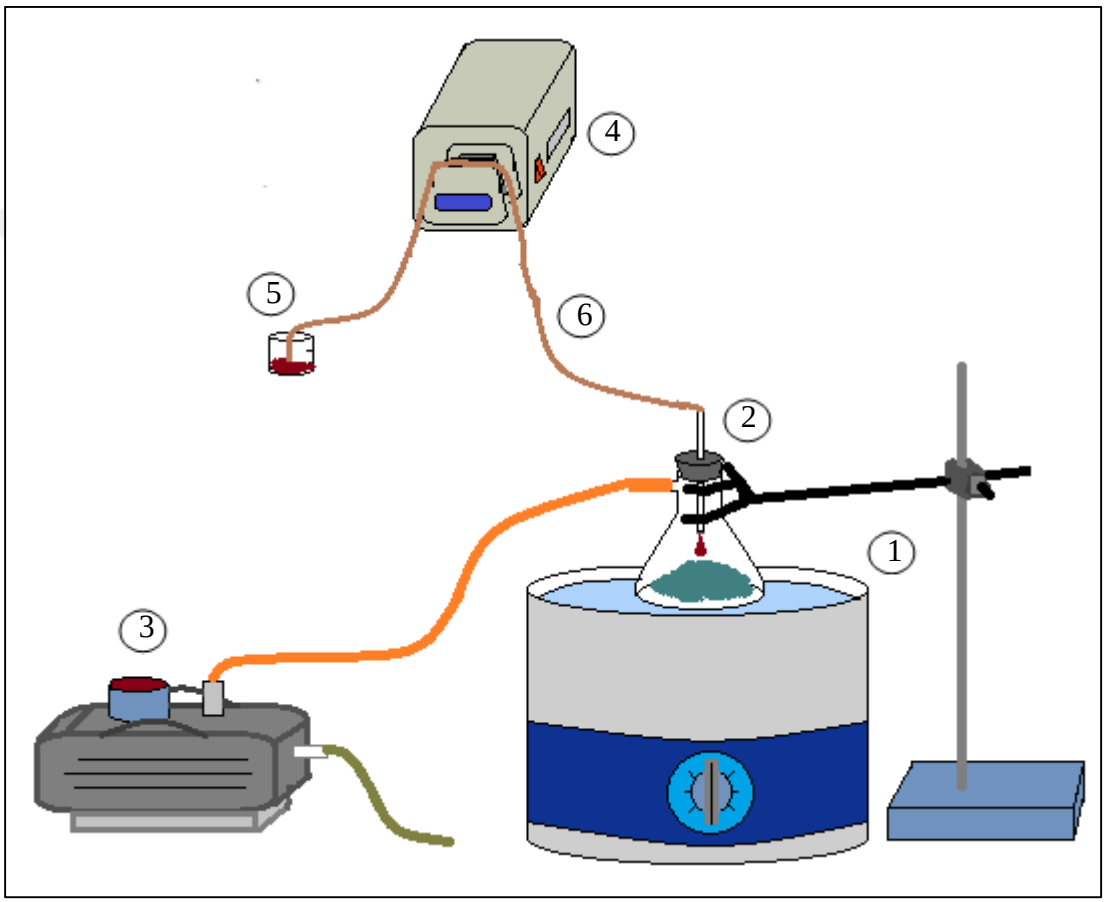

Figure 3.1. Schematic diagram of the incipient to wetness impregnation method (1. Ultrasonic mixer, 2. Büchner flask, 3. Vacuum pump, 4. Peristaltic pump, 5. Beaker, 6. Silicone tubing).

In order to synthesize the nanowire catalysts, *hydrothermal synthesis method* was used. In this method, a Retsch UR1 ultrasonic mixer, two beakers and a Gallenkamp oven and a syringe for air flow were used as in Figure 3.3. The proper amount of the active metal and urea solutions are prepared in beakers and mixed by ultrasonic mixer. The cut and clean monoliths are inserted into active metal solution. Then, urea solution is added drop by drop

to the beaker with monoliths. The beaker is kept in oven at 90 °C for the nanowire synthesis over monoliths. After synthesis, the coated monoliths are dipped into distiller water and air is flushed by air to prevent the channel clogging.

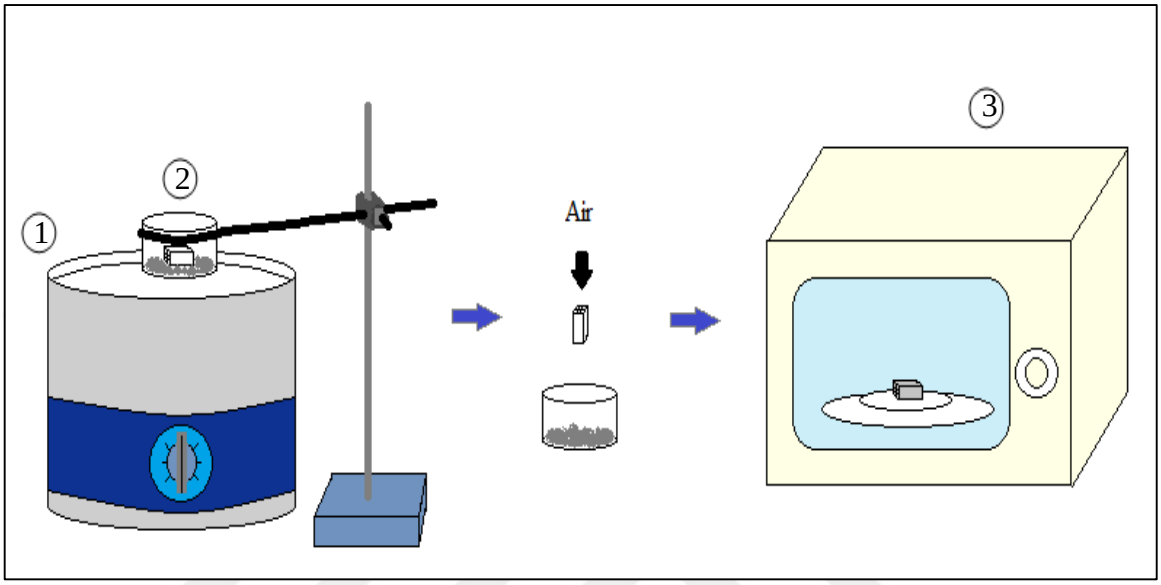

Figure 3.2. Schematic diagram of the wash-coating system (1. Ultrasonic mixer, 2. Beaker, 3. Microwave Oven).

In some cases, either a homemade Teflon autoclave (Figure 3.4a) with a Heidolph MR3001 magnetic stirrer with heating (Figure 3.4b) or an Alex Machine ultrasonic mixer with heating are also used for the hydrothermal synthesis. In these procedures, proper amount of active metal solutions and urea are well mixed by magnetic stirrer or ultrasonic mixer and directly kept at 90 °C for the synthesis, or mixed and transferred into the autoclave and kept in oven for the synthesis. After synthesis, the procedure is followed by cleaning and drying steps as in the previous methods.

All dried catalysts in this study was calcined in a temperature programmed Carbolite oven (Figure 3.4c). The detailed catalyst preparation steps will be explained in Section 3.3.

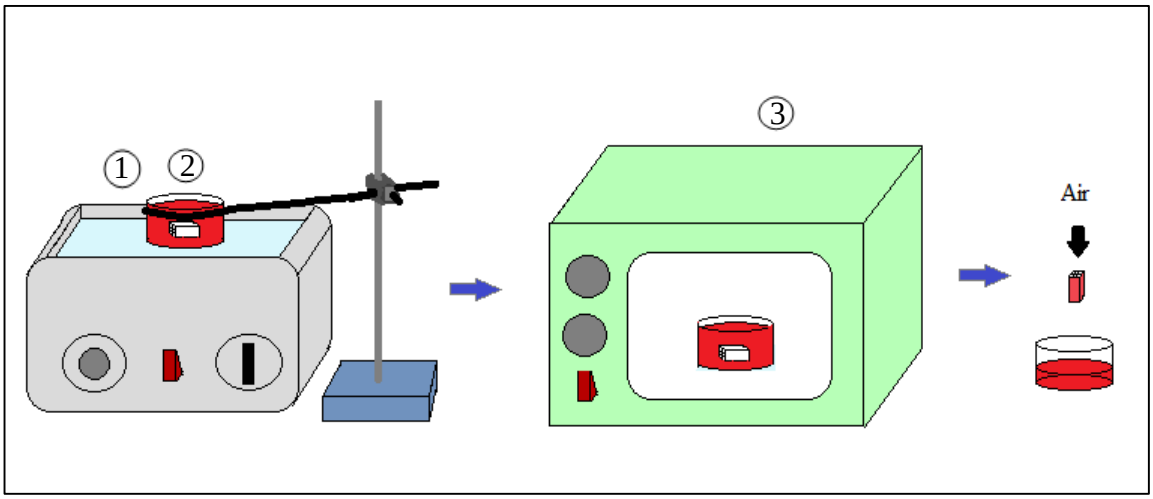

Figure 3.3. Schematic diagram of the homogeneous deposition precipitation method (1. Ultrasonic mixer with heating, 2. Beaker, 3. Oven).

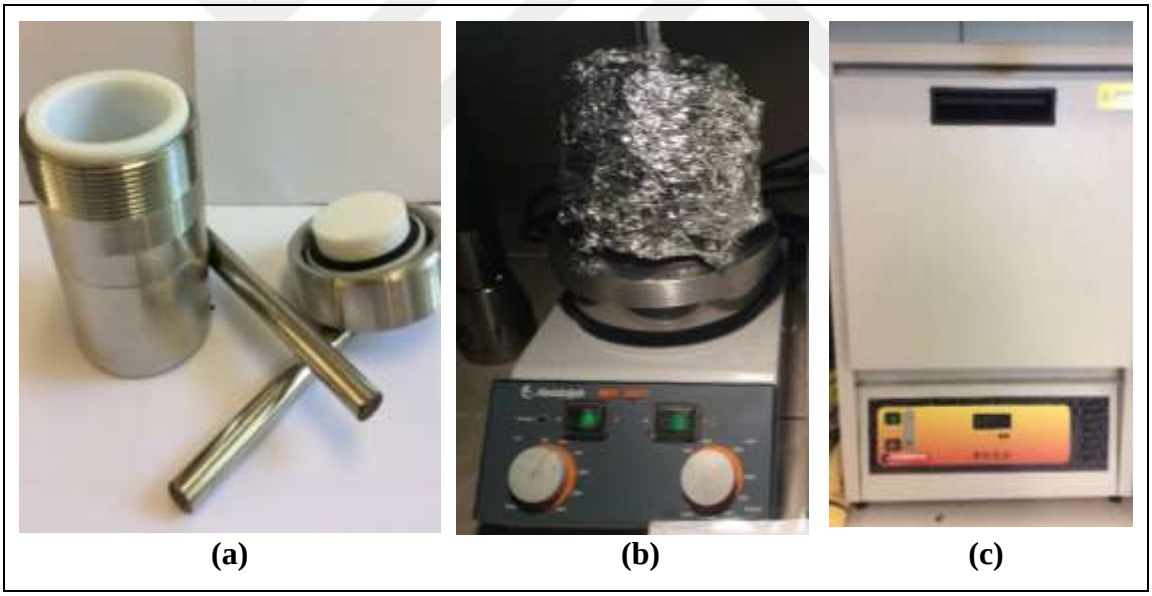

Figure 3.4. The image of Teflon autoclave(a), Heidolph MR3001 magnetic stirrer (b) and Carbolite oven (c).

3.2.2. The Reaction Systems

The constructed reaction system in our laboratories for the dry reforming of methane can be seen in Figure 3.5. The reaction system can be divided into three parts: feed, reaction and analysis. In feed section, Brooks model 5850E mass flow controllers (MFCs) were used

to control of CH_4, CO_2, N_2, H_2 inlet gases supplied by pressurized gas cylinders which are regulated as 2 bar during the reaction tests. These gases were passed through 1/4-inch stainless steel tubes after MFCs, mixed well and then sent to the reaction section for the activity test.

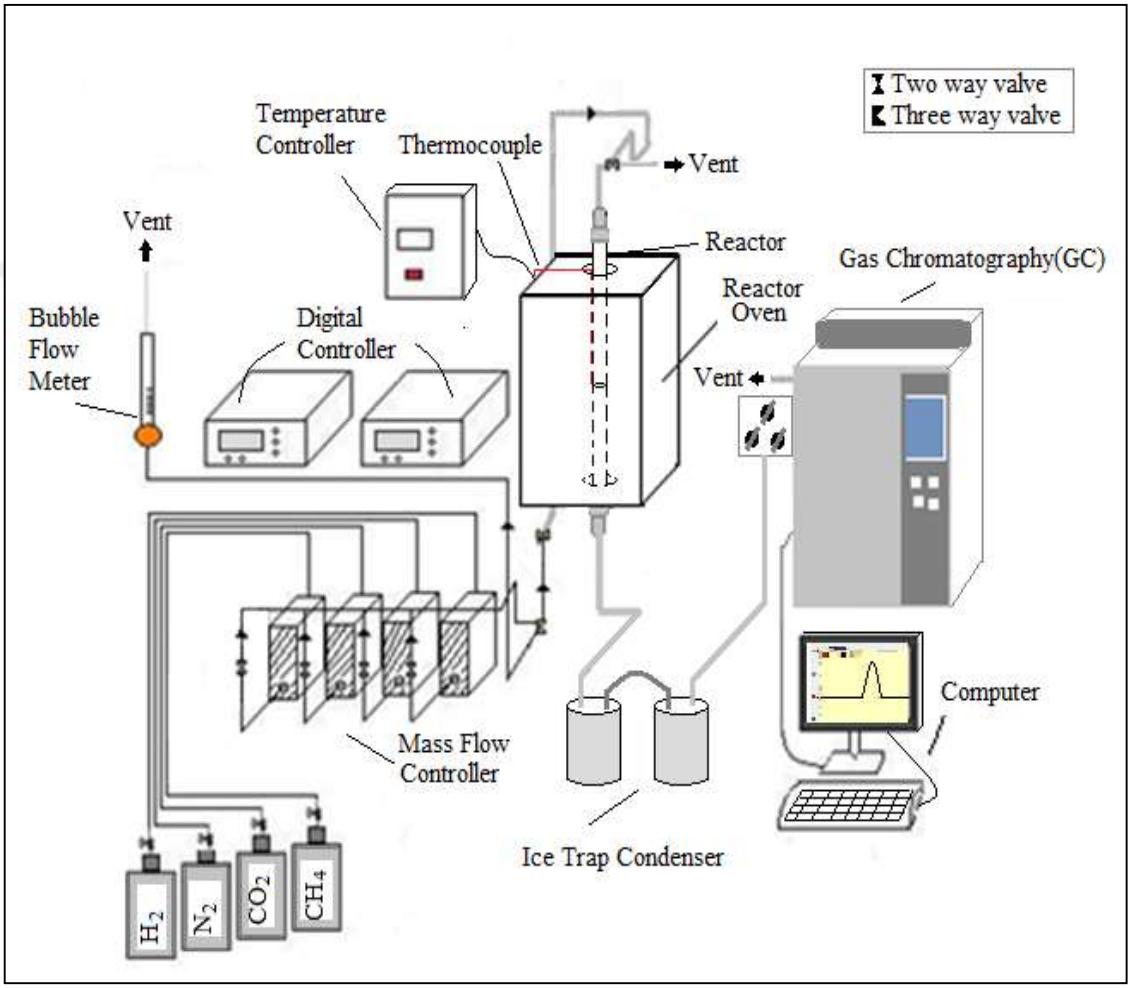

Figure 3.5. Schematic diagram of catalytic reaction system.

In the reaction part, two types of reaction system were constructed with some modifications since photocatalytic and catalytic reaction tests were performed in this study. In the photocatalytic experiments, a special design of downward tubular quartz reactor was used. The length of this reactor was 775 mm and the diameter was 10 mm. Also, there was a quartz circle part with a 45 mm diameter in the middle of the quartz reactor in order to increase photon activity through the high interaction of light with the catalyst surface (Figure 3.6a). For this purpose, first quartz wool was inserted then the circle was filled with the

catalyst as in the Figure 3.6b. The catalytic tests were also performed in a downward tubular packed-bed reactor made of quartz with a 775 mm reactor length and 10 mm inner diameter (Figure 3.6c). Small amount of quartz wool was again first insert into quartz reactor before the catalyst loading which is either in the form of particulate or monolithic (Figure 3.6d).

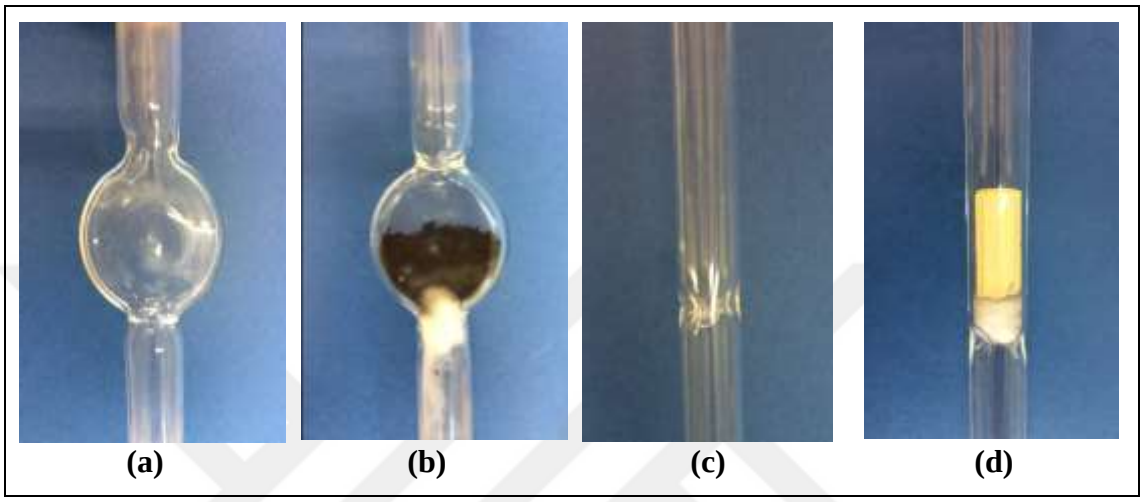

Figure 3.6. The images of the reactor configuration used in this study: empty and filled quartz reactors for photocatalytic (a-b) and catalytic (c-d) reaction tests.

In photocatalytic studies, a special design oven as seen in Figure 3.7. This oven has two blank window, which are in front and back of the oven, to allow light pass from the light source directly into the reactor circle. The inside of the oven was completely covered with quartz wool to prevent heat loss. In addition, these windows can be optionally used with a quartz window in the case of operating it at various temperatures from 0-1000 °C either in the presence or absence of the light. The designed oven was directly inserted the regular catalytic system as in Figure 3.5 with some small changes such as having cooling fan to cool the heating lamps as in Figure 3.8. Various light sources were used the photocatalytic tests such as (A) 200W UV lamp, (B) CLEO HPA 400 S 400W metal halide lamp with 87 UVA(W) Radiation 1hr and (C) ABET LS 150 Xenon Lamp Source solar simulator with 100 mW/cm^2 irradiation. The temperature is measured and controlled by a GEMO PC107 controller.

Figure 3.7. The outside(a) and inside(b) view of special design of oven.

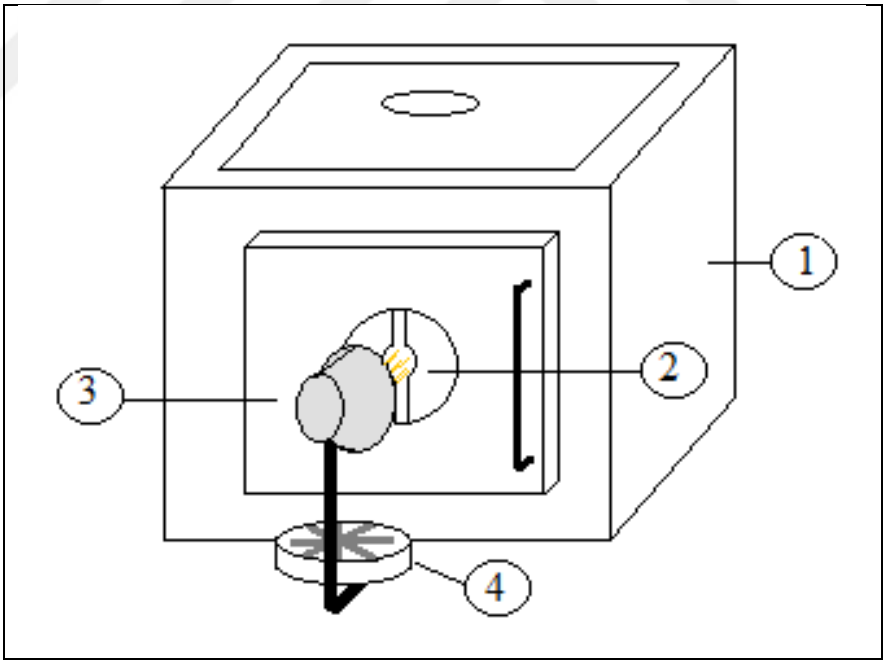

Figure 3.8. Schematic diagram of photocatalytic reaction system (1. Oven 2. Quartz reactor 3. Lamp 3. Cooling fan).

In the catalytic system, a homemade oven was used to heat the reactor. The top and the bottom of the oven were closed with quartz wool to prevent heat loss from the oven to the environment. The temperature was measured with K type thermocouple from the bottom

of the catalyst as seen in Figure 3.9 and controlled by Schimaden FP21 controller in the catalytic system. The product gases were passed through 1 cylinder and 1 spiral iced condensers to trap possible water vapor produced due to the reaction since water entrance to the gas chromatography can be harmful for the instrument working properly.

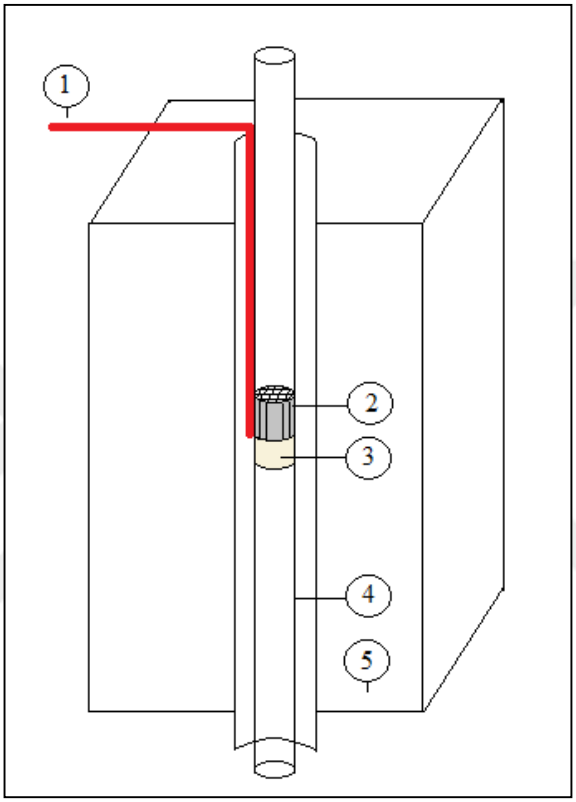

Figure 3.9. Schematic diagram of the reactor and oven used in catalytic system (1. Thermocouple 2. Monolith 3. Quartz wool 4. Quartz reactor 5. Oven).

In the product analyses section, all product and feed gases were analyzed with Schimadzu GC 2014 Gas Chromatography (GC) with a Carboxen1000 column. The product gases were carried to the GC with 1/8-inch stainless steel tubes after the condenser part. The data was taken with an hour time increment. The operating conditions of GC instrument used in this study are given in Table 3.3.

The calibration procedure conducted in this study will be explained in Section 3.4.1. Through the utilization of calibration curve, all feed and product compositions of CH_4, CO_2, H_2, CO and N_2 mixtures are calculated.

Table 3.3. Gas chromatography analyzer specifications.

GC Model	Shimadzu GC 2014
Detector type	TCD
Column temperature	150 ℃
Detector temperature	175 ℃
Injection temperature	170 ℃
Detector current	50 mA
Carrier gas	Argon
Carrier gas flow rate	30 ml/min
Column type	CBXN-1000 60/80

In all experimental studies, the results were represented in terms of CH_4 conversion, CO_2 conversion, H_2 and CO yield and H_2/CO ratio, which are calculated by using N_2 interval gases as follows:

$$X_{CH4} = \frac{X_{CH4_{in}} x F_{in} - X_{CH4_{out}} x F_{out}}{X_{CH4_{in}} x F_{in}} x100\%$$

$$X_{CO2} = \frac{X_{CO2_{in}} x F_{in} - X_{CO2_{out}} x F_{out}}{X_{CO2_{in}} x F_{in}} x100\%$$

$$Y_{H2} = \frac{0.5 x X_{H2_{out}} x F_{out}}{X_{CH4_{in}} x F_{in}} x100\%$$

$$Y_{CO} = \frac{X_{CO_{out}} x F_{out}}{X_{CH4_{in}} x F_{in} + X_{CO2_{in}} x F_{in}} x100\%$$

$$\frac{H_2}{CO} = \frac{Y_{H2}}{Y_{CO}}$$

CH_4 conversion, CO_2 conversion, CO yield and H_2 yield are represented by $X_{CH4}, X_{CO2}, Y_{H2}, Y_{CO}$ in the equations where the inlet and outlet volume of CH_4, CO_2, H_2,

CO expressed as $(X_{x_{in/out}})x(F_{in/out})$ in terms of output flow rate (F_{out}), which is calculated by composition of internal gas in the inlet and outlet (X_{N2}).

$$F_{out} = \frac{X_{N2_{in}} x F_{in}}{X_{N2_{out}}}$$

3.2.3. Catalyst Characterization Systems

Various characterization techniques such as SEM-EDX, XRD and XPS were performed to understand the physical, microstructural and electronic properties of the catalyst samples better and to investigate the changes in those properties of the catalyst after reduction and reaction process. All characterization studies were conducted in the Advanced Technologies Research and Development Center of Boğaziçi University

3.2.3.1. Scanning Electron Microscopy and Energy Dispersive X-Ray (SEM-EDX). The microstructure, morphology and the elemental analysis of fresh-reduced and used catalyst samples were investigated by SEM-EDX. Micrograph results were obtained by a Philips XL 30 ESEM-FEG system with a maximum resolution of 2 nm.

3.2.3.2. X-Ray Diffraction (XRD). The crystallographic structure of the monolithic catalyst samples was analyzed by Rigaku D/MAX-Ultima+/PC X-Ray diffraction (XRD) equipment having an X-ray generator with Cu Kα radiation (λ =0.154 nm) in a scanning angle with a range of 3-90° at a rate of 2°/min and with an accelerating voltage of 40 kV and a current of 40 mA.

3.2.3.3. X-ray Photoelectron Spectroscopy (XPS). The amount and the nature of metal species on the catalyst samples were investigated by Thermo Scientific X-ray Photoelectron Spectrometer (XPS) with a source gun of Al K Alpha X-Ray 000 and with a spot size of 400 μm. The binding energy scale of the XPS spectra were adjusted to the C1s line.

3.3. Catalyst Preparations

The Ni-based catalysts used in this study were prepared in various forms such as particulate, coated monolith and nanowire by using the preparation systems as mentioned in Section 3.2.1.

3.3.1. Ni-based Particulate Catalysts over Various Supports

Ni-based catalysts with Co addition over MgO, TiO_2 and ZnO support were prepared with the fixed 8 wt.% Ni and 2wt.%Co active metal dispersion. Dyed- Ni-Co/TiO_2 catalyst and $CH_3NH_3PbI_xCl_{3-x}$ Perovskite- TiO_2 catalysts were also particularly developed for photocatalytic system experiments.

3.3.1.1. Ni-Co/MgO. MgO supported Ni-Co based catalysts were prepared by incipient to wetness impregnation technique as in Section 3.2.1. MgO support were first crushed and sieved and then proper amount of MgO was put into the vacuum flask and mixed with an ultrasonic for 30 minutes. Then, proper amount of $Ni(NO_3)_26H_2O$ and $Co(NO_3)_26H_2O$ were dissolved in deionized water and co-impregnated to MgO support as in Figure 3.1. After impregnation process, the resulting slurry was continued to be mixed approximately 90 min till uniform distribution and then, dried for 12 h at 120 °C. Finally, they were calcined at 500 °C for 5 h.

3.3.1.2. Ni-Co/TiO_2. For TiO_2 supported Ni-Co based catalysts, same incipient-to-wetness impregnation method was used as in Section 3.2.1.1. TiO_2 (P25) as support material was first mixed under vacuum for 30 min. Then, the proper amount of $Ni(NO_3)_2.6H_2O$ and $Co(NO_3)_2.6H_2O$ were dissolved in deionized water. The prepared solution was added drop by drop through peristaltic pump to TiO_2 under vacuum. Then, the catalyst was dried at 120 °C and calcined at 500 °C.

3.3.1.3. Ni-Co/ZnO. Similar to MgO and TiO_2, ZnO support was directly mixed by ultrasonic mixer under vacuum for 30 min. Then the proper amount of $Ni(NO_3)_2.6H_2O$ and $Co(NO_3)_2.6H_2O$ solution was added to the ZnO support under vacuum. After impregnation process, the catalyst was dried at 120 ˚C and calcined at 500 °C.

3.3.1.4. Dyed-Ni-Co/TiO_2. Before impregnation of $Ni(NO_3)_2.6H_2O$ and $Co(NO_3)_2.6H_2O$ solution over support materials, firstly proper amount of dyed material (cis,bis((isothiocyanato)bis(2,2-bipyridyl-4,4-dicarboxylato)ruthenium(II)) solution in deionized water was impregnated over TiO_2 (P25) under vacuum in ultrasonic mixture and dried at 120 °C. Then, the active metal solutions were added as in Section 3.2.1.1. Dyed-Ni-Co/TiO_2 catalyst was finally dried at 120 °C and calcined at 500 °C.

3.3.1.5. $CH_3NH_3PbI_xCl_{3-x}$ Perovskite-TiO_2. The proper amount of methylamine and hydrochloric acid were mixed in a flask for 2 h with magnetic stirrer. Then the mixed solution was kept at 50 °C in order to obtain yellowish methyl ammonium iodine (CH_3NH_3I). CH_3NH_3I was then washed with diethyl ether and ethanol in turn and filtered. The filtered CH_3NH_3I, $PbCl_2$ and TiO_2 were mixed in proper amount of DMF at 60 °C to obtain $CH_3NH_3PbI_xCl_{3-x}$ over TiO_2. In order to remove the solute, the mixed material was kept in oven at 105 °C for 45 min. Since the material is sensitive to humidity, the synthesized $CH_3NH_3PbI_xCl_{3-x}$ Perovskite-TiO_2 catalyst was kept in desiccator.

3.3.2. Ni-based Coated Monolithic Catalysts

MgO, SiO_2 and CeO_2 wash-coated Ni-based catalysts monolithic catalysts with Co addition were prepared in this study as Section 3.2.1. Once again, active metals were fixed as 8 wt.% Ni and 2wt.%Co.

3.3.2.1. Ni-Co/MgO Monolith. The commercial ceramic ($2MgO.2Al_2O_3.5SiO_2$) cordierite and mullite monolithic ($3Al_2O_3.2SiO_2$) were used as monolithic support material. They were cut into the dimensions of 8 mm ×8 mm x 18 mm so that it can be easily placed into the 10 mm ID quartz tube reactor (Figure 3.6c). The channel widths of monoliths were 0.9 mm and 1mm for commercial cordierite and mullite ceramic monoliths, respectively. The cut monoliths were then washed with acetone to remove the possible impurities and open the pores from residue from the cutting procedure and dried in the oven at 120 °C for 2h. For coating, 0.2g MgO were solved in 0.5 ml deionized water for each monolith. The cleaned monoliths were then put into solution and mixed with an ultrasonic mixer for 40 min as in Figure 3.2. Every 5 min excess MgO which was clogging the openings were flushed out by pressurized air and with the help of a syringe; then they were dried for 40 min in a microwave

oven with a power of 160 W. Approximately, 10-15% of MgO was coated on monolith and the excess MgO were removed by scrubbing with the help of a needle of syringe and by tapping each monolith to the table surface. After coating process accomplished, proper amount of $Ni(NO_3)_26H_2O$ and $Co(NO_3)_26H_2O$ were dissolved in 0.3 ml deionized water for 15 min assisted with ultrasonic mixer. The prepared solution was injected drop by drop to the channels of the monolith through a syringe. Both external and internal surfaces of monolith channels were wetted. After this process, the monoliths prepared were dried at 120 °C for 4 h and then calcined at 500 °C for 5 h. The steps of the procedure can be seen in Figure 3.10.

3.3.2.2. Ni-Co/SiO_2 and Ni-Co/CeO_2 Monoliths. Either SiO_2 or CeO_2 supported Ni-based monolith catalyst was similarly prepared as discussed in Section 3.2.2.1. However, only cordierite monoliths were used in these catalysts. Also, colloidal forms of SiO_2 and CeO_2 were used instead of preparing the support solution to wash-coat the monolithic structure. Then the active metals were impregnated with the same procedure in previous Section 3.2.2.1. Prepared monoliths were similarly dried at 120 °C for 4 h and calcined at 500 °C for 5 h.

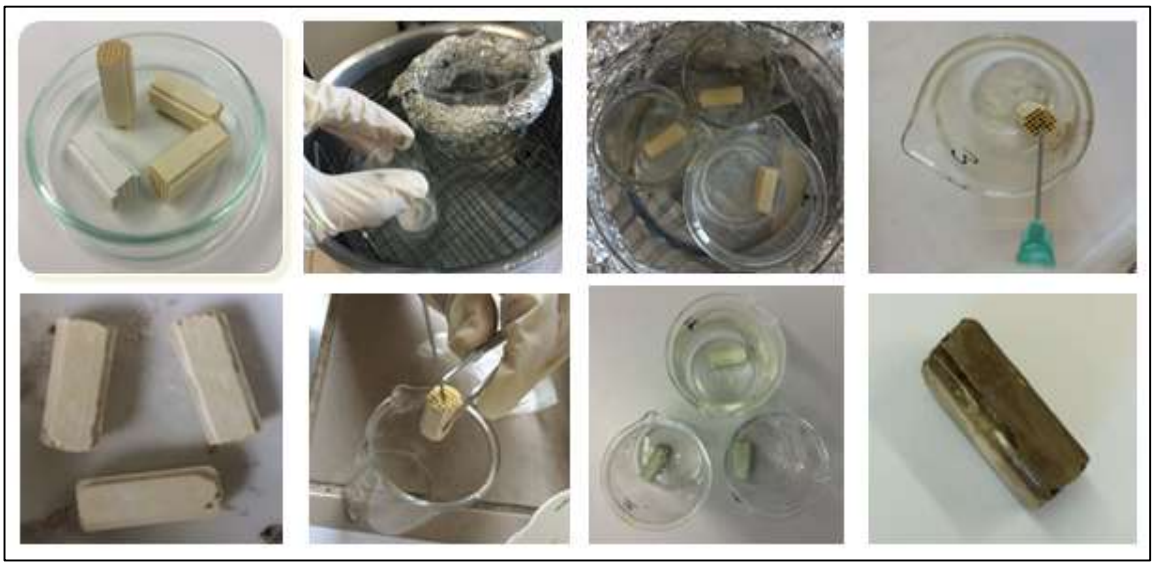

Figure 3.10. The preparation images of monolithic catalyst.

3.3.3. Ni-based Nanowire Structured Catalysts

Various $Ni_xCo_{3-x}O_4$ nanowire over monoliths and Ni-based MgO nanorod catalysts were developed. In some cases, %1 wt. Pd $Ni_xCo_{3-x}O_4$ nanowire was also used.

3.3.3.1. $Ni_xCo_{3-x}O_4$ Nanowire. The commercial ceramic cordierite ($2MgO.2Al_2O_3.5SiO_2$) with the channel with of 0.9 mm was cut into the piece (8 mm diameter x 18 mm length). The monoliths pieces were then washed with distilled water and acetone for 30min for cleaning in ultrasonic mixture. $Ni_xCo_{3-x}O_4$ nano-array synthesis (x=0,0.5,2) over these monoliths were performed following the procedure of hierarchical nickel-cobalt nano-array catalyst preparation method of Ren *et a*l. (2014). 0.5 mol/lt $Ni(NO_3)_26H_2O$ and 0.5 mol/lt $Co(NO_3)_26H_2O$ were dissolved in deionized water (20 ml, 50 ml, 100 ml, 300 ml, respectively) to prepare $Ni_xCo_{3-x}O_4$ nanowire catalyst. Unlike the studies of Ren *et a*l. (2014), low amount of solution was aimed to consume less metal nitrate chemicals in the procedure. For this purpose, the effect of using regular oven heating, ultrasonic and magnetic stirrers with heating property were also be evaluated in the synthesis of nanowire catalyst. The cut and cleaned monoliths were put into active metal solutions and mixed ultrasonically in each trials as in Figure 3.3. 5 or 10 mol urea was then added into the active metal solution in ultrasonic mixing. Then the solution was kept at 90 °C for 12 h in various systems such as ultrasonic, magnetic stirrer or oven to synthesize $Ni_xCo_{1-x}O_4$ nanowire as in Table 3.4. After the reaction proceeded, the monolith was removed from the solution and softly rinsed by distilled water, flushed out by air with the help of a syringe and dried at 80 °C for 4 h and annealed at 300 °C for 4 h with ramping 20 °C/min. In the preparation of Co_3O_4, 0.5 mol/lt of $Co(NO_3)_26H_2O$ solution was used. The rest of the preparation procedure was kept the same. the mullite type monolith was also coated with nanowire catalyst with the same procedure. The images of some preparation steps for $Ni_{0.5}Co_{2.5}O_4$ nano-array monolithic catalyst can be seen in Figure 3.11.

3.3.3.2. Pd/$Ni_xCo_{3-x}O_4$ Nanowire. In order to prepare this catalyst, first $Ni_xCo_{3-x}O_4$ nanoarray were grown over the cordierite monoliths as in Section 3.2.4. Then, proper amount of $Pd(NO_3)_2 \cdot xH_2O$ was dissolved in deionized water and impregnated over the inside of the $Ni_xCo_{3-x}O_4$ nanoarray coated monoliths. Finally, % 1 wt. Pd impregnated monoliths were dried and calcined again at the same conditions as in Section 3.2.3.2.

Table 3.4. Experimental conditions of $Ni_xCo_{3-X}O_4$ nanowire synthesis.

Trials. #	Urea amount, mol	Reaction conditions	Mixing type
1	5	Magnetic stirrer with heating	Magnetic
2	5	Oven	No mixing
3	10	Oven	No mixing
4	10	Ultrasonic stirrer with heating	Ultrasonic
5	10	Ultrasonic (2 hrs) + oven (10 hrs)	Ultrasonic

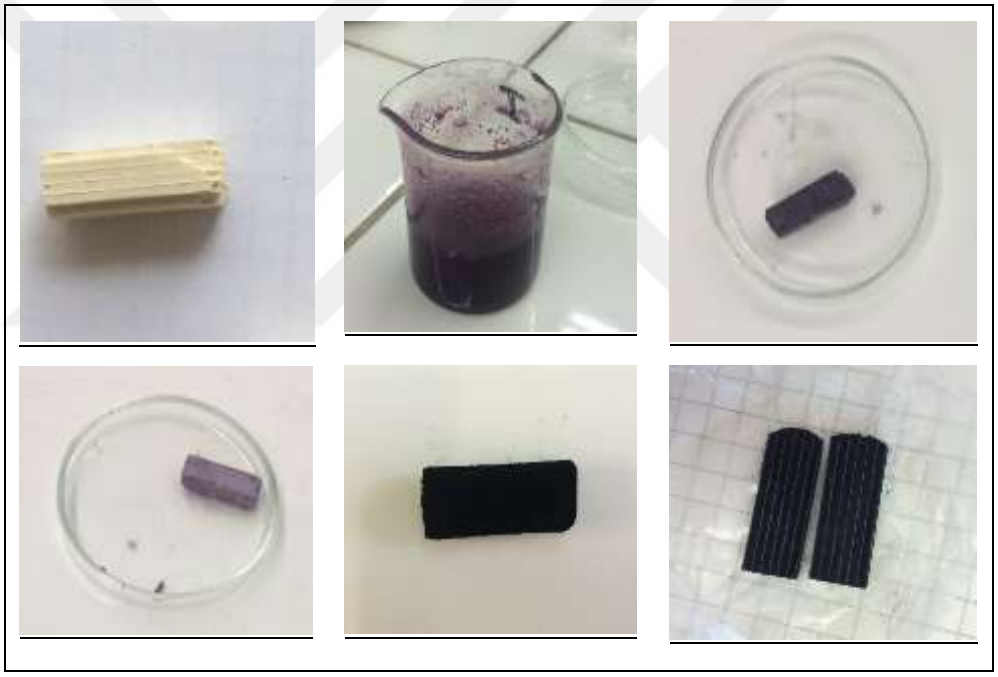

Figure 3.11. The preparation images of $Ni_{0.5}Co_{2.5}O_4$ nano-array monolithic catalyst.

3.3.4. Ni-based Nanorod Structured Catalysts

3.3.4.1. Ni-Co/MgO Nanorod. This nanorod catalyst was synthesized using two different preparation procedures. In the first one, MgO nanorod synthesized and then Ni-Co active metals were impregnated over nanorod MgO support. In the second one, MgO and Ni-Co active metals were prepared together. In the first procedure, the proper amount of urea and magnesium acetate hydrate were dissolved in 25 ml and 75 ml distilled water respectively

and mixed for 30 min with magnetic stirrer as in the MgO nanorod synthesized of Al-Hazmi *et al*. (2012). Urea solution was then added to magnesium acetate hydrate solution and mixed for 5 min. The well mixed solutions then transferred into 100 ml Teflon autoclave. The autoclave was closed well and put in the oven for 1 or 2 h in oven at 180 °C. After the reaction process 180 °C, autoclaved were cooled to room temperature. The obtained heterogonous solution inside the autoclave were transferred into centrifuge tube for the centrifugation at 4100 rpm for 10 min. Then the products were collected from the tube and filtered with distilled water and ethanol, respectively, to reduce agglomeration. The final products were dried at 60 °C for 24 and then calcined at 600 °C for 1 h. In order to obtain 8 wt.% Ni – 2wt.%Co over MgO nanowire catalysts, proper amount of Ni-Co active metal solutions were impregnated, dried and calcined as in the Section 3.2.1.1. In the second preparation method of Ni-Co/MgO nanowire catalysts, the proper amount of nickel nitrate hexahydrate, cobalt nitrate hexahydrate and magnesium acetate hydrate were co-dissolved in distilled water and mixed for 30 min. The well mixed solution was then transferred the same autoclaved and kept in oven at 180 °C for 2h. The final product was centrifuged, filtered, dried and calcined as in the procedure of MgO synthesis. The images of some preparation steps for Ni-Co/MgO nanorod catalyst can be seen in Figure 3.12.

Figure 3.12. The preparation images of Ni-Co/MgO nanorod catalyst.

3.3.4.2. Ni-Co/MgO Nanorod over Monoliths. The monolithic Ni-based over MgO nanostructured catalysts have been prepared in four different ways as in Table 3.5. In the first trial, cleaned cordierite monolith (8 mm ×8 mm x 18 mm) was inserted into the autoclave containing magnesium acetate-urea solution as in the previous section, kept for 2 h at 180 °C and cooled to room temperature. The coated monolith was taken out from the autoclave and cleaned, dried and calcined at 600 °C. In the second trial, the monolith was put again into the autoclave containing magnesium acetate-urea solution with a certain amount of Ni-Co nitrate inside. The following procedure was the same as in trial 1. In the third trial, the proper amount of the prepared MgO nanorods as in Section 3.3.4.1 was dissolved into distilled water and wash-coated over monolith surface and channels, dried and coated with active metal solutions as in Section 3.3.2.1. In the last trial, the synthesized MgO in Section 3.3.4.1 was dissolved into distilled water before calcined at 600 °C and directly wash-coated over the monolith. After the addition of active metal solution, surfaces and monolith was again dried and calcined as in Section. 3.3.2.1.

Table 3.5. Preparation methods of Ni-based MgO nanostructured monoliths.

Trials #	**Coating procedure**	**$T_{MgO,calcination}$ (°C)**	**Active metals**	**$T_{calcination}$ (°C)**
1	MgO in autoclave	600	impregnated	500
2	NiCo/MgO in autoclave	-	-	500
3	$MgO_{calcined}$ washcoated	600	impregnated	500
4	$MgO_{washcoated}$ calcined	-	impregnated	500

3.4. Reaction Test Parameters

CO_2 reforming of methane reaction tests were performed firstly in the photocatalytic system which was described in detail in Section 3.2.2. Then, the studies over monolithic and nanowire structures were continued after making the necessary changes in the reaction system mentioned above.

3.4.1. Preparation of CDRM Reaction Systems and Blank Tests

Before starting real experimental tests, several preliminary studies were performed for several reasons. Firstly, leakage test was performed with nitrogen throughout all tubes and connectors in the system and gas chromatography to be sure that no gas leakage from system to the laboratory after each experimental system construction. Then, mass flow controllers were calibrated for each reactant gases which are regulated as 2 bar. The correct amount of gases was sent to the system through calibration curve of each mass flow controllers. After that, optimal GC operating conditions (Table 3.3) were figured out to obtain separated and clear gas peaks. Certain amount of sample gas mixtures was sent to the GC at these conditions and concentration versus area graphs were obtained for each gas under optimal GC operating conditions. The curve of this graph was used to clarify the composition unknown gas mixtures. Finally, some blank tests were also performed in empty quartz reactor and quartz reactor with uncoated-reduced cordierite monolith in a temperature change 600-900 °C under 70 ml/min reactant flow (CH_4, CO_2, N_2). In addition, %8 wt. Ni-%2 wt. Co over MgO particulate catalyst was tested at 800 °C under the flow of $CH_4/CO_2/N_2$: 30/30/10 ml/min in order to check the experimental system constructed.

3.4.2. CDRM Reaction Tests over Ni-based Structures in Photocatalytic System

Performance tests of Ni-based catalysts with Co addition over MgO support and semiconductor supports such as TiO_2, ZnO were investigated in photocatalytic system under the experimental conditions as in Table 3.6. Dye added Ni-Co/TiO_2 and $CH_3NH_3PbI_xCl_{3-x}$ Perovskite to TiO_2 catalysts to increase the light absorption capacity were also tested at room conditions. Approximately, 4-5 g catalysts were used in the tests. The reduction process was conducted prior to reaction test as in the Figure 3.13.

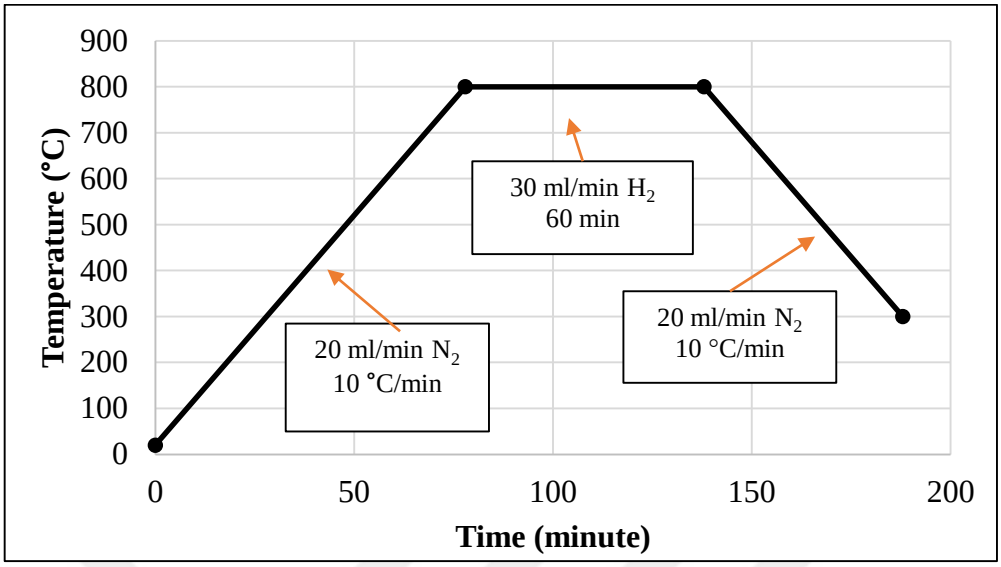

Figure 3.13. The reduction procedure for Ni-based catalysts.

Table 3.6. Experimental conditions used for DRM over various photocatalytic structures.

Exp. #	**Catalyst**	**$T_{reduction}$ (°C)**	**T (°C)**	**Feed Compositions (ml/min)**		**Lamp** closed(-), lamp or open(+)	**TOS (h)**
				CO_2	**CH_4**		
1	NiCo/MgO	800	800	30	30	-	5
2	NiCo/MgO	800	room-500	10	10	-	1
3	NiCo/TiO_2	800	room-500	10	10	-	1
4	NiCo/ZnO	800	room-500	10	10	-	1
5	NiCo/MgO	800	room-500	10	10	+	1-8
6	NiCo/TiO_2	800	room-500	10	10	+	1-8
7	NiCo/ZnO	800	300-500	10	10	+	1-8
9	NiCo/TiO_2	800	room	10	10	+	8
9	$CH_3NH_3PbI_xCl_{3-x}$ Perovskite- TiO_2	-	room	10	10	+	8
10	Dyed- Ni-Co/TiO_2	-	room	10	10	+	8

3.4.3. CDRM Reaction Tests over Ni-based Structures in Catalytic System

CO_2 reforming of methane activity of Ni-Co based particulate, wash-coated monolith and nanowires catalysts were catalytically evaluated at 600-900 °C with 50 °C temperature interval in quartz reactor. The reactor was heated to the desired reaction temperature and cooled down after the activity test with a flow rate of 30 ml min^{-1} N_2 gas. N_2 gas with a flow rate of 10 ml min^{-1} in each activity test was used as an internal gas.

3.4.3.1. CDRM Reaction Tests over Ni-Co Based Particulate and Monolithic Structures. 8% wt. Ni-%2wt.%Co over MgO particulate and 8%wt. Ni-2%wt.% Co coated over MgO, SiO_2 and CeO_2 monolith catalysts were investigated under the operation conditions as in Table 3.7. For each catalytic run, 100 mg particulate catalyst or a monolith containing 100 (±0.1) mg catalysts were used. In addition, all catalysts were reduced with H_2 gas of 25 ml min^{-1} at 800 °C (Figure 3.9).

3.4.3.2. CDRM Reaction Tests over Monolithic $Ni_xCo_{3-x}O_4$ Nanowire Structures. The catalytic tests of $Ni_{0.5}Co_{2.5}O_4$, $Ni_2Co_1O_4$ and Co_3O_4 nanowire covered monoliths were performed under the operation conditions as in Table 3.8. In addition, some catalysts were reduced with H_2 gas of 30 ml min^{-1} at 800 °C (Figure 3.13) while some was reduced at 600 °C (Figure 3.14).

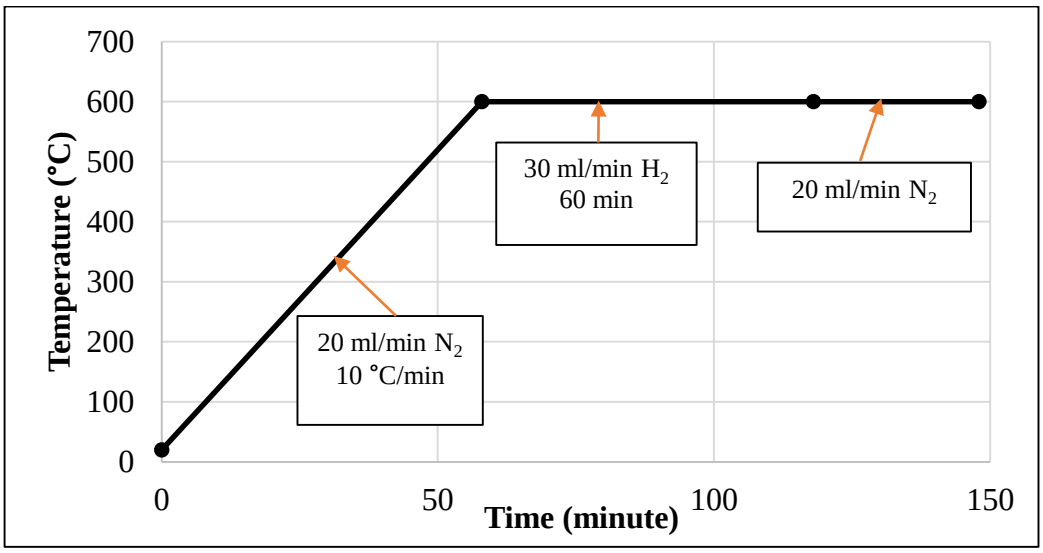

Figure 3.14. The reduction procedure for $Ni_xCo_{3-x}O_4$ nanowire structures.

Table 3.7. Experimental conditions used in CDRM over various catalysts.

Exp. #	Catalyst	T (°C)	Feed Compositions (ml/min)			TOS(h)
			CO_2	CH_4	O_2	
1	Ni-Co/MgO particulate	600-900	30	30	-	1
2	Ni-Co/MgO cordierite	600-900	30	30	-	1
3	Ni-Co/MgO mullite	600-900	30	30	-	1
4	Ni-Co/SiO_2 cordierite	600-900	30	30	-	1
5	Ni-Co/CeO_2 cordierite	600-900	30	30	-	1
6	Ni-Co/MgO cordierite	600-900	20	20	-	1
7	Ni-Co/MgO cordierite	600-900	30	30	-	1
8	Ni-Co/MgO cordierite	600-900	20	40	-	1
9	Ni-Co/MgO cordierite	600-900	40	20	-	1
10	Ni-Co/MgO cordierite	600-900	30	30	0.70	1
11	Ni-Co/MgO cordierite	600-900	30	30	1.44	1
12	Ni-Co/MgO cordierite	600-900	30	30	2.10	1
13	Ni-Co/MgO cordierite	750	30	30	-	8
14	Ni-Co/MgO cordierite	800	30	30	-	8
15	Ni-Co/MgO cordierite	750	30	30	0.70	8
17	Ni-Co/MgO cordierite	750	30	30	1.44	8
18	Ni-Co/MgO cordierite	750	30	30	2.10	8
19	Ni-Co/MgO cordierite	750	30	30	2.10	48

3.4.3.3. CDRM Reaction Tests over Ni-based MgO Nanorod Structures. The catalytic performances of Ni bases MgO nanorod structures was tested under the operating conditions as in Table 3.9. In tests, 60 ml/min $^{-1}$ of feed flow balanced with 10 ml min^{-1} of N_2 as an internal gas was used with a CH_4/CO_2 ratio of 1. All samples were reduced with H_2 gas of 30 ml min^{-1} at 800 °C for 1 h as in Figure 3.13. NiCo labeled catalyst in Table 3.9 represents

the 8% wt. Ni-2% wt.% Co active metal amount while Ni means 8% wt. Ni content over MgO support.

Table 3.8. Experimental conditions used in CDRM over $Ni_xCo_{3-X}O_4$ coated monolith catalysts

Exp. #	**Catalyst**	**$T_{reduction}$ (°C)**	**T (°C)**	**Feed Compositions (ml/min)**			**TOS (h)**
				CO_2	**CH_4**	**O_2**	
1	$Ni_{0.5}Co_{2.5}O_4$	-	600-900	30	30	-	1
2	$Ni_{0.5}Co_{2.5}O_4$	600	600-900	30	30	-	1
3	$Ni_{0.5}Co_{2.5}O_4$	800	600-900	30	30	-	1
4	$Ni_2Co_1O_4$	600	600-900	30	30	-	1
5	Co_3O_4	600	600-900	30	30	-	1
6	$Ni_{0.5}Co_{2.5}O_4$	600	750	30	30	-	8
7	$Ni_2Co_1O_4$	600	750	30	30	-	8
8	$Ni_2Co_1O_4$	-	750	30	30	-	8
9	Co_3O_4	600	750	30	30	-	8
10	$Ni_{0.5}Co_{2.5}O_4$	600	750	30	30	2.1	8
11	$Ni_2Co_1O_4$	-	750	30	30	2.1	16
12	%1 Pd added $Ni_2Co_1O_4$	600	600-900	30	30	-	8

3.4.3.3. CDRM Reaction Tests over Ni-based MgO Nanorod Structures. The catalytic performances of Ni bases MgO nanorod structures was tested under the operating conditions as in Table 3.9. In tests, 60 ml/min $^{-1}$ of feed flow balanced with 10 ml min^{-1} of N_2 as an internal gas was used with a CH_4/CO_2 ratio of 1. All samples were reduced with H_2 gas of 30 ml min^{-1} at 800 °C for 1 h as in Figure 3.13. NiCo labeled catalyst in Table 3.9 represents the 8% wt. Ni-%2wt.%Co active metal amount while Ni means 8% wt. Ni content over MgO support.

Table 3.9. Experimental conditions used in CDRM over Ni-based MgO nanorod structures.

Exp. #	**Catalysts as to metal addition method over MgO**	**$T_{MgO,calcination}$ (°C)**	**W_{gcat} (mg)**	**T (°C)**	**TOS (h)**
1	NiCo impregnated	600 °C in oven	50	600-900	1
2	NiCo impregnated	600 °C in air	50	600-900	1
3	NiCo co-prepared	-	50	600-900	1
4	NiCo impregnated	600 °C in oven	20	600-900	1
5	NiCo impregnated	600 °C in oven	100	600-900	1
6	Ni impregnated	600 °C in oven	50	600-900	1
7	NiCo impregnated	600 °C in oven	50	750	8
8	Ni impregnated	600 °C in oven	50	750	8
9	NiCo impregnated monolith	600 °C, pre-calcined	50	600-900	1
10	NiCo impregnated monolith	600 °C, after coating	50	600-900	1

4. RESULTS AND DISCUSSION

As mentioned in Section 2.3, Ni-based catalysts for CDRM process have been widely studied due to its low cost and high activity. However, the studies have been still in progress to overcome the industrial utilization problems such as lack of stability. In this aspect, the aim of this study is to obtain an efficient CDRM process over Ni-based structured catalysts with less energy consumption, low coke formation, optimum syngas ratio as well as high stability. The steps taken in this work for this purpose are as follows:

- CDRM process over Ni-based particulate catalyst was first investigated in the presence of photocatalytic assistance for the expectancy of decreasing CDRM thermal energy demand.
- Afterwards, CDRM was performed over Ni-based wash-coated monoliths comparing with particulate catalyst to seek out whether monolithic structures will improve the catalytic activity of Ni-based catalysts or not.
- In further step, Ni-based structures as in the form of $Ni_xCo_{3-x}O_4$ nanowires were for the first time studied in CO_2 reforming of methane to observe their catalytic contributions to CDRM.
- Then, Ni-based active metals over MgO nanorod structure were studied to evaluate their catalytic performance in CDRM.
- Finally, thermodynamic analysis was conducted in the presence of carbon to evaluate the thermodynamic consistency of experimental results.

Prior to representing the results of these investigations, a blank test and some preliminary findings will be given to clarify the effect of catalyst utilized in the experiments.

4.1. Results of Preliminary Studies

First of all, some blank tests were performed in empty quartz reactor and over an uncoated but reduced cordierite monolith in quartz reactor at various temperature form room temperature to 900 °C with 50 °C temperature interval, and at a total flow of 60 ml min^{-1}

reactant (CH_4/CO_2:1/1) also containing 10 ml min^{-1} N_2 as internal standard. After 800 °C, negligible amounts of CH_4 and CO_2 conversions as well as trace amount of H_2 and CO product (seen only at 900 °C) have been obtained; they can be disregarded considering the level products obtained in the presence of catalyst. As the result, either quartz reactor or uncoated monolith itself has not any significant impact on catalytic performance of CDRM.

Afterward, some catalytic tests were performed to check the experimental system constructed. For this aim, %8 wt. Ni- %2 wt. Co over MgO particulate catalyst was chosen as reference since it was previously tested and stated as well working catalyst by the Huo *et al.* (2014). Furthermore, the addition of Co metal to Ni catalyst was suggested to reduce coke formation with reasonable activity by enabling the oxidation of surface carbon to CO or CO_2 according to several studies (Gao *et al.*, 2017; Son *et al.*, 2014b; Zhang *et al.*, 2008). Also, MgO was a preferable basic support to increase CO_2 activation ability and hence suppress coke formation (Asencios *et al.*, 2011; Monroy *et al.*, 2012; Titus *et al.*, 2016). For catalytic test, 100 mg catalyst was examined at 800 °C under the flow of $CH_4/CO_2/N_2$: 30/30/10 ml/min. The results shown in Figure 4.1 was quite coherent with those obtained in reference study. It led to 84% CH_4 conversion, 90% CO_2 conversion and high H_2/CO ratio 0.94, which means that the constructed system works quite well. this test also show that the catalyst has indeed a good catalytic activity in CDRM. Therefore, the metal loadings of catalyst were fixed to 8wt.% Ni and 2wt.% Co in the remain parts of this study.

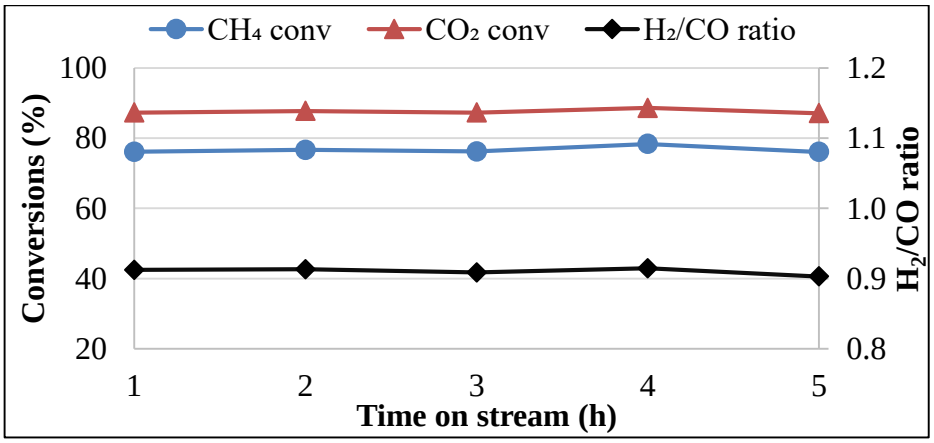

Figure 4.1. Activity results of 8wt.%Ni-2wt%Co/MgO particulate catalyst.

4.2. Performance Analysis of Photocatalytic Assisted CDRM over Ni-based Particulate Structures

One of the main obstacles for the commercialization of CDRM process is high energy demand of the reaction. Therefore, photocatalytic systems can contribute to decrease this demand through the activation of semiconductor supports with light either at room or mild conditions such as 300-500 °C.

8wt.%Ni- 2wt.%Co over various semiconductor supports such as TiO_2 and ZnO as well as MgO support were first tested with 30 ml/min total flow of $CH_4/CO_2/N_2$: 1/1/1 from various temperatures form room to 500 °C to understand the catalyst beaviors in the absence of any photocatalytic enchancement. The results were as in Figure 4.2.

The catalytic activity of the catalysts increased with the increased temperature as it was excepted since CDRM is an endothermic reaction. A temperature such 300 °C was insufficient to convert CH_4 and CO_2 into synthesis gas at all. Among these catalysts, 8wt.%Ni-2wt.%Co over TiO_2 gave way to better catalytic activity than 8wt.%Ni-2wt.%Co over MgO, which was better than 8wt.%Ni-2wt.%Co over ZnO particulate catalyst. The results for the catalytic experiments performed below 300 °C did not shown on the graph since there was not any catalytic conversions or products.

In order to investigate the effect of photocatalytic assistance in CDRM, same experiments over Ni-based particulate structures were conducted in the presence of photocatalytic lights with various power. The findings can be summarized as follows:

- Although TiO_2 and ZnO are known to be efficient semiconductors in photocatalytic activities, there was no improvement in the activity tests performed at temperatures from room to 500 °C. Probably they could not achieve to work as a photocatalyst and be insufficient to meet the necessary conditions for CDRM reaction at mild temperatures.
- Even if the irradiation time over catalyst was lasted for 8 h in some cases; no remarkable catalytic activity change was observed.

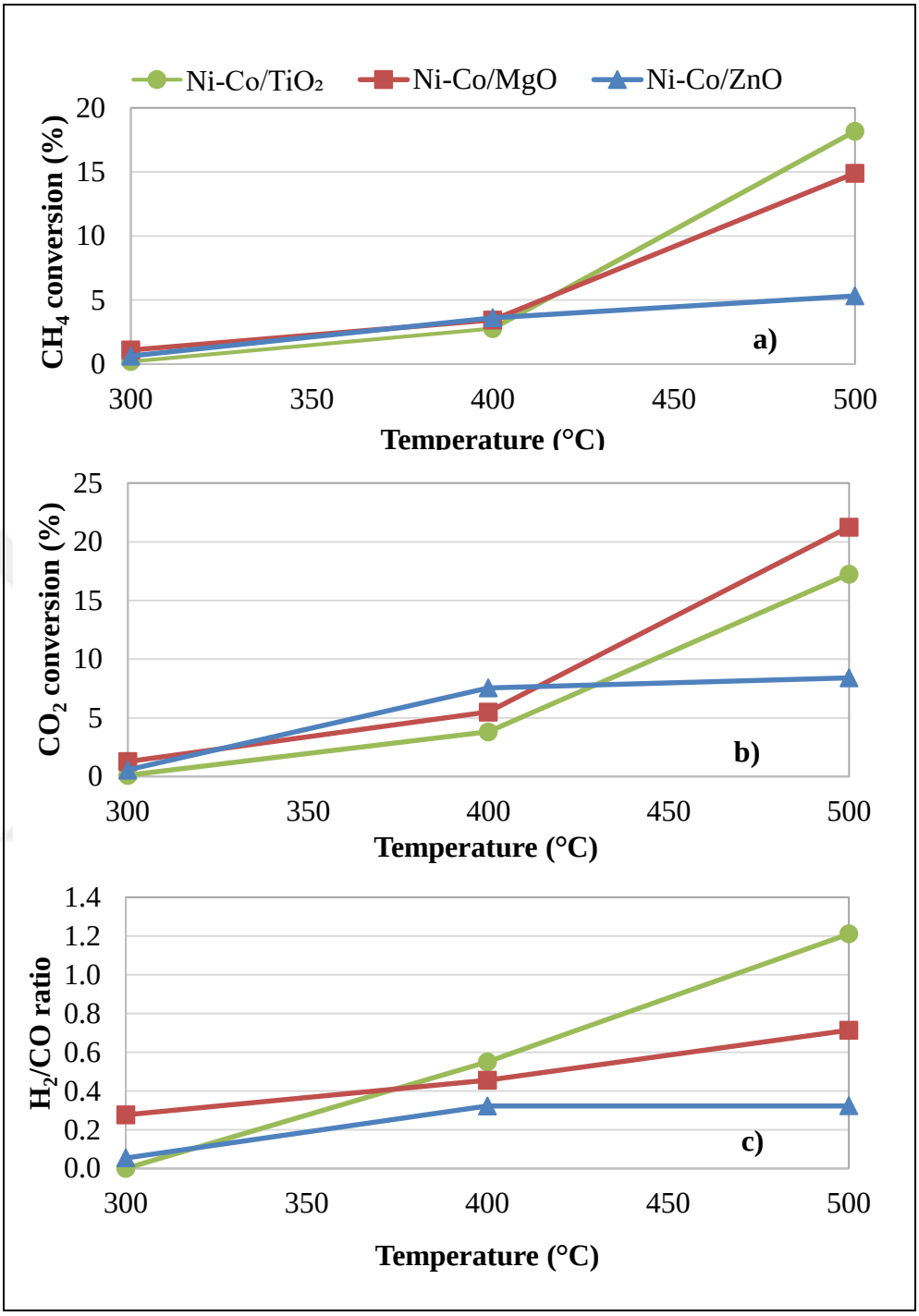

Figure 4.2. Activity results of 8wt.%Ni-2wt.%Co over TiO_2, MgO, and ZnO particulate catalysts: a) CH_4 conversion, b) CO_2 conversion, c) H_2/CO ratio.

- In order to increase the light sensitivity of TiO_2 photo catalyst in photocatalytic assisted CDRM, dye material (cis, bis ((isothiocyanato) bis (2,2-bipyridyl-4,4-dicarboxylato) ruthenium (II)) added Ni-Co/TiO_2 and $CH_3NH_3PbI_xCl_{3-x}$ perovskite,

which is known to be a good sensitized in photovoltaic cells, over TiO_2 were tested at the previous experimental conditions for 8 h as well. Unfortunately, dye addition or perovskite structures did not modify the photocatalytic activity of TiO_2.

- In contrast to the most of the studies in literature, neither the utilization visible light or UV used in this study made any contribution on the CDRM performance.

To sum up, the developed photocatalytic system and modified photo catalysts did not work properly as expected. Operating conditions such as working under continuous flow while some photocatalytic experiments in the literature were performed in batch system may be one of the reasons. Also, the distance between the photo reactor and light source which is larger than 20 cm due to the nature of constructed system may lead an adequate condensed light reaching to catalyst surface as well as less contact time of the light with catalyst surface. Finally, light sensitivity of developed catalyst may not be sufficient to break and convert the highly stable CH_4 and CO_2 gases. Therefore, the system and catalyst should be improved with further investigations.

4.3. CDRM Performance Analysis of Ni-based Particulate and Monolithic Structures

Most of the CDRM studies in the literature were conducted in a fixed bed reactor with the particulate form of the catalyst while there were also a few studies performed over the monolith structures although they offer several superiorities against the packed bed reactors such as low pressure drop (thus low energy loss), higher mechanical strength and easier to be scaled up by just regulating the number of channels (Ciambelli *et al*., 2010; Giroux *et al*., 2005; Heck *et al*., 2001; Özyönüm and Yildirim, 2016; Ryu *et al*., 2007; Qui *et al*., 2012). In this part of the study, CDRM performance tests of 8wt.%Ni-2wt.%Co based MgO wash-coated mullite and cordierite monolithic structures were tested and compared to particulate form at various temperatures. Besides to the effect of the monolith type and temperature, the impacts of various support types, CH_4/CO_2 feed ratios, gas hourly space velocity (GHSV) and low amount of additional oxygen gas on the catalytic performance of monoliths were investigated to understand the catalytic behavior of monoliths in CDRM. The results were better clarified through performed SEM-EDX, XRD and XPS analysis.

4.3.1. Effect of Temperature

8wt.% Ni- 2wt.% Co over MgO particulate catalyst were tested at various temperatures from 600 °C to 900 °C with a 50 °C temperature increment under the flow of 60 ml/min reactant gas mixture (CH_4/CO_2:1/1) with 10 ml/min N_2 internal standard. The catalytic activity results of 8wt.% Ni- 2wt.% Co over MgO particulate, cordierite and monolith catalyst can be seen in Figure 4.3. The reaction test with particulate catalyst verified its high performance reaching to 70% CH_4 conversion, 80% CO_2 conversion and a H_2/CO ratio of 0.89 at 750 °C; these values were increased further with increasing temperature. This performance improved further with the use of cordierite and mullite monolithic structures especially at low temperatures (equivalent to about 50 °C reduction in reaction temperature); at higher temperatures, both CH_4 and CO_2 conversions were nearly the same probably due to the fact that they approached to equilibrium conversion while H_2/CO ratio was approaching to unity.

The higher performance of the monolithic catalyst is in agreement with the observations of Soloviev *et al.* (2011) over Nickel-alumina on cordierite honeycomb monolith and of Liu *et al.* (2008) over the Ni catalysts on SiC monolithic. Miguel *et al.* (2012) found that monolithic Ni/MgO catalyst also showed higher stability and higher conversion than particulate catalyst for steam reforming of methane process. This was probably due to the fact that monolithic form enhanced the heat transfer (Heck *et al.*, 2001). Luisetto *et al.* (2017) has also found that CH_4 and CO_2 conversions of Ni-Ru cordierite monolith were higher as against powdered catalysts. In our case, the advantage of monolithic catalyst seems to diminish at high temperature as far as the CH_4 and CO_2 conversions are concerned; however, it should be still more desirable due to the other properties as easy to scale up and low pressure drop.

Especially, for Ni-based catalysts, which have a tendency of pressure drop by plugging the reactor, the monolithic structure can be a good option. In addition, monolithic structures may helpful to increase the contact time of reactant gases with MgO support surfaces which has lower surface area then other proper supports such as Al_2O_3 (Abdollahifar *et al.*, 2014, Zhang *et al.*, 2014). The application of MgO over monolithic structures may be enhanced its role in CDRM and may give way to an increase in the catalytic activity. Furthermore, the

enhanced catalytic activity of cordierite monoliths may be related that it has higher number of the channels comparing to mullite type monoliths; namely it can provide higher coated surface area.

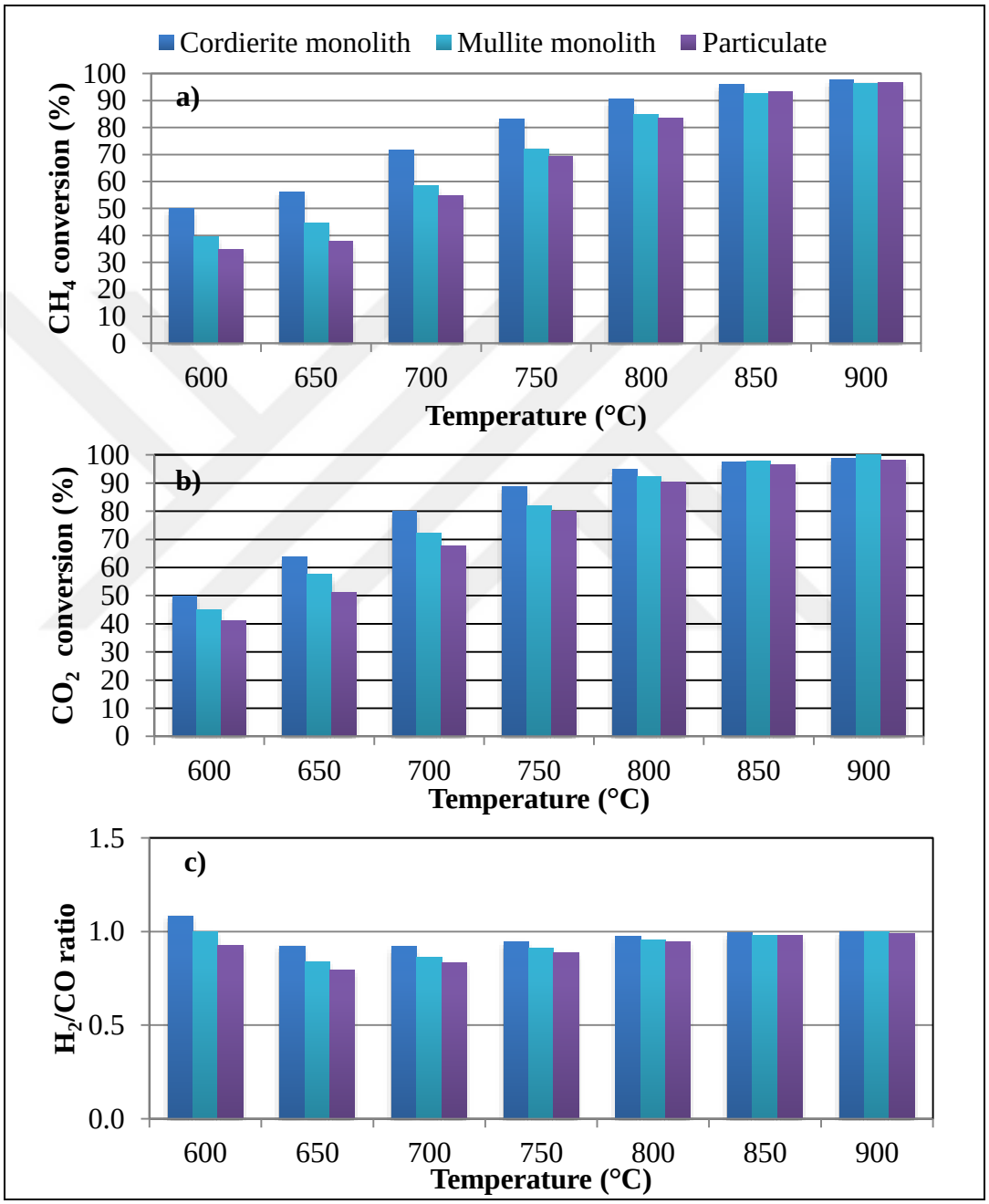

Figure 4.3. Activity results of 8wt.%Ni-2wt%Co/MgO catalyst in the form of particulate, coated over cordierite and mullite monolith: a) CH_4 conversion, b) CO_2 conversion, c) H_2/CO ratio.

Since the cordierite catalyst monolith has better performance, of which reasons are not clear at this stage (possibly due to the more suitable heat transfer properties or narrower channel wide), 8wt.%Ni-2wt.%Co metals over MgO coated cordierite monolith was used in the remaining part of the study.

4.3.2. Effect of Support Type

The coating material in monolithic structures has known to be a significant parameter which affects the catalytic activity of structures. In order to investigate this effect wash-coated various supports such as CeO_2, SiO_2 and MgO over cordierite monolith, 8wt.%Ni-2wt.%Co based MgO, CeO_2 and SiO_2 coated monoliths was tested at a temperature change from 600 °C to 900 °C with a 70 ml/min reactant gas mixture (CH_4/CO_2:1/1, 10 ml/min N_2 internal).

Among tested these monolithic structures, MgO supported Ni-Co based catalyst resulted in higher CH_4 and CO_2 conversions than CeO_2, and SiO_2 ones as in Figure 4.4. In terms of H_2/CO ratio, after 800 °C, CeO_2 and MgO supported catalyst similar ratio but still lower than the MgO has. It was obvious that the interaction between colloidal CeO_2 with the active metals were poor and CeO_2 supported catalyst did not successfully work as in the colloidal form over monolith although the particulate form of Ni-Co/CeO_2 catalyst was previously suggested a highly active catalyst for CDRM in literature (Ay and Üner, 2015). The performance test of monolith prepared with colloidal SiO_2 seemed to be slightly better; it gave an over 60% conversion for CH_4 and 60% conversion for CO_2 with a H_2/CO ratio of 0.8 at 750 °C; however, it was still behind the catalytic performance of MgO coated monoliths, which was compatible with in some studies resulting higher catalytic activity over MgO support then SiO_2 catalysts in the literature. At 900 °C, all coated monoliths nearly gave way to the same performance.

Among these catalysts, Ni-Co/MgO monolithic catalyst was found to be the most active alternative. Therefore, the next performance test was conducted over this monolithic structure. Prior to main tests, some time on stream (TOS) test results was performed at 750 °C and 800 °C for 8h in order to check its stability. As to Figure 4.5, during these

temperatures both CH_4 and CO_2 conversion were highly stable and the ratio of H_2/CO was 0.94 and 0.97, respectively.

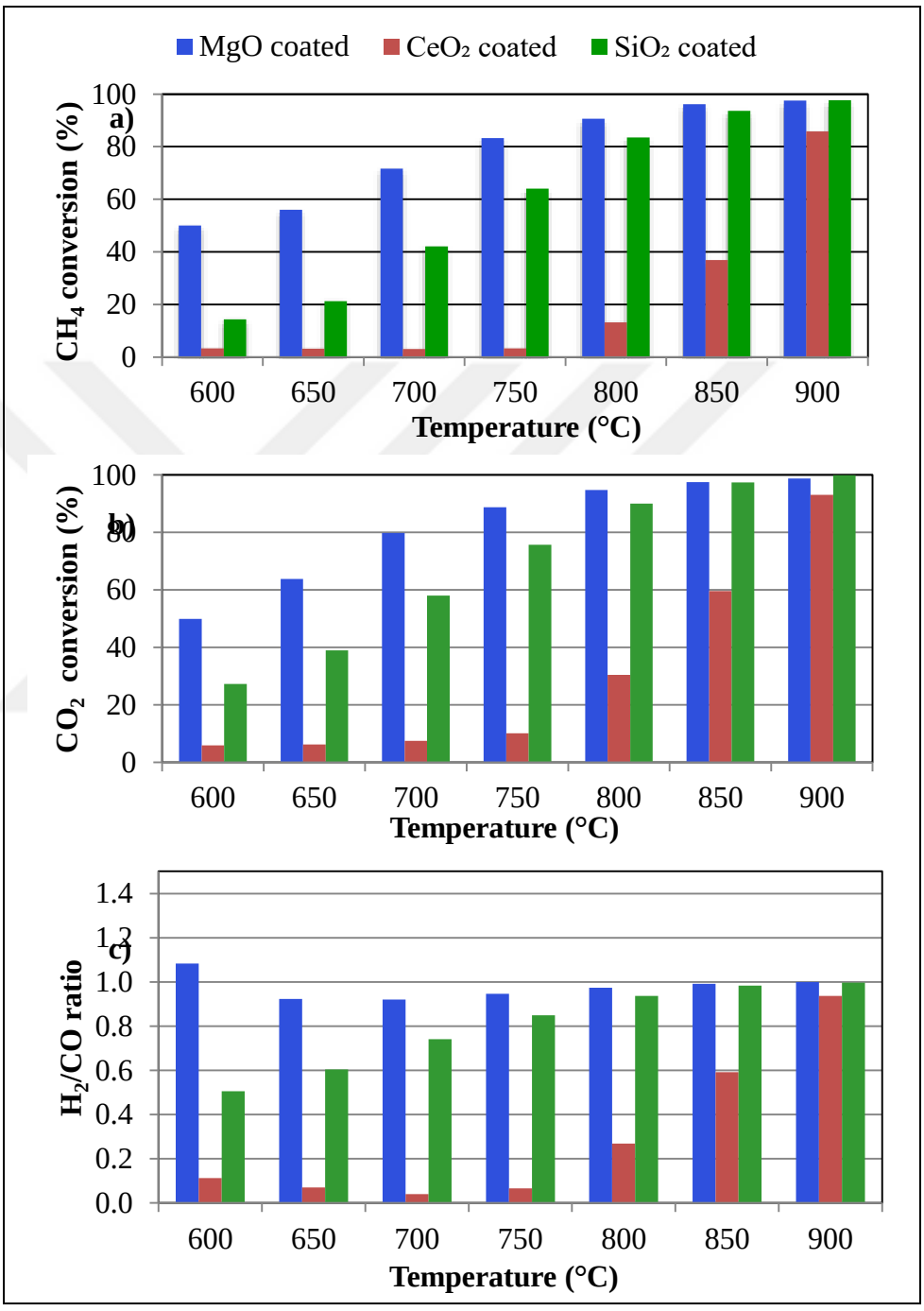

Figure 4.4. Activity results of 8wt.%Ni-2wt.%Co based MgO, CeO_2 and SiO_2 coated monoliths: a) CH_4 conversion, b) CO_2 conversion, c) H_2/CO ratio.

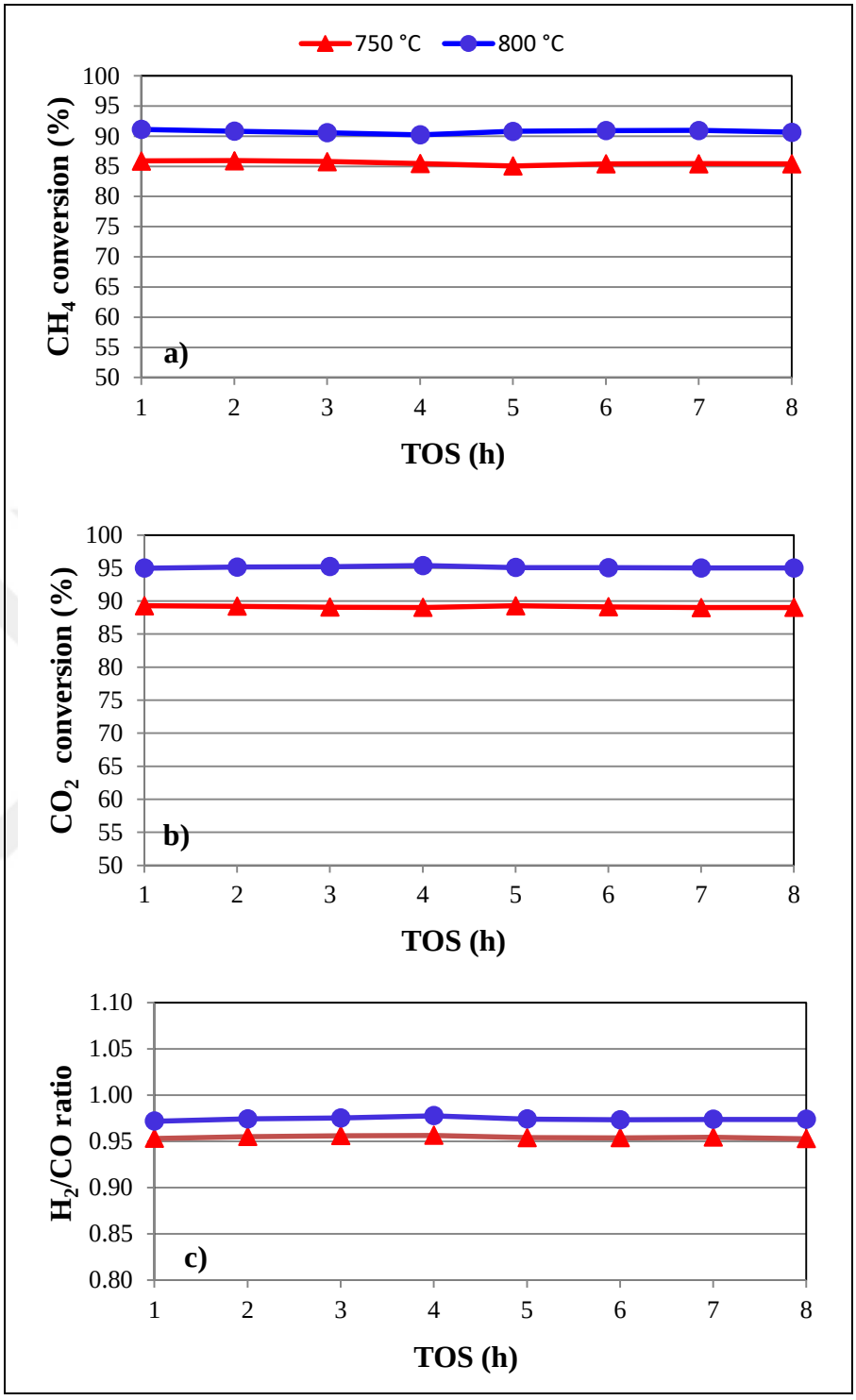

Figure 4.5. TOS results of 8wt.%Ni-2wt.%Co based MgO coated monoliths for 8 h: a) CH_4 conversion, b) CO_2 conversion, c) H_2/CO ratio.

This test also indicated that making 50 °C temperature interval test from 600 °C to 900 °C or working on only one temperature condition did not affect the activity performance of the catalysts. For example, CH_4 conversion was 90.65% in former case at 800 °C, while 90.83% was second case. At 750 °C, the change was approximately 3%.

4.3.3. Effect of Gas Hourly Space Velocity (GHSV)

The effect of gas hourly space velocity (GHSV) was also tested to make sure that the performance is not due to the excess use of catalyst. Figure 4.6 shows the results obtained at 18000, 30000, 42000 $mlg_{cat}^{-1}h^{-1}$ (calculated based on the weight of Ni-Co/MgO content excluding the mass of monolith); these values reasonable represent the ranges reported in the literature by various investigators. CH_4 and CO_2 conversions were slightly higher at 18000 $mlg_{cat}^{-1}h^{-1}$ at low temperatures as expected (high contact time of the reactant gases with monolith surfaces) but the difference disappeared at high temperatures; H_2/CO ratio was not affected by this change at all. In addition, this results also proved that monolithic structures can be capable of working at higher reactant flow rates with low activity lost.

4.3.4. Effect of CH_4/CO_2 Ratio

Since the resulting syngas ratio of dry reforming of methane play a crucial role in the Fisher-Tropsh synthesis and mainly depend on the feed gas ratio (Frontera *et al*., 2013), CH_4/CO_2 is an important variable that should be investigated. When the ratio of CH_4/CO_2 was changed from 0.5 to 1.5, CH_4 conversion decreased while the CO_2 conversion increased (Figure 4.7) as expected. At the ratio of 0.5, CO_2 became the limited reactant and consumed 100% at high temperatures while CH_4 conversion become significantly lower; it was just opposite at the CH_4/CO_2 of 1.5 (CH_4 consumed fully at high temperatures).

The CH_4/CO_2 ratio of 1.0 seems to be the best considering that it leads to high conversion for both reactants and H_2/CO ratio close to unity; this is an expected and desirable result, which was also reported by other investigators (Abdollahifar *et al*. 2016; Du *et al*., 2013).

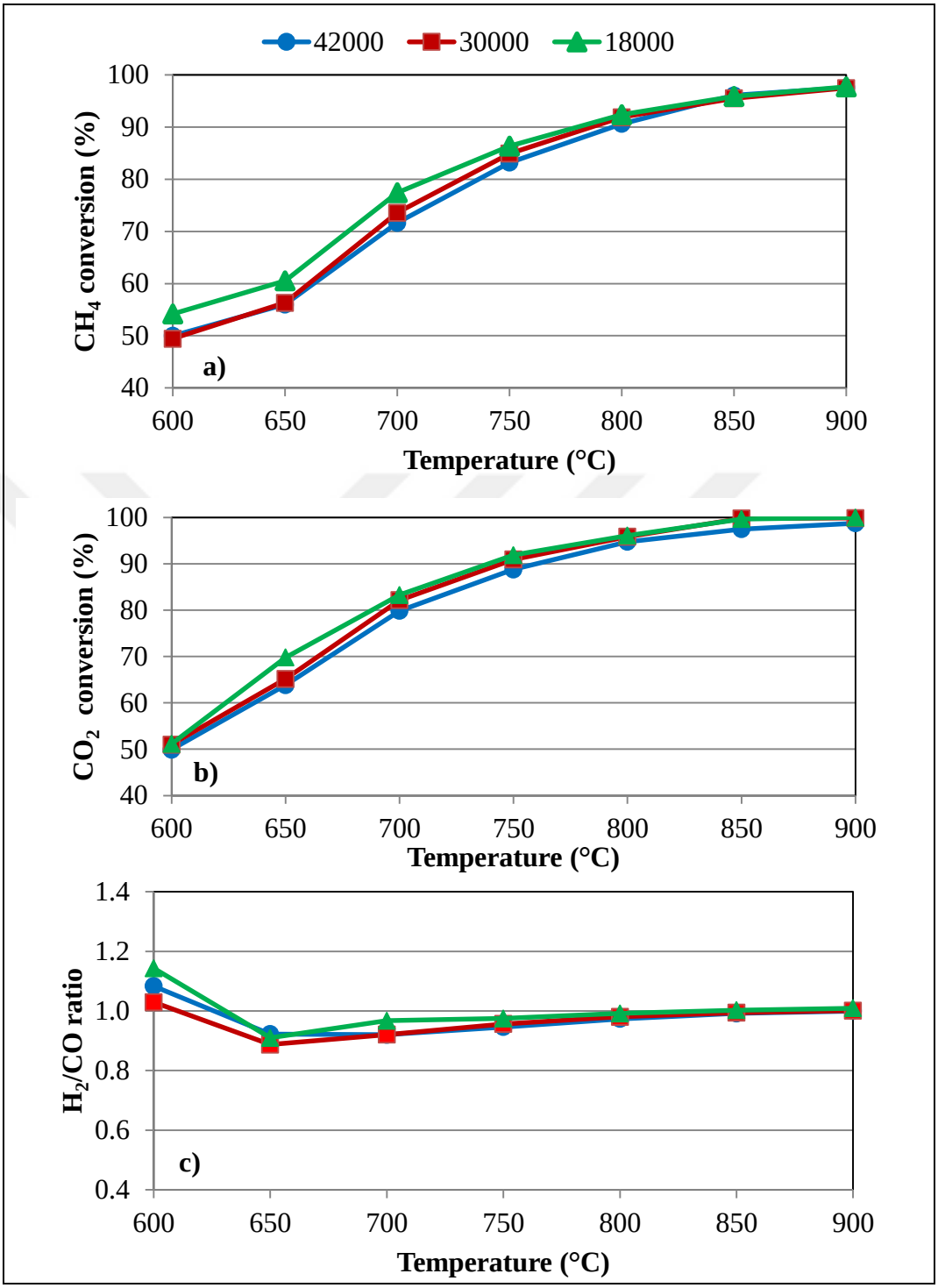

Figure 4.6. Activity results at various GHSV($mlg_{cat}^{-1}h^{-1}$) over 8wt.%Ni-2wt.%Co/MgO monolithic catalyst when CH_4/O_2 is 1: a) CH_4 conversion, b) CO_2 conversion, c) H_2/CO ratio.

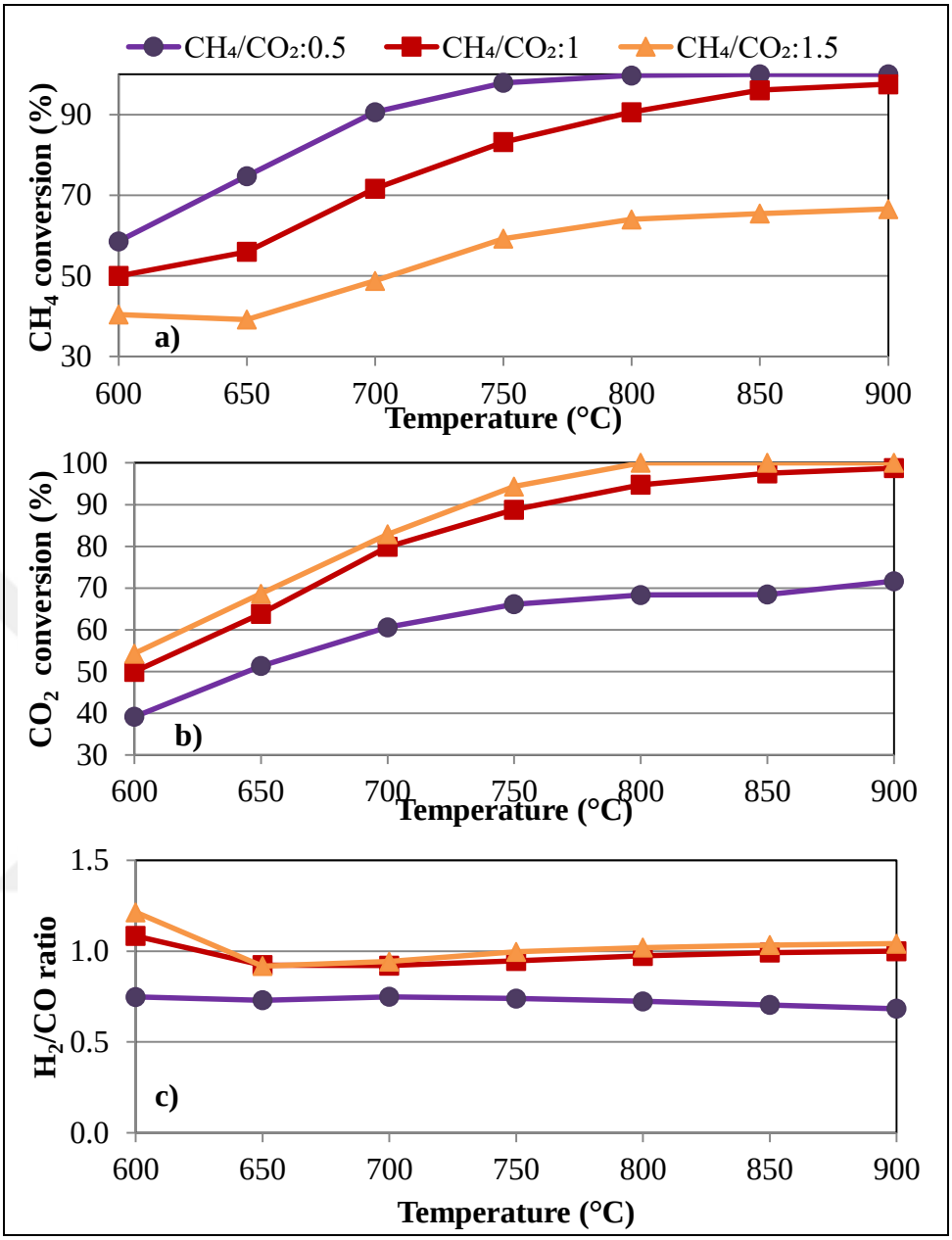

Figure 4.7. Activity results at various CH_4/CO_2 ratio over 8wt.%Ni-2wt.%Co/MgO monolithic catalysts when GHSV is 42000 $ml g_{cat}^{-1} h^{-1}$: a) CH_4 conversion, b) CO_2 conversion, c) H_2/CO ratio.

4.3.5. SEM- EDX Test of Ni-Co/MgO Coating over Monolith

In order to examine whether MgO wash-coating procedure and dispersion of active metals over monolithic structures were successful or not, SEM-EDX analysis was conducted

on fresh wash-coated monolithic catalysts. The SEM images of 8wt.%Ni-2wt.%Co over MgO coated monolithic structures are given in Figure 4.8.

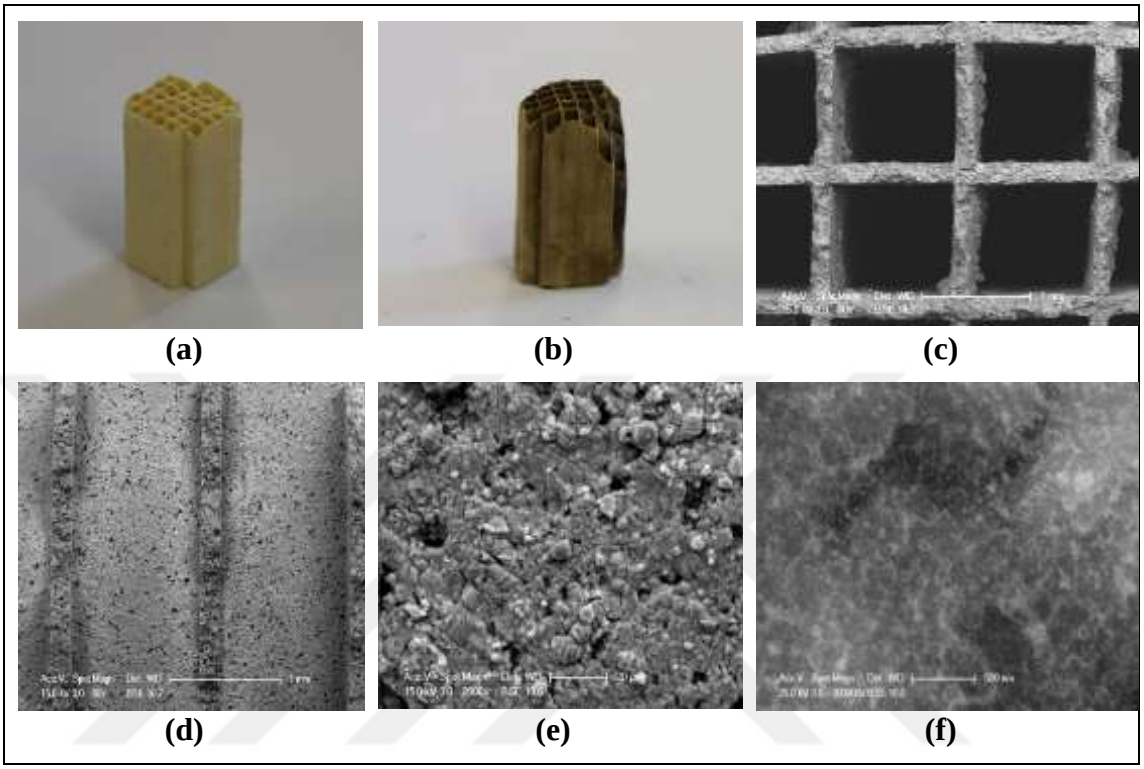

Figure 4.8. Images of (a) bare monolith, fresh-reduced Ni-Co/MgO coated monolith (b) and SEM images of coated monolith; (c) (80x), (d) (90x), (e) (2000x) and (f) 100000x.

The support was seemed to be uniformly coated on the monolithic structure as a thin film as it apparent from the comparison of images of bare (Figure 4.8a) and coated (Figure 4.8b) monolithic pieces and from the cross-sectional (Figure 4.8c) and lateral (Figure 4.8d-e) SEM images of coated catalyst although cross-sectional images (c) also show some local accumulations (especially in corners) probably stemmed from the support wash-coating procedure. In the image with 2000x (Figure 4.8e), it is clearly seen that monolith is coated well with the catalyst. Dark points these images mean natural pore structure of the monoliths, while the white balls signify the coated MgO support. Also, from the images, it is not easy to distinguish Ni and Co active metals; however, the white bands in Figure 4.8f are thought to be Ni clusters. The average value of EDX analysis of the images taken from three different point in 2000x (Figure 4.8e) with 60 scans was resulted in the Table 4.1 below, which gave good Co and Ni content as 1.88 wt.% and 7.69 wt.%, respectively. That proves that the active

metals are well dispersed on the MgO coated monolith; this is also verified from the EDX elemental mapping images of these elements in Figure 4.9. Al, Si, some Mg and O metals were seen in the analysis probably due to the monolith itself, which consists of $2MgO.2Al_2O_3.5SiO_2$.

Table 4.1. The average value of EDX analysis taken in 2000x.

Element	Avg. Wt.%	Avg. At%
C	2.61	4.96
O	29.07	41.36
Mg	14.08	13.21
Al	18.63	15.74
Si	25.52	20.70
Ca	0.51	0.29
Co	1.88	0.73
Ni	7.69	3.00
Total	100.00	100.00

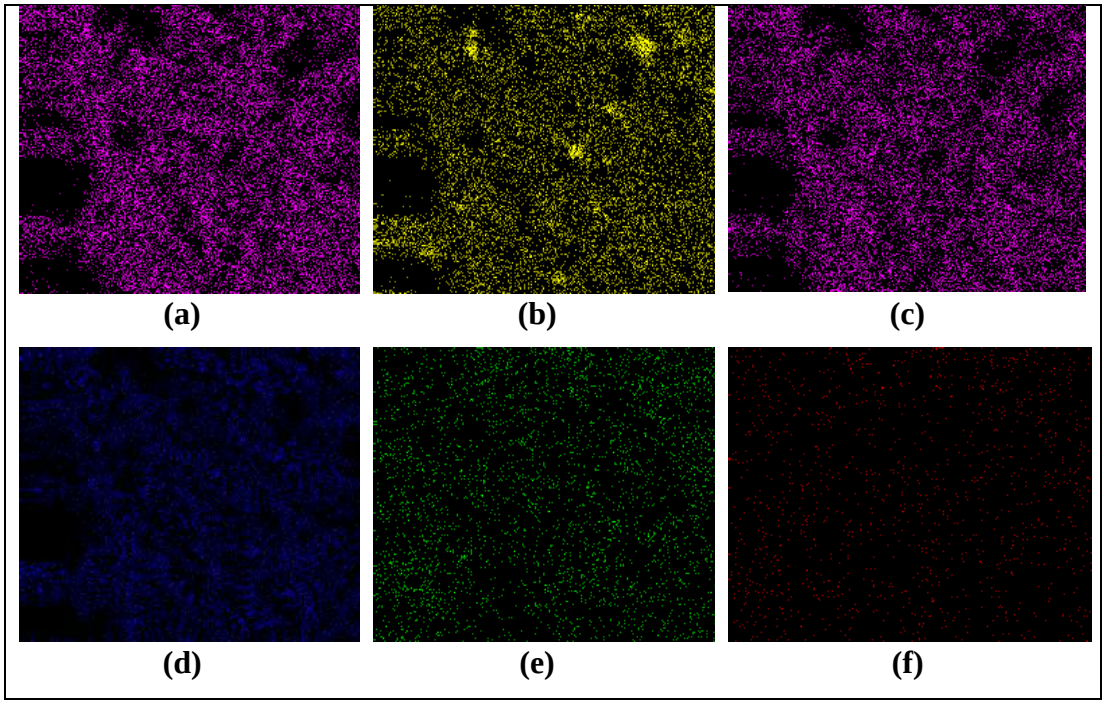

Figure 4.9. EDX elemental mapping of fresh-reduced Ni-Co/MgO sample: (a) Si, (b) Mg, (c) Al, (d) O, (e) Ni and (f) Co.

4.3.6. Coke Formation and Effect of O_2 Addition to the Feed

It is well known that Ni-based catalysts suffer from coke deposition weakening the commercial potential of dry reforming of methane process (Damyanova *et al.*, 2012; Huo *et al.*, 2014). Ni-Co/MgO coated monolithic catalysts used at 750 °C for 8h with a CH_4/CO_2 ratio of 1 and at 42000 $mlg_{cat}^{-1}h^{-1}$ GHSV was characterized for coke formation (Figure 4.10).

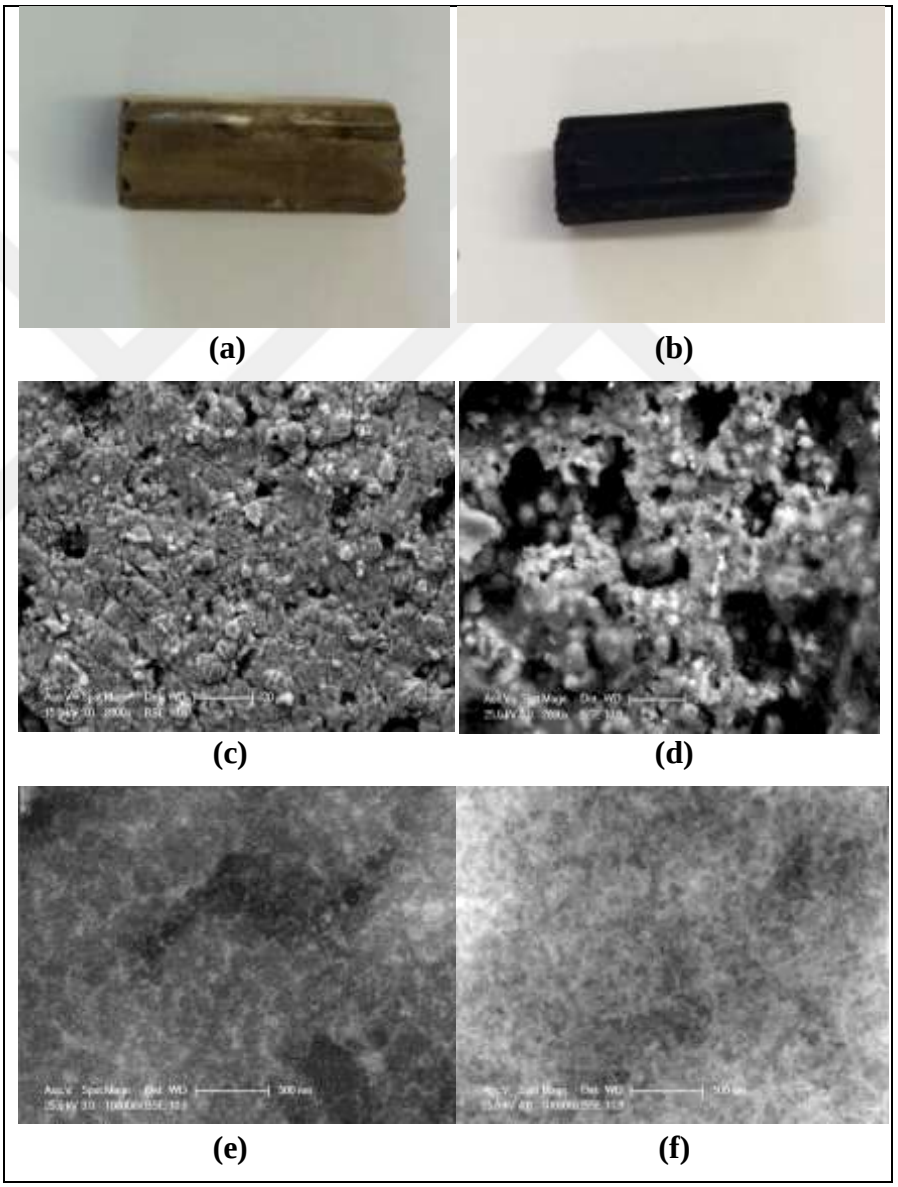

Figure 4.10. Images of the fresh-reduced (a) and spent (b) monolithic Ni-Co/MgO catalysts and SEM Micrographs reduced-fresh (b) 2000x, (b)100000x and spent catalysts (e) 2000x, (f)100000x.

The common argument was also true in this work; as it can be seen from Figure 4.10b the coke deposition over the monolithic piece was apparent from the color of used monolithic piece compared with the coated but unused monolith presented in Figure 4.10a. The coke deposition was also observable in the internal SEM images of used monolithic catalyst (Figure 4.10d). This carbon formation can also be seen in SEM Micrographs (Figure 4.10f) as white, thin nanotubes. The average value of EDX analysis taken in 2000x also showed that carbon weight percent remarkably increased to 40wt.% as in Table 4.2, while Ni and Co elements decreased.

Table 4.2. The average value of EDX analysis taken in fresh-reduced and spent samples.

Element	**Fresh catalyst, Avg. Wt%**	**Spent Catalyst, Avg. Wt%**
Ni	7.69	4.67
Co	1.88	1.31
C	2.62	41.30

Then we decided to add small amount of oxygen (1-3%) to see whether the coke deposition was successfully depressed without any negative effect on conversion and product distribution. Although there are works in the literature aiming to combine dry reforming with partial oxidation (oxy-CO_2 reforming) (Chen *et al.*, 2011), steam reforming (Danilova *et al*., 2015) or to regenerate the deactivated catalyst with cyclic O_2 addition (Assabumrungrat *et al*., 2009), our aim was to test the possibility of reducing coke formation without fundamentally changing the nature of dry reforming process; hence we kept the oxygen ratio of in the feed as low as possible. The effects of oxygen addition to coke deposition were presented in Figure 4.11. As can be seen from the comparison of Figure 4.11a and Figure 4.11b was well as Figure 4.11c-d, 3% O_2 addition significantly prevented coke deposition; the EDX mapping images for C element in the absence (Figure 4.11e) and presence of 3% oxygen (Figure 4.11f) also verify this result. The color change in monolithic surface was also observed in the presence of 1-2% oxygen but the difference was not as apparent as in the case of 3% indicating that a certain amount of oxygen is needed. EDX elemental mapping other metals such as Ni and Co for used Ni-Co/MgO in the absence and presence of 3% O_2 addition can be seen Appendix A. Even if the average amount of Ni and

Co active metals were decreased after reaction, they were still well dispersed on the monolith and C element was seemed to dispersed on especially over Ni metals.

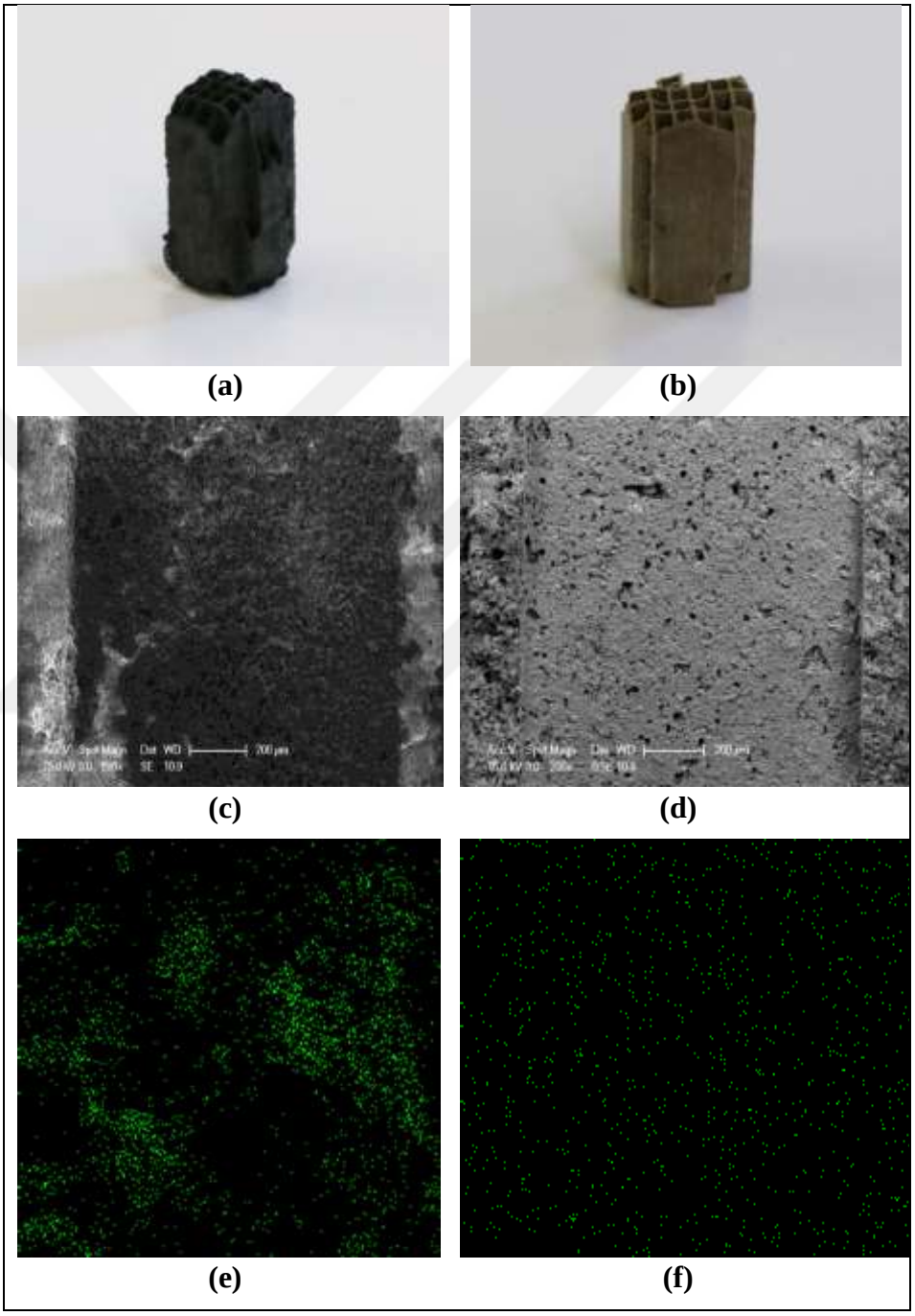

Figure 4.11. Images of spent Ni-Co/MgO coated monoliths without (a), with (b) 3% O_2 and SEM-EDX Images for spent samples without (c), (e) and with (d), (f) 3% O_2.

We also performed XRD analyses for both reduced and used catalyst (in the absence and presence of O_2) in order to understand whether O_2 addition caused any changes in crystalline phases. The XRD patterns of bare monolith, after MgO coating and reduction, after Ni and Co loading, after reaction without O_2 and after reaction with 3% O_2 are given in Figure 12. The possible crystalline phases for these patterns are also added to the Figure 12.

Main peaks at 2θ=10.35, 18, 18.94 21.66, 26.3, 28.38, 29.36, 33.82, 54.22, 69.64° in all samples clearly correspond to the cordierite monolith while peaks at 2θ=42.78, 62.16° are for cubic MgO. Generally, the spectra of used catalyst in the presence of 3% is much closer to the fresh catalyst compared with the spectra of the used catalyst without oxygen; apparently the presence of 3% oxygen did not change the crystalline phases of the catalyst, on the contrary it helped the preserve the structure. For three cases, the crystallite size of the MgO peaks at around 2θ=62° was calculated by the Scherrer equation with the measurement of the FWHM (full width at half maximum) of the diffraction peaks. 20.08 nm of crystallite size in the reduced samples increased to 36.09 nm in the reacted samples while it was measured as 19.71 nm over the reacted samples in the presence of 3% oxygen. There may be also NiO and CoO in the catalyst, however it is impossible to be sure because their peaks has close 2θ with MgO, hence they may be overlapping. Huo *et al.* (2014) has stated that diffraction peaks at 2θ=75, 79° indicates the formation of solid solution in the form of either Ni-Mg-O, Co-Mg-O or their composites. We observed such a peak in the spectra of used catalysts (without oxygen); this may be supporting the results of article mentioned above although it is not fully conclusive.

XPS analysis was also conducted to measure the binding energies of the components in the reduced and reacted samples. The detailed Ni 2p and Co 2p scans of fresh-reduced and reacted samples in the presence of 3% oxygen as in Figure 4.13. Unfortunately, the detailed XPS scans of the reacted samples in the absence of oxygen did not clearly obtain since there was huge coke over the samples. As seen in Figure 4.13, both Ni 2p and Co 2p scans have a complex shape having a mixture of core level and satellite features. In the reduced samples (Figure 4.13a-b), BEs at 856.32 eV and 873.99 eV show the Ni $2p_{3/2}$ and Ni $2p_{1/2}$ spin orbit peaks while BEs at 780 eV and 796.71 eV are Co $2p_{3/2}$ and Co $2p_{1/2}$ spin orbit peaks.

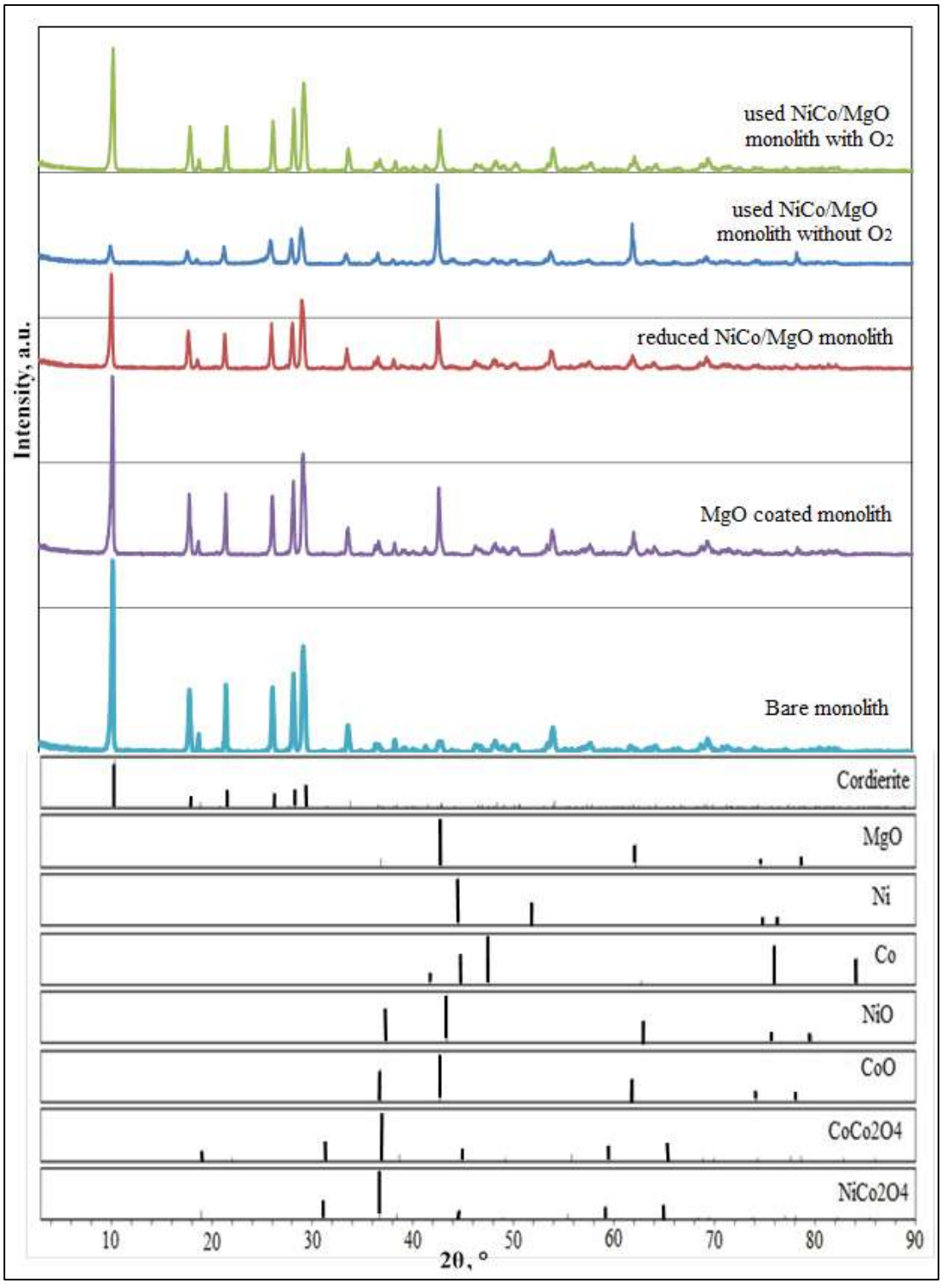

Figure 4.12. The XRD spectra of monolith samples at various conditions.

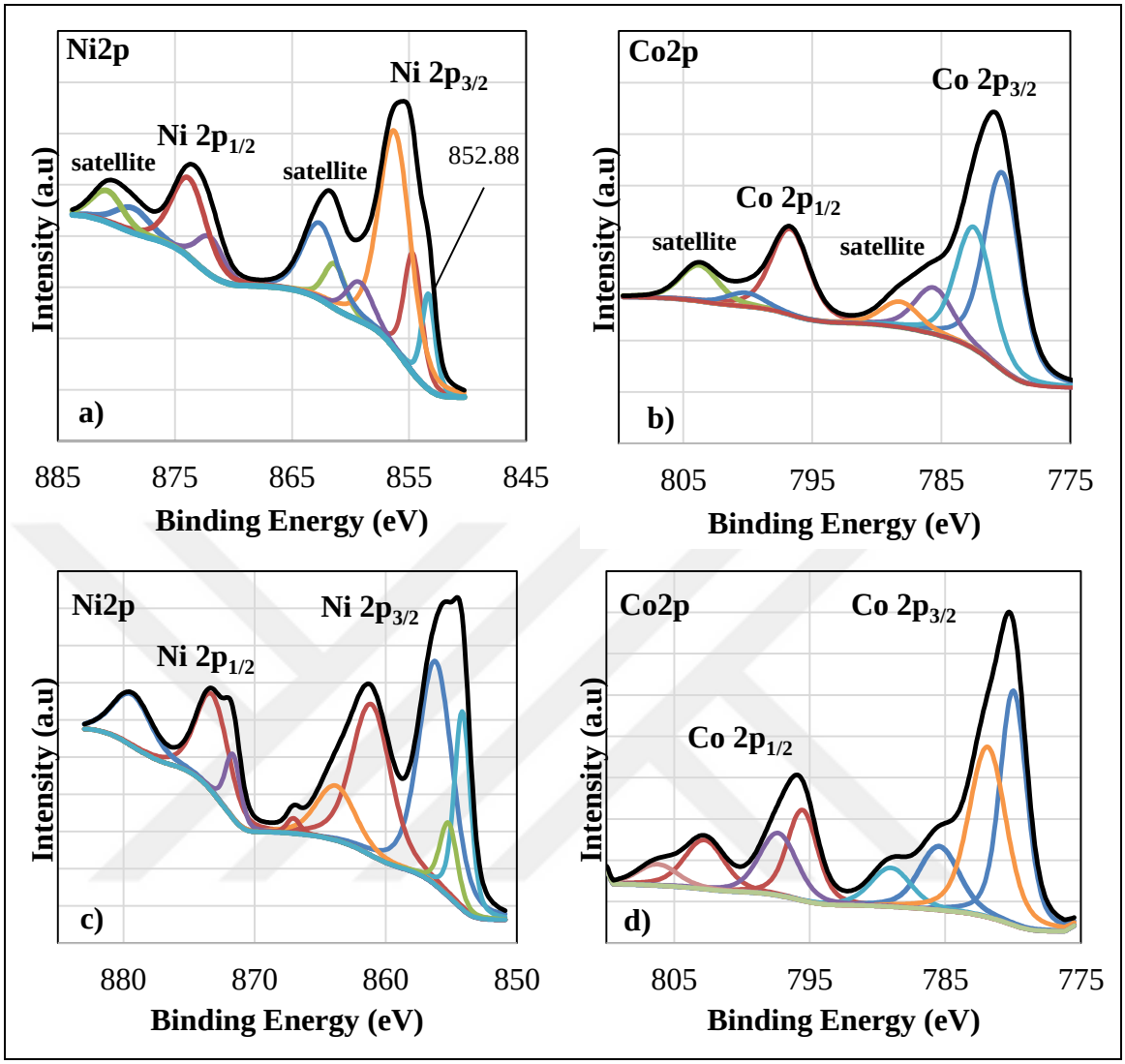

Figure 4.13. XPS scan results of fresh-reduced (a), (b) and spent samples in the presence of3% oxygen (c), (d).

The other peaks as labeled in the Figure 4.13a-b are the satellites of these spin orbits. The peak 856 eV was previously related to oxidized Ni due to the interaction of mixed oxide support, MgO or hydroxyl groups while the one at 853 eV was only accepted as the sign of metallic Ni in the study of Walker *et al.* (2012). Similarly, Xu *et al.* (2013) indicated the peaks at 852.0 eV as the reduction state of Ni and the ones at 855.1 eV as the oxidation states of Ni. The peaks at 855.5 and 852.2 eV in Ni $2p_{3/2}$ spectra were also accepted as the Ni^{+2} and Ni^{0} phases of the nickel respectively while the ones at 780.7 and 777.4 eV in the Co $2p_{3/2}$ spectra were stated as Co^{+2} and Co^{0}, respectively (Zhang *et al.*, 2014). Fan *et al.* (2010), binding energies of Ni^{+2} and Co^{+2} were shifted from 855.4 to 861.8 and from 784 eV to 779.9

eV in the XPS studies of Ni-Co bimetallic catalysts. As it seen in Figure 4.13, both Ni 2p and Co 2p scans were quite changed after the reaction in the presence of oxygen. The changes in Ni 2p scan and Co 2p scans in Figure 4.13c-d can be attributed as the NiO and CoO spectra; showing the oxidation of metals during the reaction.

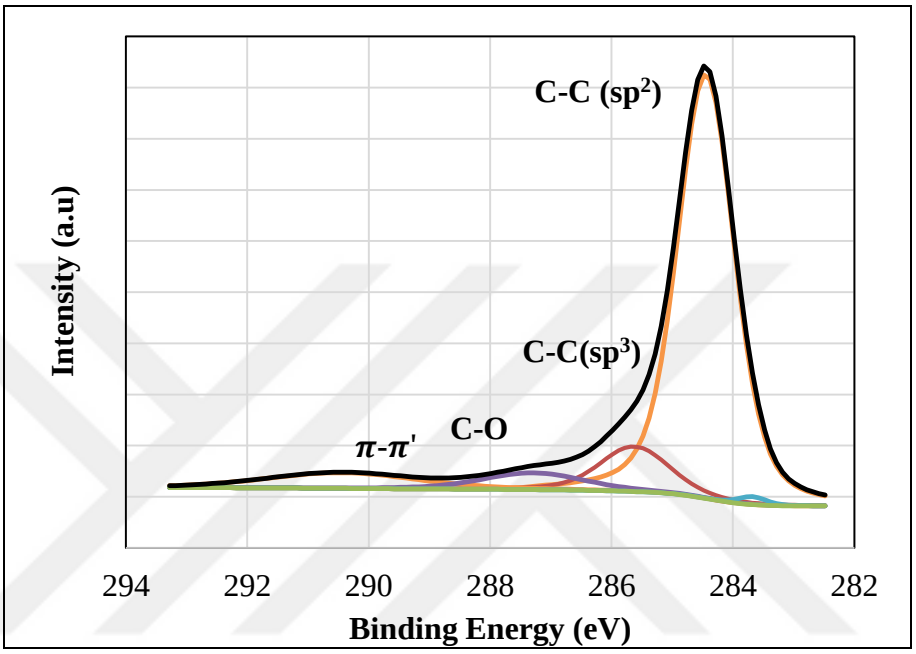

Figure 4.14. C1s XPS spectra of reacted samples in the absence of oxygen.

In order to clarify carbon formed in the reacted samples, C1s XPS spectra was evaluated as in Figure 4.12. The main peaks at 284.38 eV and 285.48 eV were assigned as the sp2 and sp3 hybridized carbon atoms which can be related to the graphitic type of carbon on the catalyst.

4.3.7. Effect of O_2 addition on CDRM Catalytic Activity

The results of performance test in the presence of 1, 2 and 3% oxygen in the feed is given in Figure 4.15; the results without oxygen in the feed was also added for comparison; the effects of oxygen over conversions and H_2/CO ratio was minor. CH_4 conversion was increased a few percent while CO_2 conversion decreased (effects over CO_2 conversion was slightly more than CH_4 conversion); H_2/CO ratio was also increased slightly. The decrease of CO_2 conversion in the presence of oxygen may be due to the fact that O_2 is more reactive than CO_2, and besides it oxidizes coke and CO producing additional CO_2 (Assabumrungrat

et al., 2009). Nikoo and Amin (2011) has also declared that it is thermodynamically possible to avoid carbon formation, and to have a syngas yields of 90% and unity ratio of H_2/CO at a temperature 800 °C and the feed containing 1:1:0.1 ratio of CH_4:CO_2:O_2. O'Connor and Ross (1998) also reported a similar result (O_2 ratio was higher than ours in both studies). These results suggest that the land fill gases as the feedstock in dry reforming of methane could be also used since it has approximately 45–55% CH_4, 30–40% CO_2, 10–15% N_2, 0–5% O_2 as used by Kohn *et al.* (2010).

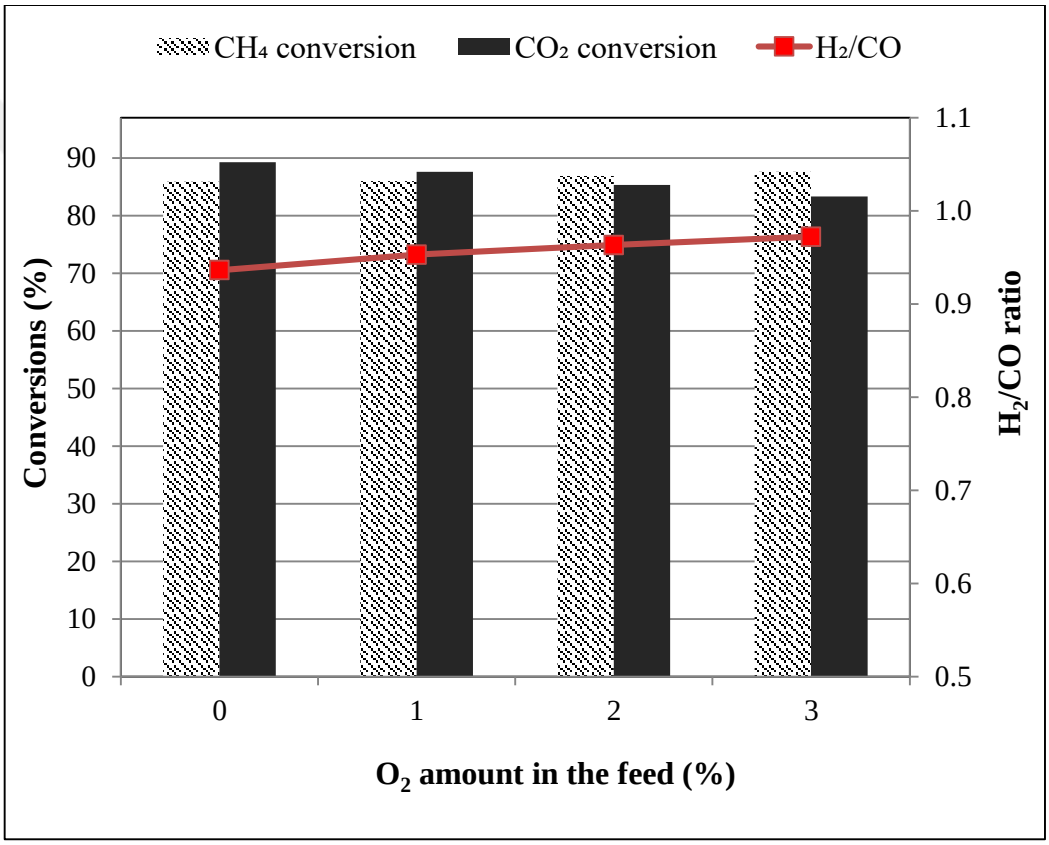

Figure 4.15. Catalytic activity of Ni-Co/MgO cordierite monolithic catalyst in presence of O_2 (0%-3%) at 750 °C under 42000 $mlg_{cat}^{-1}h^{-1}$ GHSV with a CH_4/O_2 ratio of 1.

4.3.8. Stability Test of Ni-based Monolithic Structures on CDRM

The stability tests of the Ni-Co/MgO over cordierite catalyst was also performed for 48 h in the presence of 3% O_2 at 750 °C, the gas hour space velocity (GHSV) of 42000 $mlg_{cat}^{-1}h^{-1}$ and CH_4/CO_2 feed ratio of 1. As in Figure 4.16, the CH_4 conversion, CO_2 conversion

and H_2/CO ratio were almost constant (with some small fluctuation) for 48 hours. This indicates that the catalyst is quite stable. The coke deposition at the end of the test was also lower than that observed in the absence of oxygen (even in much shorter times on stream); however, it was still exist requiring some additional precautions.

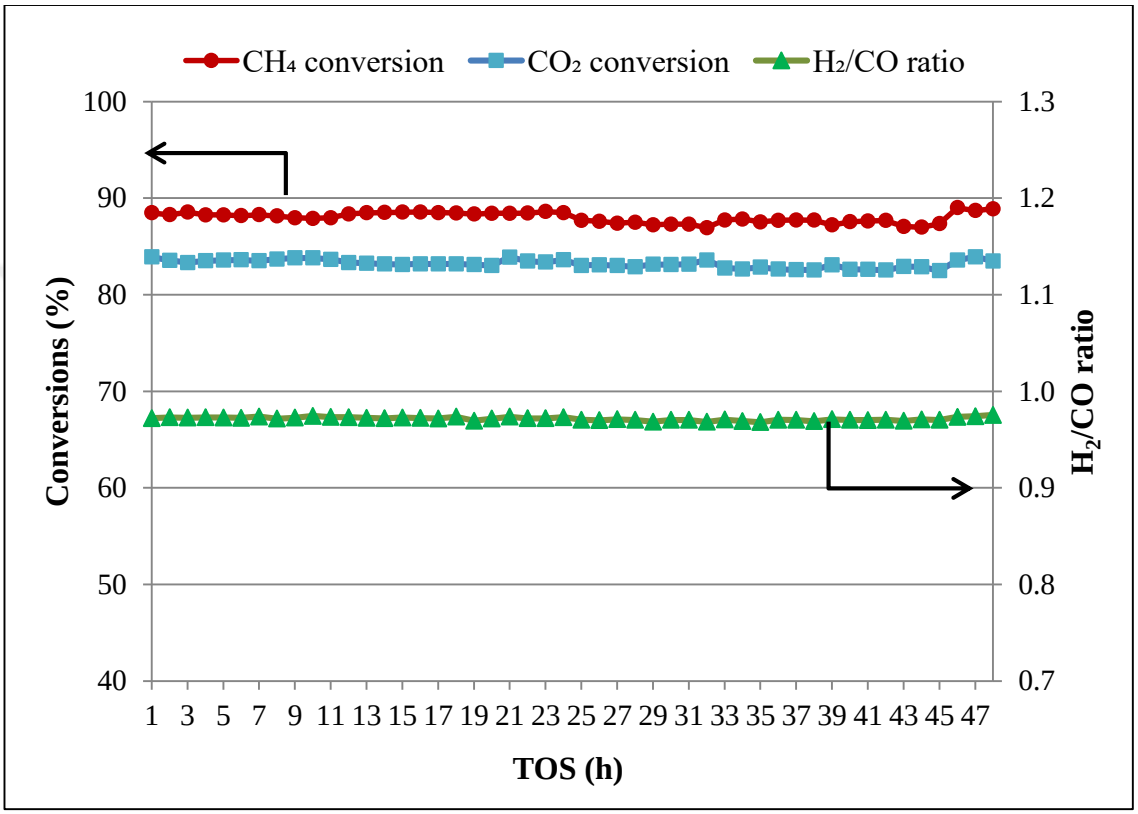

Figure 4.16. Stability test for cordierite monolithic catalyst.

4.4. CDRM Performance of Ni-based $Ni_xCo_{3-x}O_4$ Nanowire Structures

The small sized Ni catalyst have suggested in the literature to enhance the catalyst activity and stability due to the increased surface area (Han *et al*., 2017). The nanostructured monolithic catalysts may be beneficial in this aspect since they can provide enhanced surface due to their special morphology comparing regular coated monolithic structures. In this study, for the first time, the catalytic performance of $Ni_xCo_{3-x}O_4$ nanowire structured monolithic catalysts has been investigated at various temperatures in CDRM. In addition, the morphology of the synthesized structured catalysts was examined in detail through the

SEM and XRD tests. Furthermore, time on stream tests were performed in order to check the catalytic stability of the catalyst.

4.4.1. SEM Test of $Ni_xCo_{3-x}O_4$ Synthesis over Monolith Structures

The preparation method of $Ni_xCo_{3-x}O_4$ nanoarray structures over monoliths developed by Ren *et al*. (2014) was also used in this study. The nanowire catalyst, which was synthesized quite well using the procedure of Ren *et al*. (2014) can be seen in Figure 4.17; however, the procedure was needed to be modified to reduce the consumption of metal precursor. Therefore, several set of experimental conditions have been tested to achieve a uniform grown of $Ni_xCo_{3-x}O_4$ nanowire over monolithic surfaces (Table 3.4.) There were lots of unsuccessful and successful trials to synthesize Co_3O_4 and $Ni_{0.5}Co_{2.5}O_4$ nanowire structures. SEM test results of some these structures are as in Figure 4.18 and 4.19. Considering these test results, the major findings can be summarized as follows:

- The amount of urea affects the formation of nanowires as in Figure 4.18a-b. When it was low, nanowires were not synthesized at all. When it was high amount, the catalyst could be blow in calcination steps (Figure 4.18c-d).
- The mixing is an important parameter to obtain a uniform and well grown nanowire synthesis over monolithic structure. If it was insufficient, the solutions did not reach the inside of the monolith channels and thus the nanowires were not effectively grown inside (Figure 4.18e-f).
- $Ni_{0.5}Co_{2.5}O_4$ nanowire was also tried to be grown over mullite type monolith instead of cordierite ones; however, synthesis was not successful at whole monolith surfaces probably due to weak cohesion of nanowire solutions and monolithic surfaces (Figure 4.18g-h).
- Although magnetic stirrer with heating resulted good nanowire formation all over the monolith support, the heat loss leading deviation in the reaction temperature from set value as well as the high amount of solution demand due to evaporation of solution made this method hard and uneconomical for our study.
- Diluted solution was also used to obtain low amount of nanowire growth over monolithic structures. The attained wires were quite thin, weak and not uniform (Figure 4.19a-b).

- The ultrasonic mixture with heating was a good option to synthesize nanowire with high wire distribution inside the channels; however, it could not operate properly after 1 or 2 hrs. due to the instrument failure (Figure 4.19c-d).
- Direct usage of oven at 90 °C for hydrothermal reaction of reactant solutions helped to synthesize the nanowire but the diffusion of them inside the channels was a major problem in some synthesis.
- The best nanowire synthesis over monolithic structures were obtain in the case of first usage of ultrasonic mixing for 1 or 2 h followed by keeping them at oven set 90 °C with high amount of urea (Figure 4.19e-h).

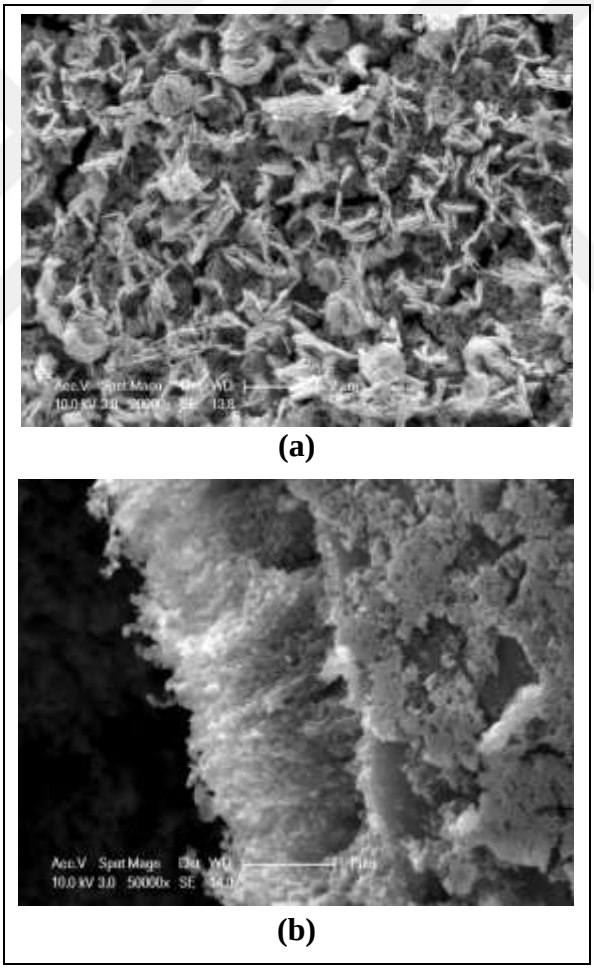

Figure 4.17. SEM results of synthesized $Ni_{0.5}Co_{2.5}O_4$ nanowires as to Ren *et al*. (2015) procedure at various magnifications: (a) 2000Ox, (b)50000x.

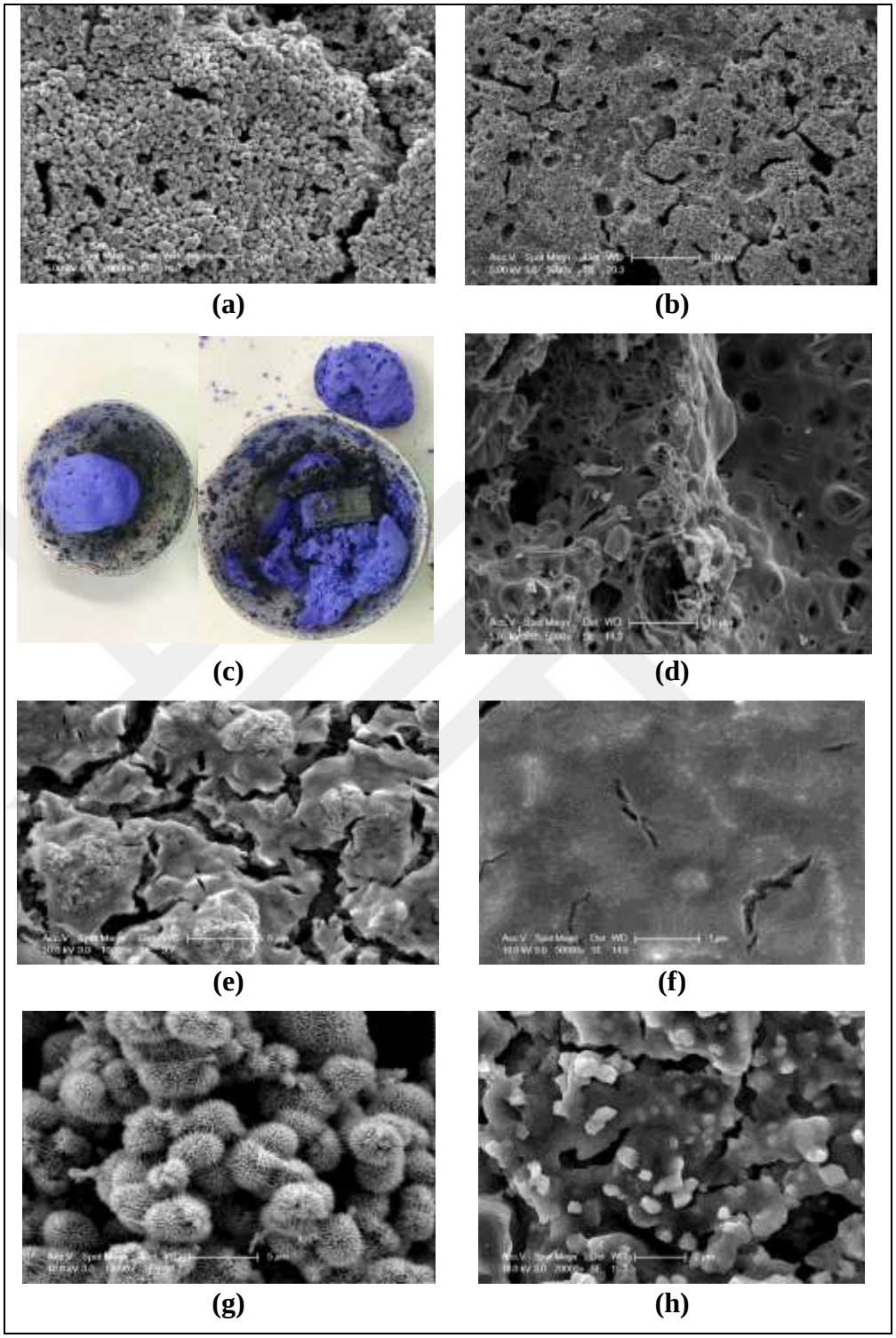

Figure 4.18. SEM results of synthesized $Ni_xCo_{3-x}O_4$ nanowires with (a-d) various urea amount, (e-f) insufficient mixing and (g-h) over mullite monoliths.

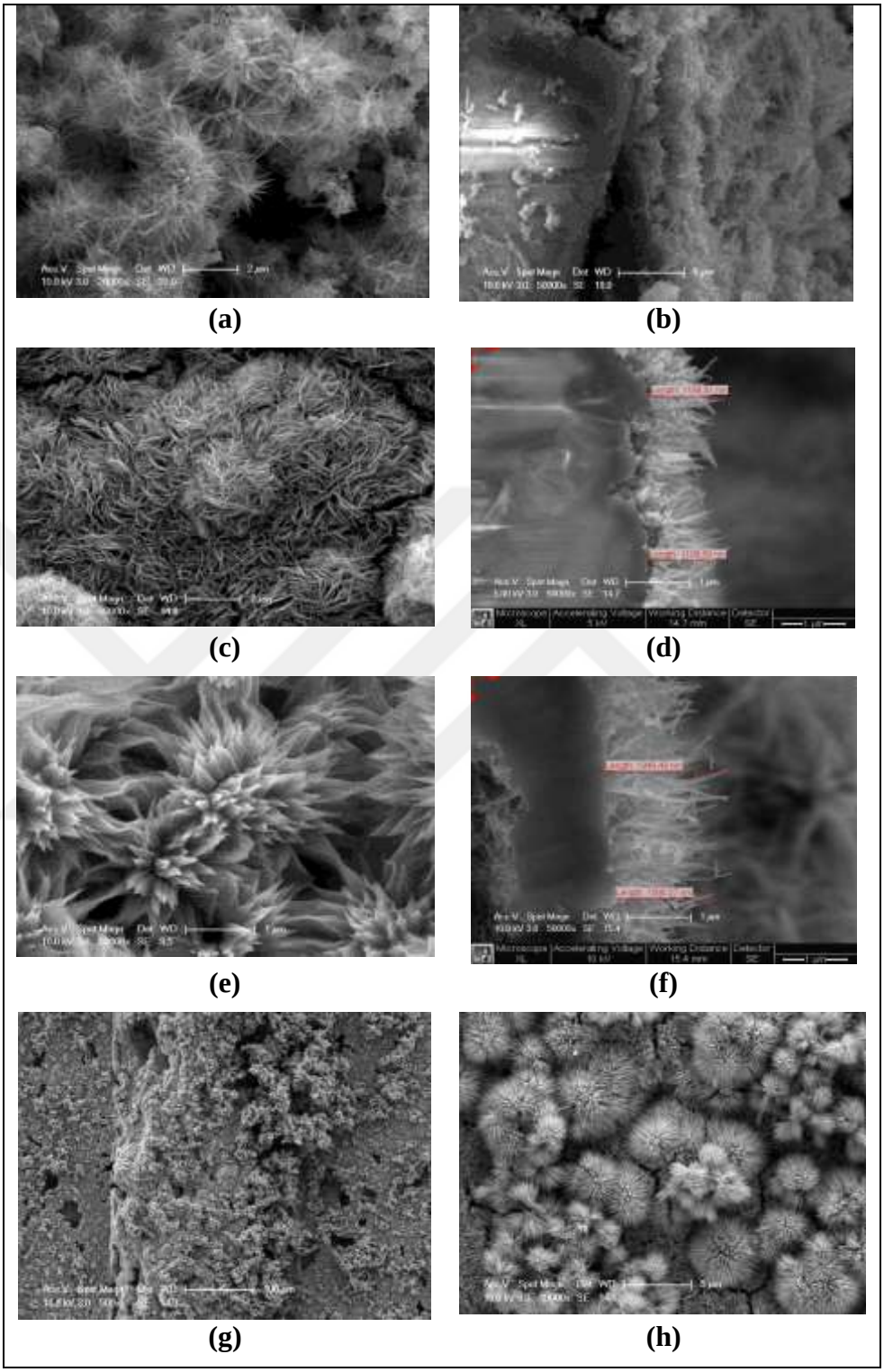

Figure 4.19. SEM results of synthesized $Ni_xCo_{3-x}O_4$ nanowires with (a-b) diluted solution, (c-d) ultrasonic mixing, (e-f) well mixing and (g-h) well mixing with lower magnification ratio.

The SEM results of the internal surfaces of $Ni_{0.5}Co_{2.5}O_4$ nano-array monoliths in various magnifications (500x, 10000x, 2000x, 20000x) in Figure 4.19e-h showed that nanowires were well dispersed on the monolith surfaces and they tend to accumulate on each other within the monolith channels. Lateral characterization of the monolith showed that approximately 1600-2000 nm of wire were formed. Therefore, the procedure with ultrasonic mixing for 1 or 2 h followed by reaction in oven set 90 °C and containing a proper amount of urea were used in the rest of the study.

4.4.2. Effect of Reduction Temperature

Prepared $Ni_{0.5}Co_{2.5}O_4$ catalyst was tested under various temperatures from 600 °C to 900 °C in order to see the effect of reduction procedure at 600°C, 800 °C or unreduction on the catalytic performance (Figure 4.20).

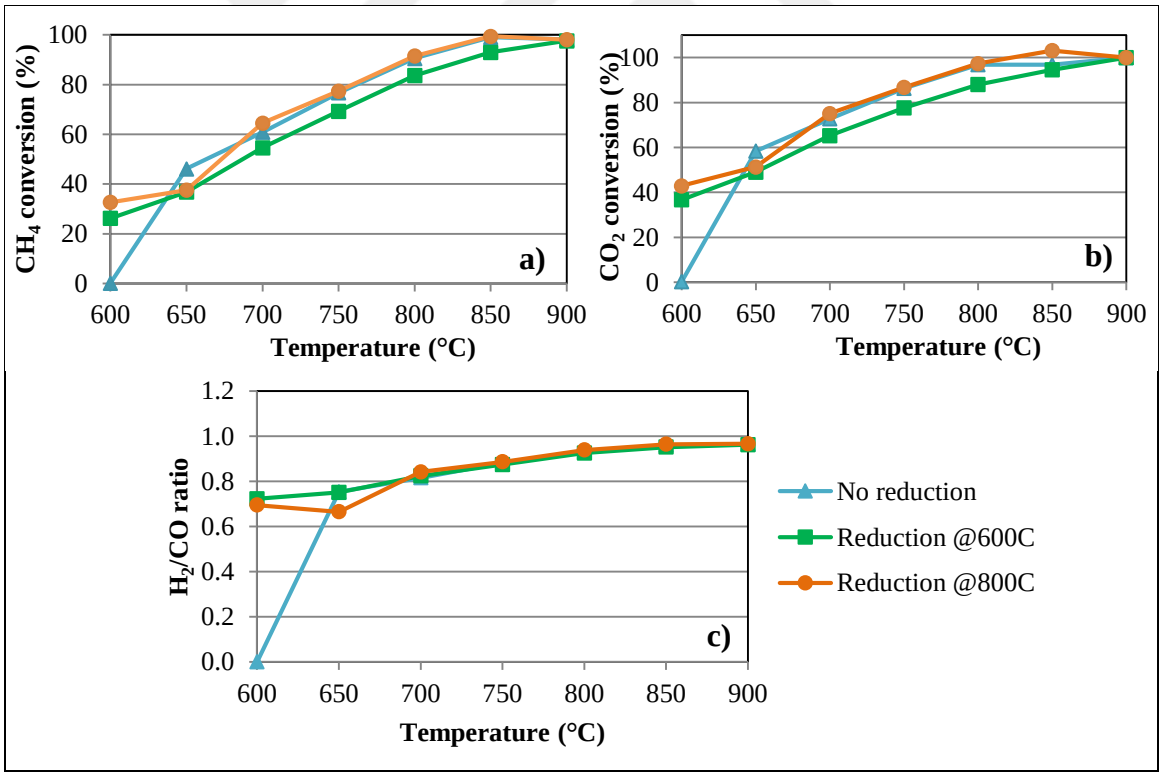

Figure 4.20. Performance test results of $Ni_{0.5}Co_{2.5}O_4$ catalyst depending on the reduction procedure: a) CH_4 conversion, b) CO_2 conversion, c) H_2/CO ratio.

As it seen in Figure 4.20, the reduction has definitely affected the catalytic performance. It seemed to be higher at 800 °C while the product ratio was not affected with this change at all. The higher temperature probably increased the number of active sites which lead to higher reactant interaction and conversion. Since CO_2 and CH_4 conversions increased at the same time, CO and H_2 product yields were also increased in similar rate resulting in the similar ratios. However, at lower temperatures such as 600 °C and 650 °C, reduction at 600 °C gave way to higher ratio than the others. When the catalyst was unreduced, the results did not make any sense at 600 °C. Probably, the catalyst was not active without the reduction process, and with the increasing temperature it may be reduced by the produced H_2.

4.4.3. Effect of Ni/Co Ratio

Various $Ni_xCo_{3-X}O_4$ nano-array catalysts (x=0, 0.5 and 2) were prepared, reduced at 600 °C and catalytically tested at a temperature range from 600 °C to 900 °C under 70 ml/min feed flow. The catalytic test results can be seen in Figure 4.21 in terms of reactant conversions and product gas ratio as H_2/CO. As it seen from the figure, as Ni content in $Co_{3-x}O_4$ nano-array increased, CH_4 conversion increased proportionally until 750 °C. After this temperature, nano-array catalysts having high amount of Ni inside ($Ni_2Co_1O_4$) or not having (Co_3O_4) led to higher amount of conversion than $Ni_{0.5}Co_{2.5}O_4$. Since the experiments were performed with a 50 °C temperature increment, the active sites of Ni metal may be blocked by the coke formation or sintered with the increasing temperature and lost its catalytic activity for methane consumption. In the case of CO_2 conversion, having high amount of Ni led to highest CO_2 conversion at all temperatures. After 700 °C, nano-array catalysts without Ni started to reach the one having highest amount of Ni (x=2). However, in terms of product ratio, H_2/CO, highest amount was obtained in the case of x=0.5. On this basis, it can be said that the amount of Ni in the nano-array catalyst significantly affect the product distribution. In the absence of it, really low amount of H_2/CO ratio was observed until 750 °C. In this aspect, the best results were obtained over $Ni_{0.5}Co_{2.5}O_4$ catalyst (x=0.5); after this point, the product distribution was almost the same.

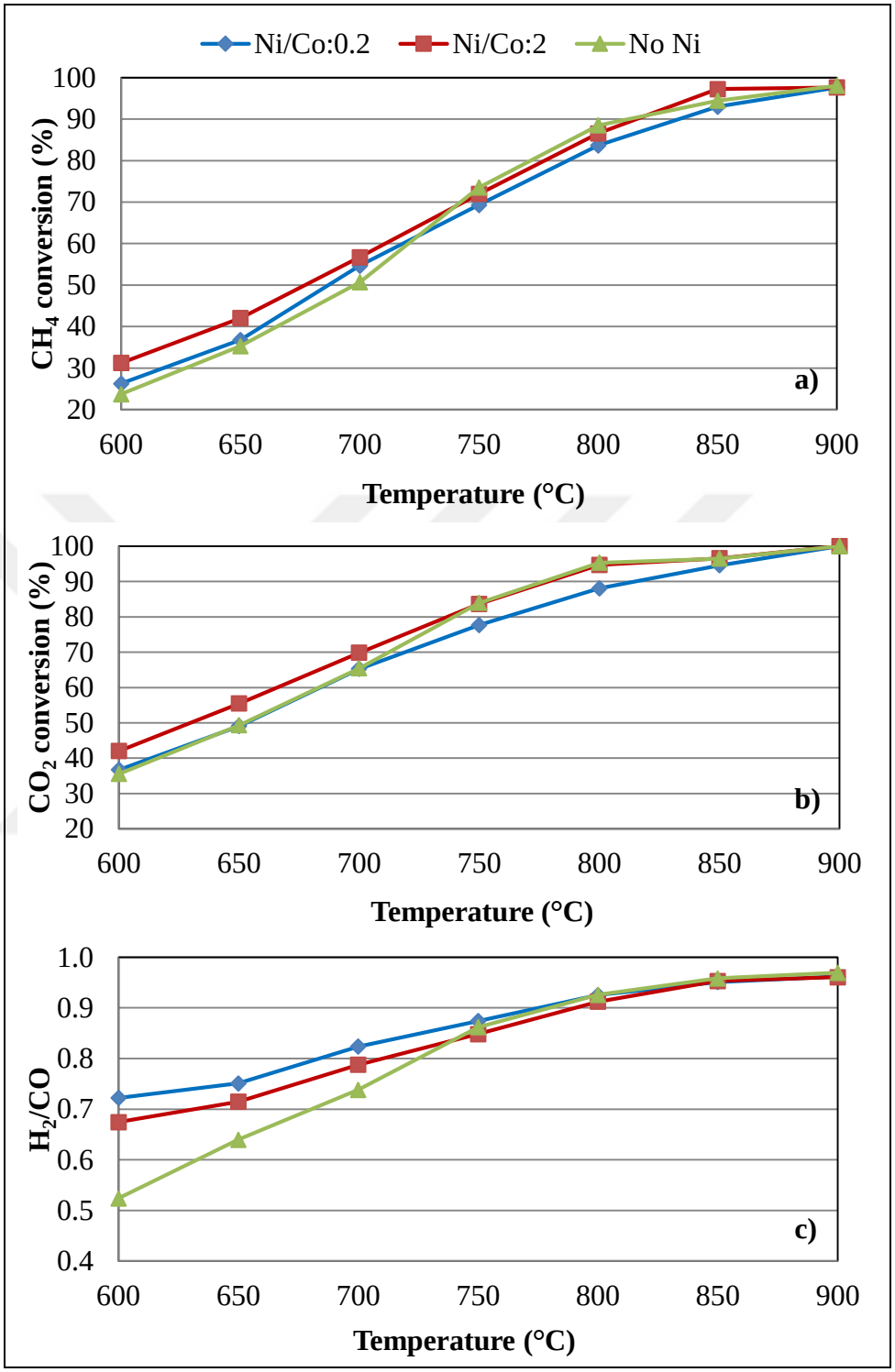

Figure 4.21. Performance test results of nanowire catalyst with changing ratio of Ni/Co: a) CH_4 conversion, b) CO_2 conversion, c) H_2/CO ratio.

4.4.4. Effect of Total Feed Flow

The catalytic test of $Ni_{0.5}Co_{2.5}O_4$ catalyst was evaluated under feed flow such as 15, 30, 50 and 70 ml/min with a CH_4/CO_2 ratio of 1 at 750 °C. The results in Figure 4.22 showed that both CH_4 and CO_2 conversions as well as product ratio was highly affected by this feed flow change. The lower feed flows increased the catalytic performance since they led to higher contact time between the reactant gases and catalyst surface. On the other hand, monolithic structures were known as to be able to work at higher flows with less catalytic activity change. Therefore, $Ni_{0.5}Co_{2.5}O_4$ structured monolith catalyst used in this study was probably highly sensitive to flow velocity and resulted in various CH_4 and CO_2 conversions as well as product ratios.

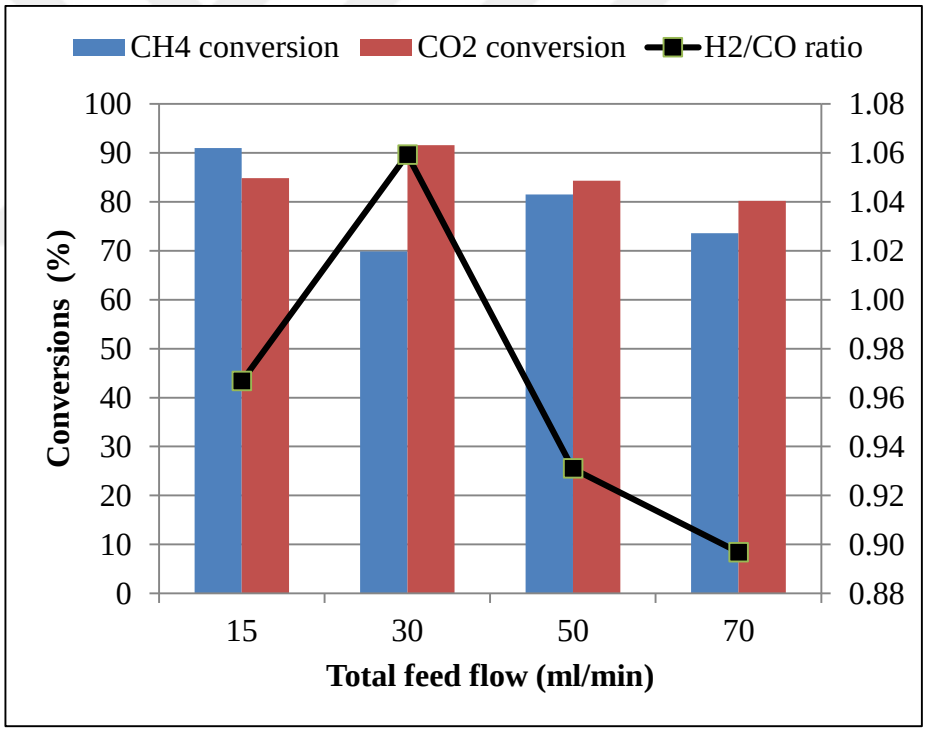

Figure 4.22. Performance test results of nanowire catalyst under various feed flow in which the ratio of CH_4/CO_2 is 1 and balanced with 10ml/min (N_2).

4.4.5. Time on Stream Tests

$Ni_xCo_{3-X}O_4$ nano-array catalysts was also tested at 750 °C for 8 h in order to check the catalyst stability during these hours. As it seen in Figure 4.23, the unreduced $Ni_{0.5}Co_{2.5}O_4$ and $Ni_2Co_1O_4$ structured monolithic catalysts were easily lost their catalytic activity under these conditions. Even if they are reduced under H_2 flow, they are still not stable. The catalytic performance of reduced $Ni_{0.5}Co_{2.5}O_4$, for instance, decreased from 84.5% CH_4 conversion, 91.3% CO_2 conversion with a 0.93 H_2/CO ratio to 75.2%, 84.5% and 0.87 in 8 h, respectively. However, their catalytic performance was improved as to unreduced ones. The reduced Co_3O_4 structures gave way to similar decline but with the lowest catalytic activity.

Coke formation may be the main reason for these catalytic lost; therefore, low amount of oxygen (3%) was added to the feed in order to prevent this formation but without aiming the change in product distribution. For instance, CH_4 conversion increased to 91.3% and CO_2 conversion CO_2 conversion was decreased 87.0% in the presence of oxygen over reduced $Ni_{0.5}Co_{2.5}O_4$ while product ratio was also increased to 0.96. However, there was no change in the stability; catalyst significantly lost its activity during these hours reaching 81.% CH_4 conversion, 81.4% CO_2 conversion with a 0.91 H_2/CO ratio, which were still higher than the one obtained in the absence of oxygen. On the other hand, $Ni_2Co_1O_4$ structured catalysts in the presence of additional O_2 was quite stable for 8 h. After these hours, it also started to lost its catalytic performance. It was obvious that adding low amount of oxygen to the system gave way to better product distribution.

For another solution, small amount of Pd, which is a coke resisted active metal, was added to reduced $Ni_2Co_1O_4$ structured catalysts, which had the highest catalytic activity among reduced ones. This addition did not improve the catalytic stability of this catalyst. As a result, although O_2 addition to the feed on reduce $Ni_2Co_1O_4$ catalyst experiments seemed to be best option among these solutions to increase stability, the results were not satisfactory to meet the industrial demand.

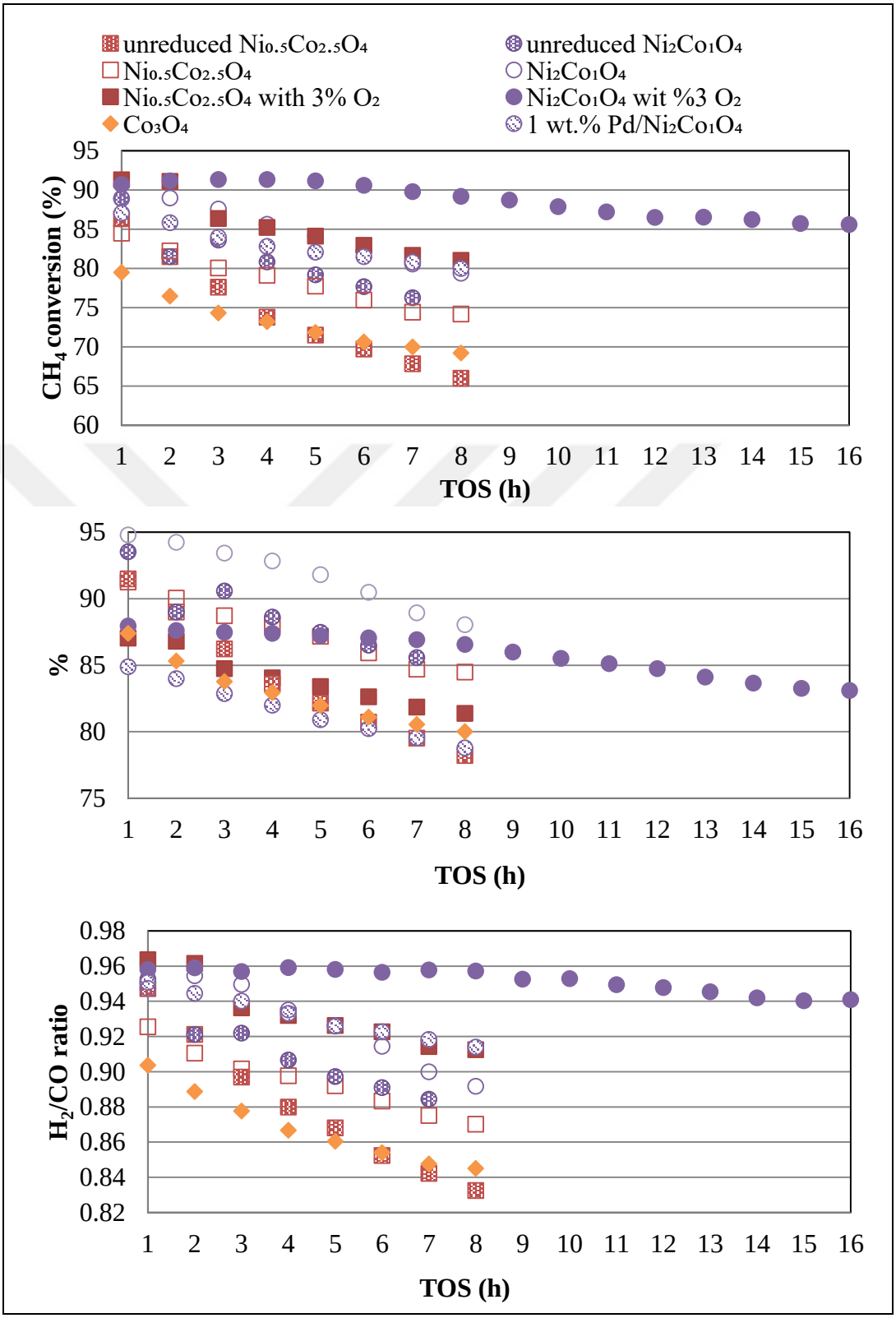

Figure 4.23. TOS test results of nanowire catalyst at 750 °C.

4.4.6. Characterization of Reduced and Spent $Ni_xCo_{3-x}O_4$ Nanowire Structures

The $Ni_xCo_{3-x}O_4$ nanoarray monolithic structures could be sensitive to temperature and reactant flow. For the sake of further understanding of catalyst morphology under the conditions that are least likely to deform the nanowire morphology, the reduced and spent $Ni_{0.5}Co_{2.5}O_4$ nanoarray coated of monoliths at reaction 600 °C for 1 h were analyzed. In addition, spent catalyst in the presence of 3% O_2 at 600 °C was evaluated to examine how O_2 affected nanowire structures. SEM results was in Figure 4.24.

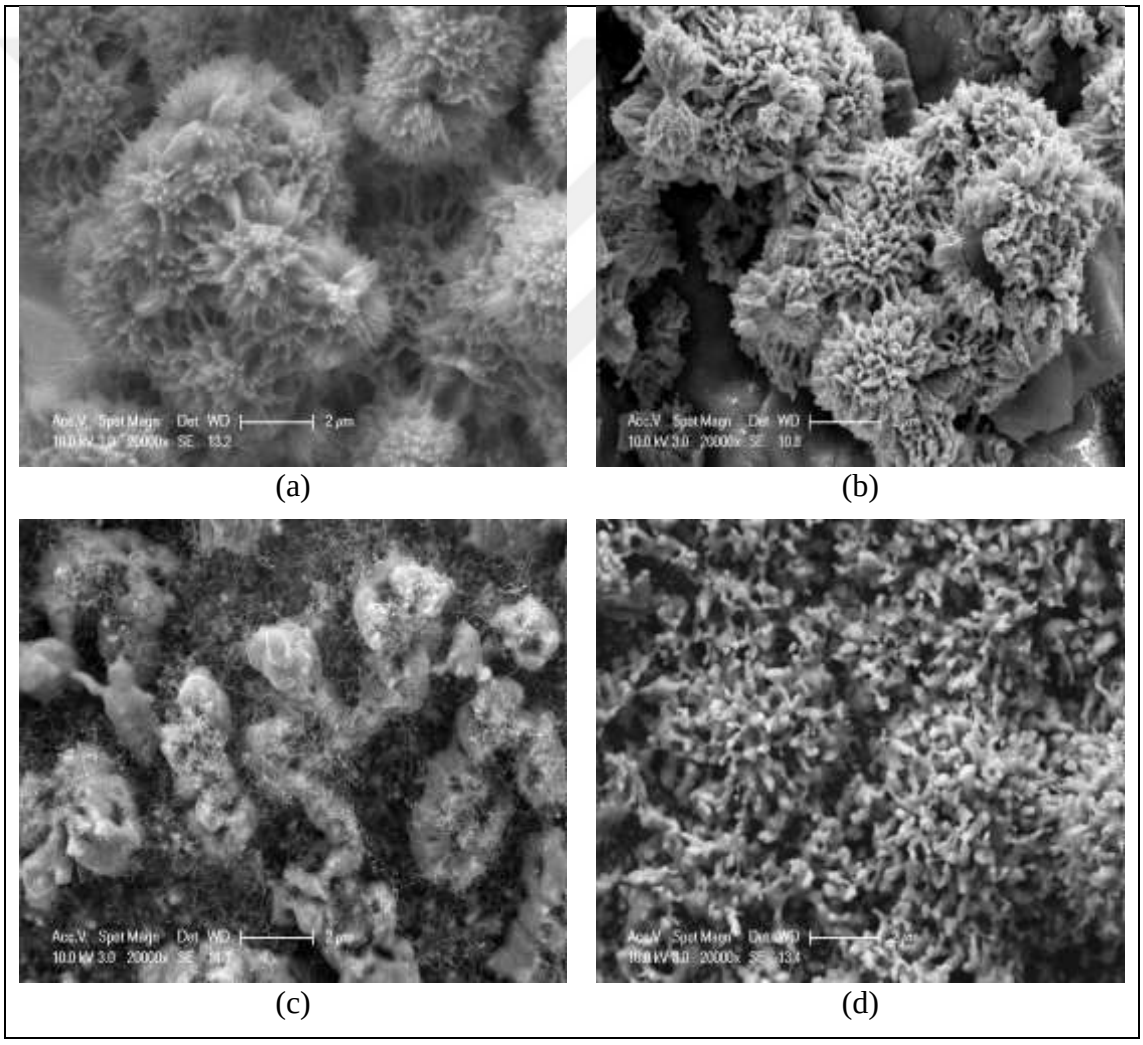

Figure 4.24. SEM images of $Ni_xCo_{1-x}O_4$ nanowire catalyst: fresh (a), reduced at 600 °C (b), reacted in the absence (c) and presence of 3% O_2 (d).

According to these results, the morphology was drastically changed when it was reduced under H_2 flow (Figure 4.24b). The main structure of wires was seemed to remain; however, wires could be thicker. After the reaction at 600 °C, the nanowire structure was seemed to turn into clusters (Figure 4.24c). In addition, as it was expected huge amount of carbon wires were observed between these clusters. The spent nanowire catalysts under the feed flow in which 3% O_2 was added indicated very low amount of carbon wires comparing the one in the absence of O_2 (Figure 4.24d). However, the nanowires were still seemed to turn into clusters after the reaction.

The XRD patterns of $Ni_{0.5}Co_{2.5}O_4$ nano-array in the form of fresh, reduced with H_2 600 ℃ and reacted in the absence and presence of 3% O_2 at 600 ℃ were as in Figure 4.25. Before reduction, the nano-array showed only the structure of small amount of cordierite and huge amount of $Ni_{0.5}Co_{2.5}O_4$ with the peaks at 2Θ = 19.2, 31.5, 36.8, 38.44, 44.8, 65.18, 69.6°, which are related the $Ni_xCo_{3-x}O_4$ pattern. After reduction, $Ni_{0.5}Co_{2.5}O_4$ pattern diminished and new clear peaks at around 2Θ = 44.4, 51.7, 76° related to metallic Ni and Co were occurred. After the reaction, it was observed that these peaks lost their intensity and the XRD patterns of cordierite monolith become more visible. It can also be said that the intensity of metallic Ni and Co metals were higher in the crystal structure of $Ni_{0.5}Co_{2.5}O_4$ nano-array catalyst reacted in the presence of O_2 than the one in the absence of O_2, where the intensity of cordierite structure was higher. In terms of carbon formation, it was really hard to claim something since the XRD pattern of the carbon types were overlaps the cordierite peaks, such as at 2Θ= 26.1°.

The crystallite size of the samples was also calculated from the XRD data through the Scherrer equation. In the unreduced samples the crystallite size of $NiCo_2O_4$ and Co_3O_4 species were 10.90 nm and 14.46 nm., respectively. In the reduced sample, $NiCo_2O_4$ and Co_3O_4 had 19.02 and 23.73 nm crystallite sizes while Ni and Co species had 21.68 and 19.24 nm crystallite sizes, respectively. In the reacted samples in the absence of oxygen, they increased further to 28.98, 25.38 and 28.69 for $NiCo_2O_4$, Ni and Co species. In detailed analysis, Co_3O_4 species did not observe on this sample. In the reacted samples in the presences of oxygen it was harder to distinguish peaks and decide its crystallite sizes from the detailed XRD analysis.

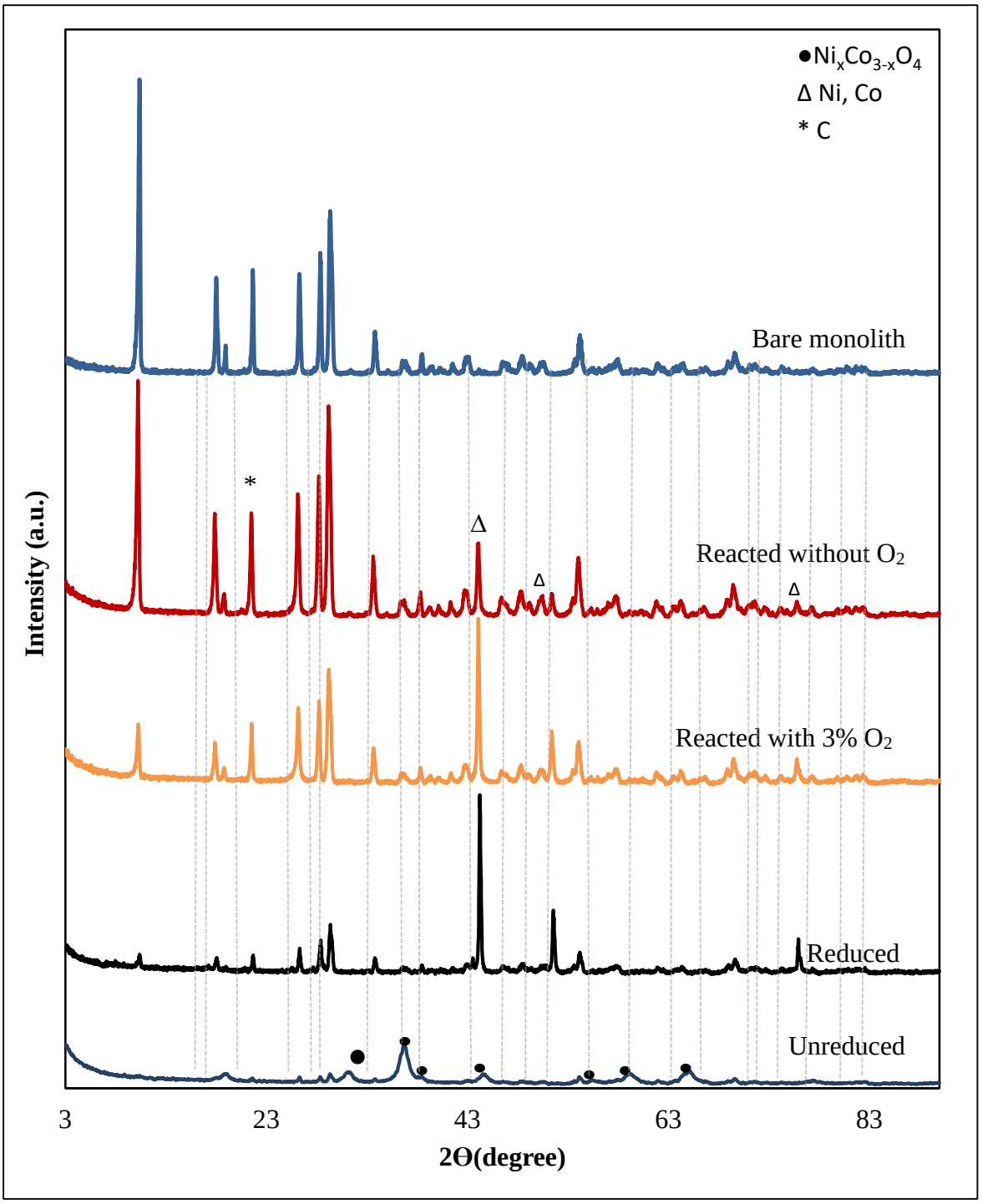

Figure 4.25. The XRD patterns of $Ni_{0.5}Co_{2.5}O_4$ nanowire catalyst operated under various conditions.

4.5. CDRM Performance of Ni-based Catalysts over MgO Nanorods

As mentioned in Section 2.4, MgO as a support for Ni-based catalysts have been widely studied by various researcher since it has a positive effect on CDRM processes due to its high basicity (Asencios *et al.*, 2011). However, its surface area is lower than the other suggested supports such as Al_2O_3 (Hang *et al*., 2014). In this aspect, the utilization of MgO support in nanosized forms can be beneficial to increase its surface area. In literature, there have been some attempts to prepare and use nano sized Ni-based catalyst over MgO containing support as the studies of Abdollahifar *et al*., (2014), Zhang *et al.* (2016) and Bian *et al*. (2016). As different from these studies, MgO nanorod were prepared, in this work, using a method similar to that developed by Al-Hazmi *et al.* (2012) for the antibacterial studies. As far as we know, the catalytic performance of Ni-based catalysts over this kind of MgO nanorod were examined in CDRM for the first time. Moreover, some experimental studies were also performed to coat or grow it over monolithic structures for the sake of enhanced performance such as workable with low pressure drop.

4.5.1. Characterization of Synthesized MgO Nanorods

In order to check whether MgO nanorods were synthesized as in the study of Al-Hazmi *et al.* (2012) or not, the MgO samples prepared were analyzed by SEM analysis first. Then, the Ni-based catalysts over these MgO nanorod samples were investigated for better understanding of the catalyst surface morphology through SEM, XRD and XPS analyzes.

4.5.1.1. SEM Test Results**.** As mentioned in Section 3.2.4.1, MgO was synthesized in oven during either 1 h or 2 h. Figure 4.26 shows these MgO nanorods in various magnifications. The synthesis of MgO nanorod was seen to be quiet successful in both situations although there were some nano MgO balls which were unable to form the road or were broken during the synthesis procedure. Human intervention during the transferring samples from one cup to other or any kind of similar reasons may be the cause of these deformations in the structure. The time for the synthesis may be also insufficient; this is not clear at this step and needs further clarification with additional studies. Previously, Al-Hazmi *et al.* (2012) has synthesized nanorod MgO with the same chemicals but they used microwave furnace for hydrothermal processes for 15 minutes. In our case, however, we used conventional thermal

furnace, and the synthesis was achieved at 180 ˚C and 1 h. The thinnest nanorod was approximately 100 nm with a length of 2-4 μm as in seen Figure 4.26d.

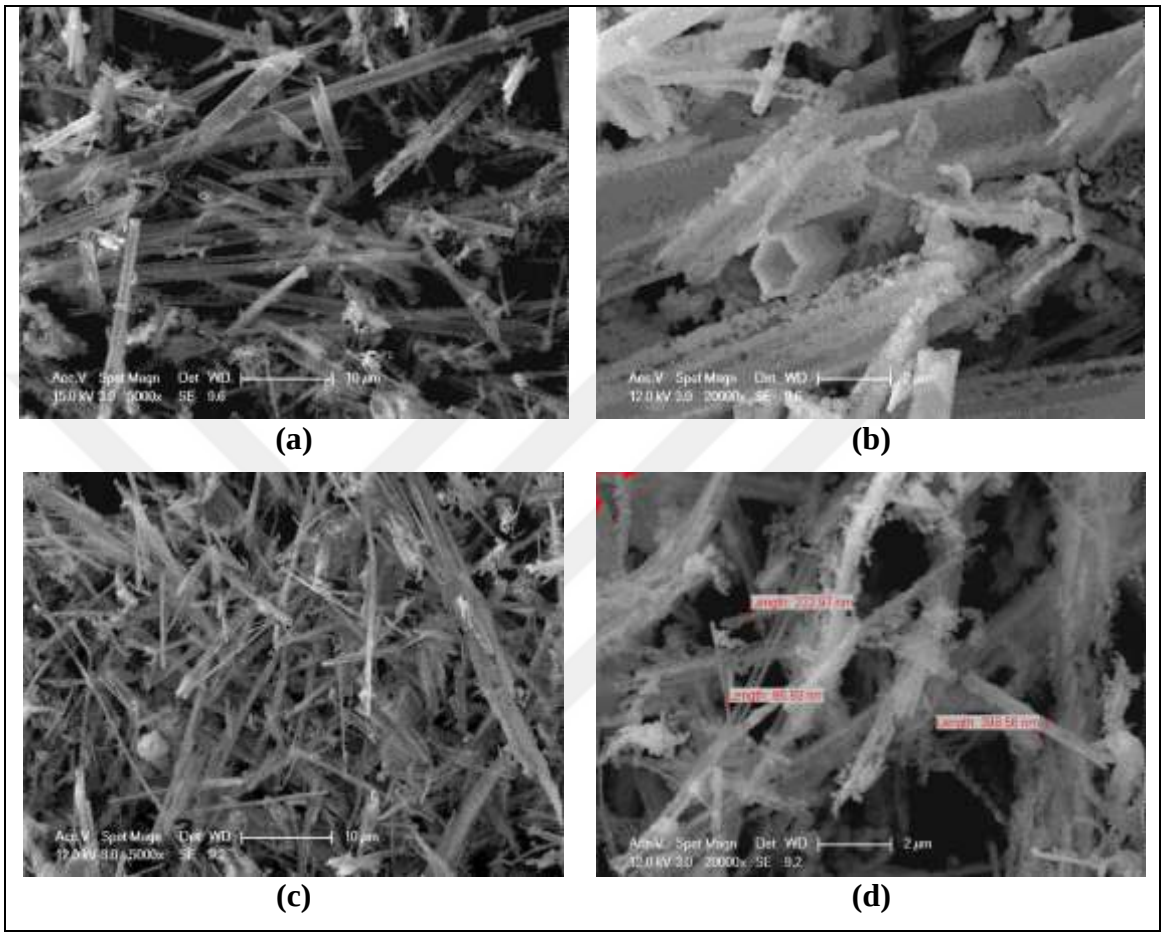

Figure 4.26. SEM Images of MgO synthesized during 1 h (a, b) and 2 h (c, d).

As a second step, Ni-based catalysts over MgO prepared through 2 different ways as in Section 3.2.4.1 were analyzed by SEM instrument. SEM images in Figure 4.27a-b represents the impregnated 8wt.%Ni and 2wt.%Co active metals over MgO nanorods while Figure 4.27c-d shows the images of co-prepared active metals and MgO nanorods in various magnifications. As seen in Figure 4.27a-b, the impregnated active metals formed a new thin structures, like nano sheets over the nanorods with a 40-67 nm thickness. Similarly, Han *et al.* (2014) obtained a flower-like nano-architecture composed of nano-sized flakes in MgO-Al_2O_3 aerogel samples for CO_2 capture process. In addition, Zhang *et al.* (2016) observed a similar morphology (thin sheets which were intercrossed with each other) in the sample of Ni/MgO containing 15% Al_2O_3 for dry reforming of methane.

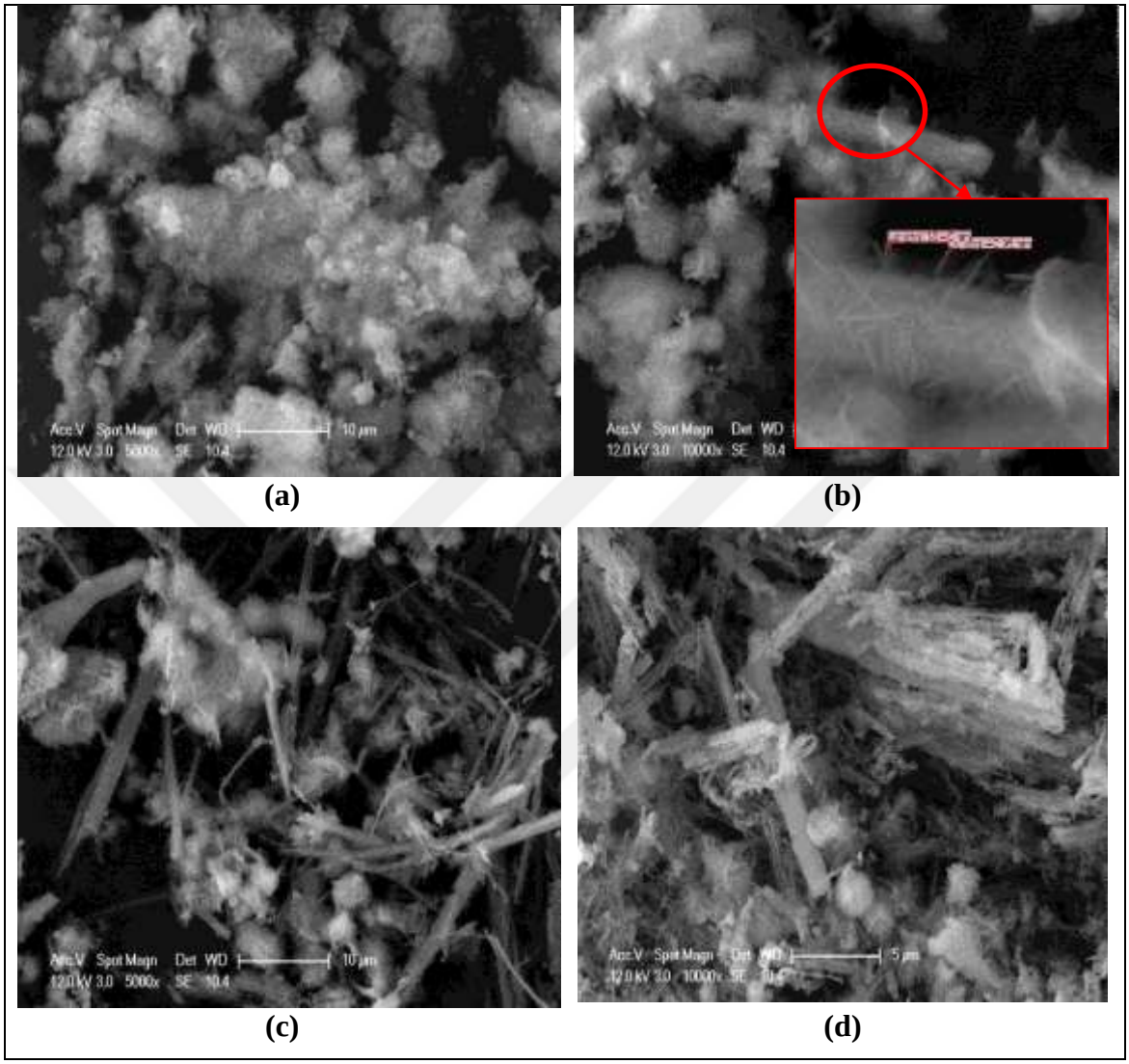

Figure 4.27. SEM images of synthesized catalyst with impregnation (a,b) and co-preparation (c, d).

On the other hand, the co-prepared samples showed more mix structures as seen in Figure 4.27c-d. Bian *et al.* (2016) has synthesized a Mg phyllosilicate nanotube over silica for dry reforming of methane through the hydrothermal process of Mg nitrate, Ni nitrate and sodium silicate solutions. Their TEM images showed that ball shaped Ni metals were well dispersed into the synthesized nanotubes. In our case, they were either smooth nanorods similar to the one in pure MgO nanorod samples or nano sheets as in the impregnated samples. If both methods used in our study are compared, it can be said that the impregnation of active metals over MgO nanorods gave way to more uniform distribution as to the co-

preparation of the metals with MgO. Needless to say, further investigations should be conducted such as mapping of the active metals or TEM to clarify their distribution through the support.

4.5.1.2. XRD Test Results. In order to examine the crystal morphology of the Ni-based MgO nanorod catalysts prepared by the impregnation of active metals over MgO nanorods, XRD analysis were performed over fresh and reduced samples (Figure 4.28).

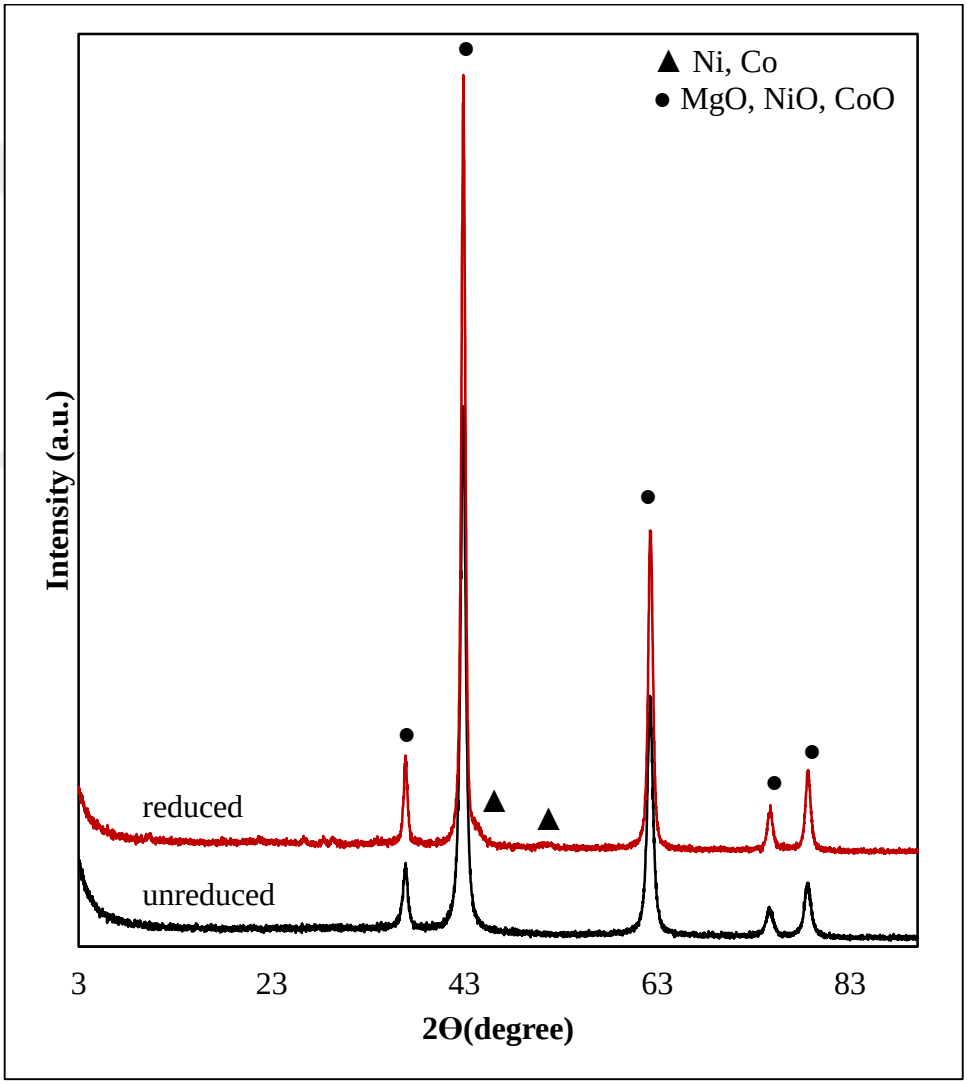

Figure 4.28. XRD graph of the unreduced fresh and reduced Ni-based MgO nanorod structured catalyst.

As seen in Figure 4.28, the unreduced samples showed clear peaks at 2Θ= 36.92°, 42.92°, 62.26°, 74.62° and 78.64° which are probably related to MgO support and/or NiO

and CoO phase of active metals which were completely overlaps with MgO peaks. The reduced samples showed additional peaks at around 2Θ= 44° and 51° which can be indication of metallic Ni and Co phases. Even if the peaks of these metals were quite low in XRD graph, the average crystallite size of the Ni and Co metals were also calculated from Scherer equation and found as 15.76 nm and 47.27 nm, respectively. On the other hand, before the reduction process, the average MgO crystallite size was found as 15.58 nm; then, it was increased to 18.92 nm with the reduction process at 800 °C.

4.5.1.3. XPS Test Results. The surface of impregnated Ni and Co species over MgO nanorod structures were also analyzed by XPS measurements. Ni2p and Co2p XPS scans of the unreduced and reduced Ni-based MgO nanorod samples were represented in Figure 4.29.

Highly clean XPS spectra were obtained as seen in the figure. The binding energies at 855.68 and 873.28 eV can be assigned as the Ni $2p_{3/2}$ and Ni $2p_{1/2}$ while BES at 781.48 and 796.78 eV can be related to Co $2p_{3/2}$ and Co $2p_{1/2}$ phases. The energies at 881.38, 861.98, 803.98, 788.68 eV are the shoulder peaks of these phases. After reduction process, these phases seemed to be remained their BES but lowered in the intensity. In other words, atomic weight percentages of these metals were quite changed. In some studies, binding energies at around 852.5 eV were assigned to Ni^0 species; however, in our case it did not observed clearly. On the other hand, Zhen *et al*. (2016) declared that peaks at 852.6 and 870.0 are the Ni metallic states. XPS scan results were also used to determine the atomic and weight percentages of the Ni and Co metal contents on MgO nanorod samples. In the unreduced Ni-based MgO nanorod, 6.33 att.% Ni, 2.52 att.% Co metals, in other words, 18 wt.% Ni and 7.2wt.%Co metals were calculated from the XPS deconvoluted areas. In the reduced sample, these ratios were 3.20 att.% for Ni, 2.15 att.% for Co, namely 14 wt.% and 10 wt.%, respectively. Since MgO nanorod was impregnated as to 8wt.%Ni and 2wt.%Co, these values were quite higher than we excepted.

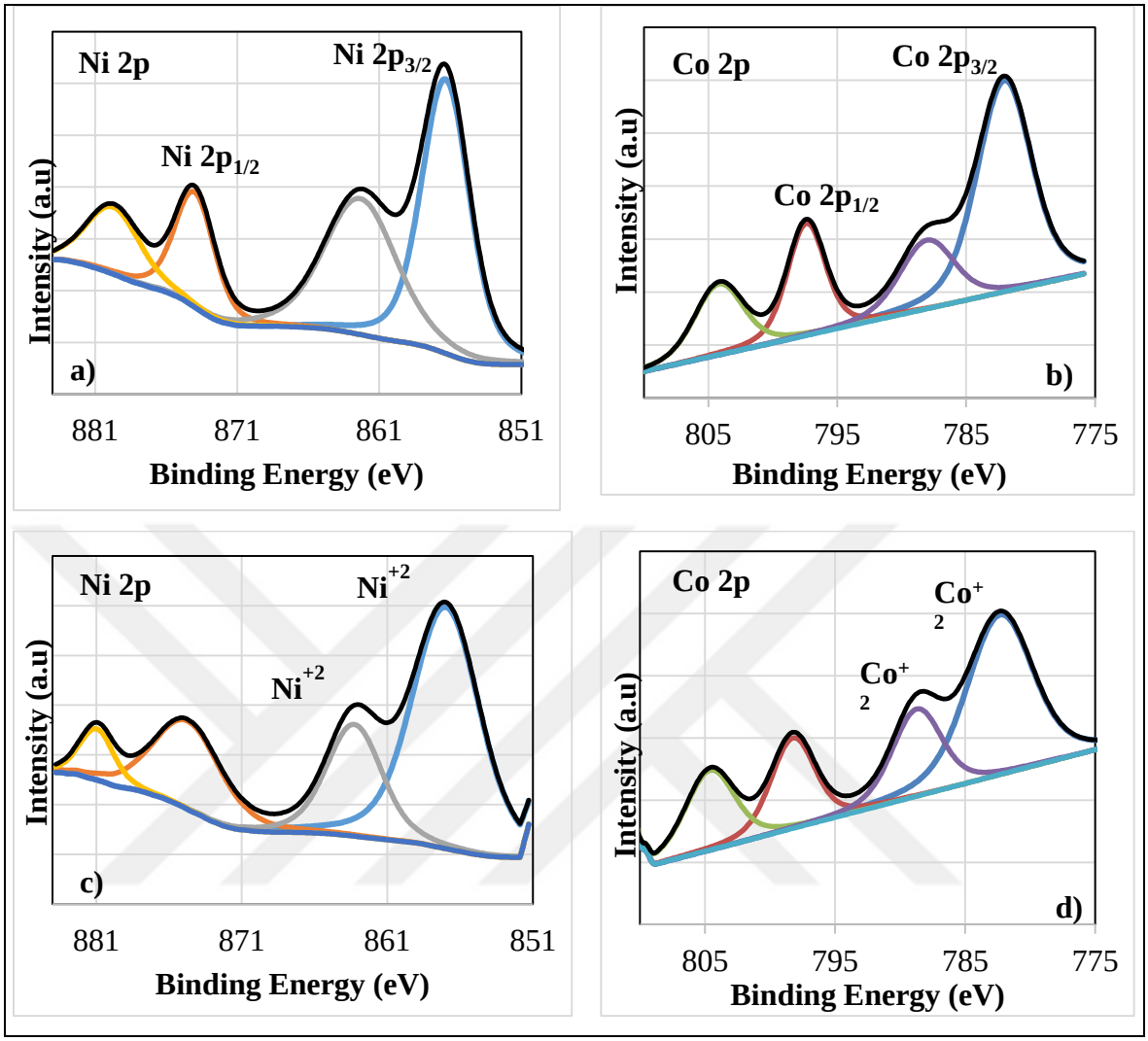

Figure 4.29. XPS scans of the unreduced (a-b) and reduced (c-d) Ni-based MgO nanorod structured catalysts.

4.5.2. Effect of Calcination Procedure of MgO Nanorod

As is known, pretreatment of the catalysts such as drying, calcination or reduction may have significant impact on the catalytic performance since they may influence the active metal dispersion over support, porosity of the support, active sites of the catalysts etc. Therefore, before the impregnation of 8wt.%Ni and 2wt.%Co metals over MgO nanorods, the synthesized MgO nanorods were calcined in two ways such as calcination under stagnant air in a furnace or under 20 ml/min of air flow in the quartz reactor at 600 °C for 1 h.

As it seen from Figure 4.30, the change of calcination procedure did not affect the catalytic performance of the catalysts; the catalyst calcined both ways resulted nearly the same CH_4 conversion, CO_2 conversion and product yields. Therefore, from now on, all catalysts were calcined in furnace without air flow since this method is easier than the calcination in the air flow.

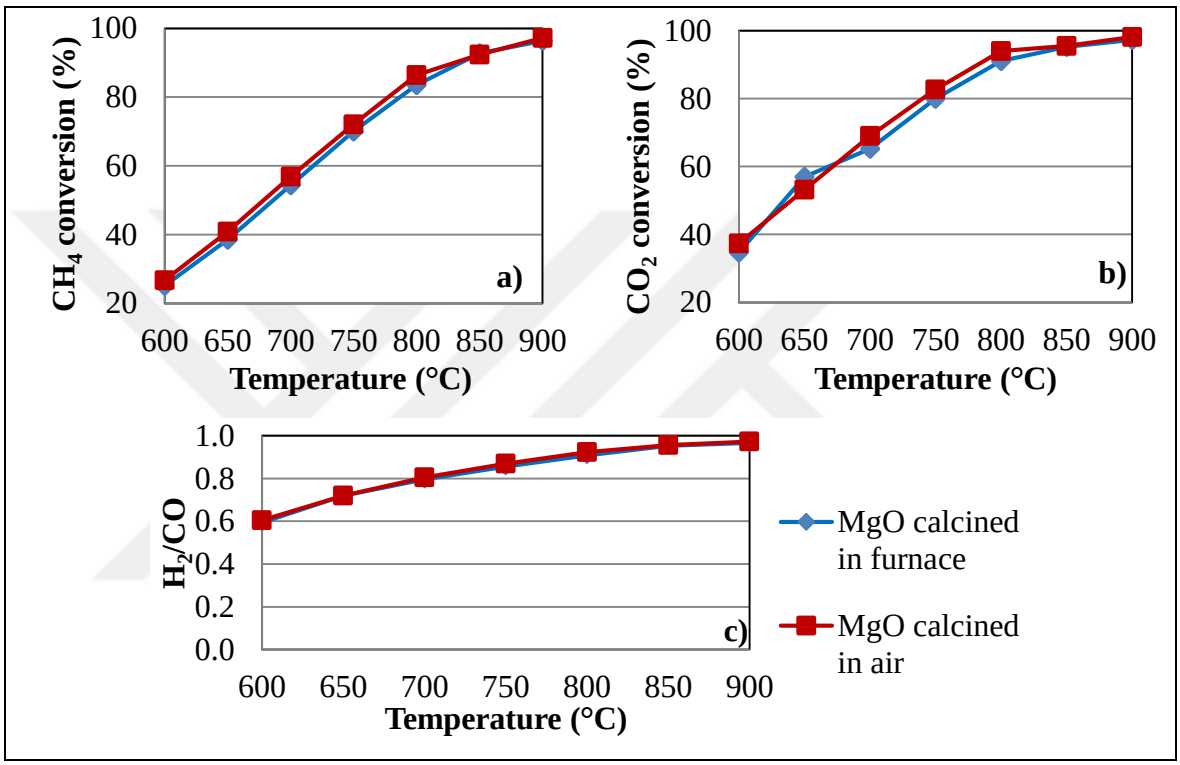

Figure 4.30. The effect of MgO nanorod calcination procedure on CDRM catalytic performance: a) CH_4 conversion, b) CO_2 conversion, c) H_2/CO ratio.

4.5.3. Effect of Preparation Method of Ni-based MgO Nanorod

The catalytic performance of the catalyst prepared in various ways such as impregnated NiCo active metals over MgO nanorods or co-prepared NiCoMgO nanostructured catalysts were evaluated at a temperature change from 600 to 900 °C under the reactant flow of 70 $mlmin^{-1}$ (CH_4/CO_2:1/1) with a 10 $mlmin^{-1}$ N_2 internal gas flow. In addition, same amount of catalyst (50mg) were used under the same condition to compare the effect of MgO structure in CDRM. The results are given in Figure 4.31.

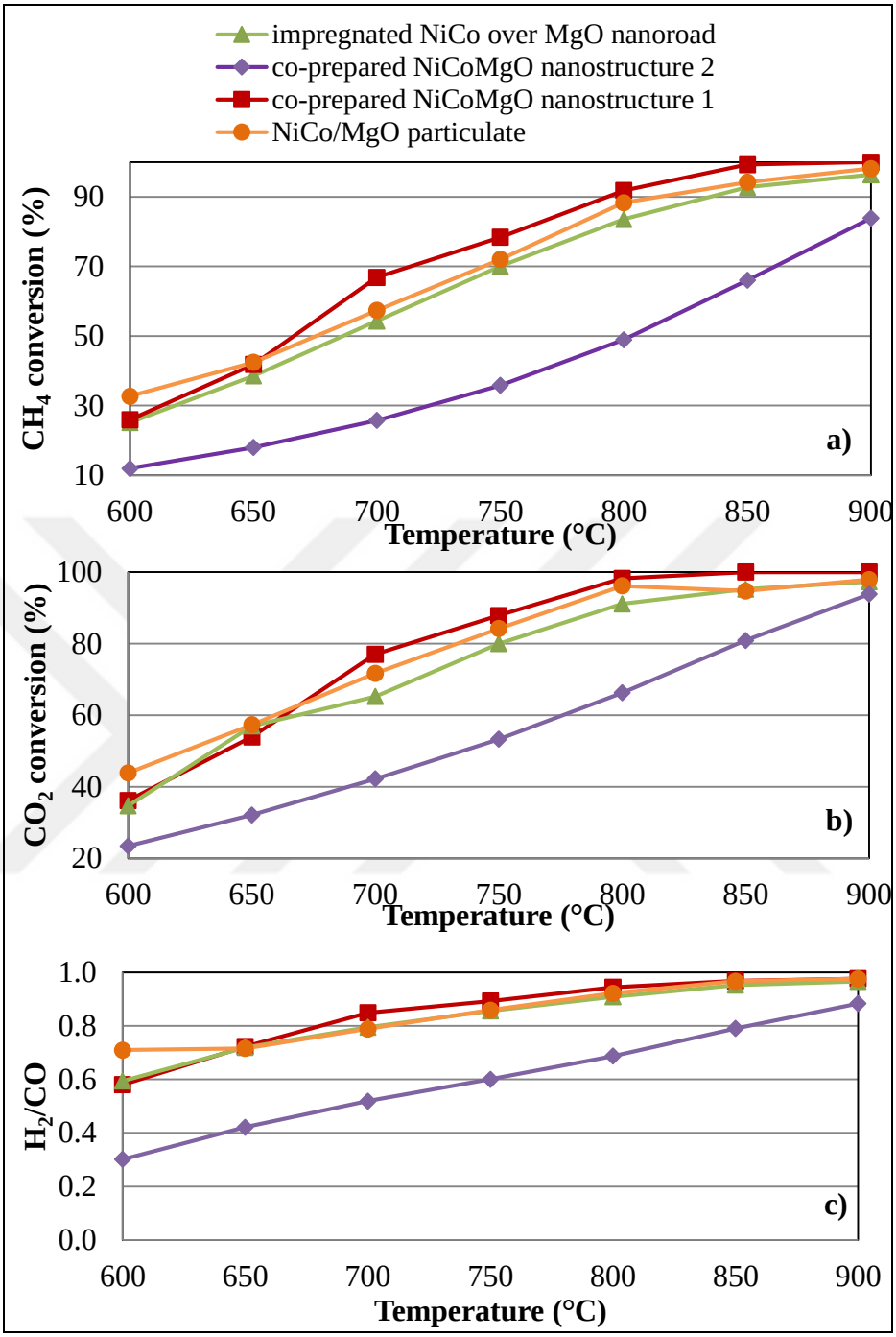

Figure 4.31. The effect of preparation method of NiCoMgO catalysts on CDRM catalytic performance: a) CH_4 conversion, b) CO_2 conversion, c) H_2/CO ratio.

Expect co-prepared NiCoMgO nanostructured 2, the catalytic performances of these catalysts were generally good and similar wit some minor differences. For example, at 600 °C, both CH_4 and CO_2 conversion as well as the product ratio was higher on the particulate catalysts; however, at 650 °C, all samples showed the nearly same catalytic performances.

When the temperature increased further, the highest catalytic activity was observed over co-prepared NiCoMgO nanostructured catalyst followed by the impregnated NiCo over MgO nanorod and NiCoMgO particulate catalyst followed it, respectively. On the other hand, when the experiments were repeated, co-prepared NiCoMgO nanostructured catalyst, which is labeled as 2 in Figure 4.31, showed significantly different performance compared to the first trial; this situation may be stemmed from that active metals could not successfully synthesized with MgO in each preparation trials and were not uniformly dispersed. Similarly, the higher catalytic activity of particulate NiCoMgO may be also related to the more successful metal dispersion than MgO nanorods, even though its surface area was expected to be lower than nanostructured catalysts.

4.5.4. Effect of GHSV

The amount of the catalyst used in the reaction is an important parameter since it directly affects the contact time of the reactants with the catalyst surface and thus the catalytic activity. The relation can be expressed by gas hourly space velocity (GHSV) as the volumetric flow rate over the mass of the catalyst. In order to investigate this relation, various amount of NiCo impregnated MgO nanorods samples such as 20 mg, 50 mg and 100 mg were loaded to the quartz reactor and their catalytic performances were evaluated under the same operating conditions. The results explained in terms of GHSV ($mlg_{cat}^{-1}h^{-1}$) respectively as in the Figure 4.32. CH_4 and CO_2 conversions as well as H_2/CO ratio decreased with the increasing amount of GHSV; this could be an excepted result since the contact time is also decreases with the decreasing amount of the catalyst. For instance, 100 mg catalyst gave way to 54% CH_4 and 72% CO_2 conversion with a 0.79 H_2/CO ratio while these values were increased to 70%, 80%, 0.87 ratio over 50 mg and 78%, 86%, 0.9 ratio over 20 mg catalyst, respectively.

In addition, the catalytic performance dependency on the change in GHSV values were more drastic at high temperatures such as 700 °C and more. In particular, when GHSV is 210,000 $mlg_{cat}^{-1}h^{-1}$, the catalytic activity improvement with increasing temperature were much lower at higher temperatures than the one in 84,000 $mlg_{cat}^{-1}h^{-1}$ and 42,000 $mlg_{cat}^{-1}h^{-1}$.

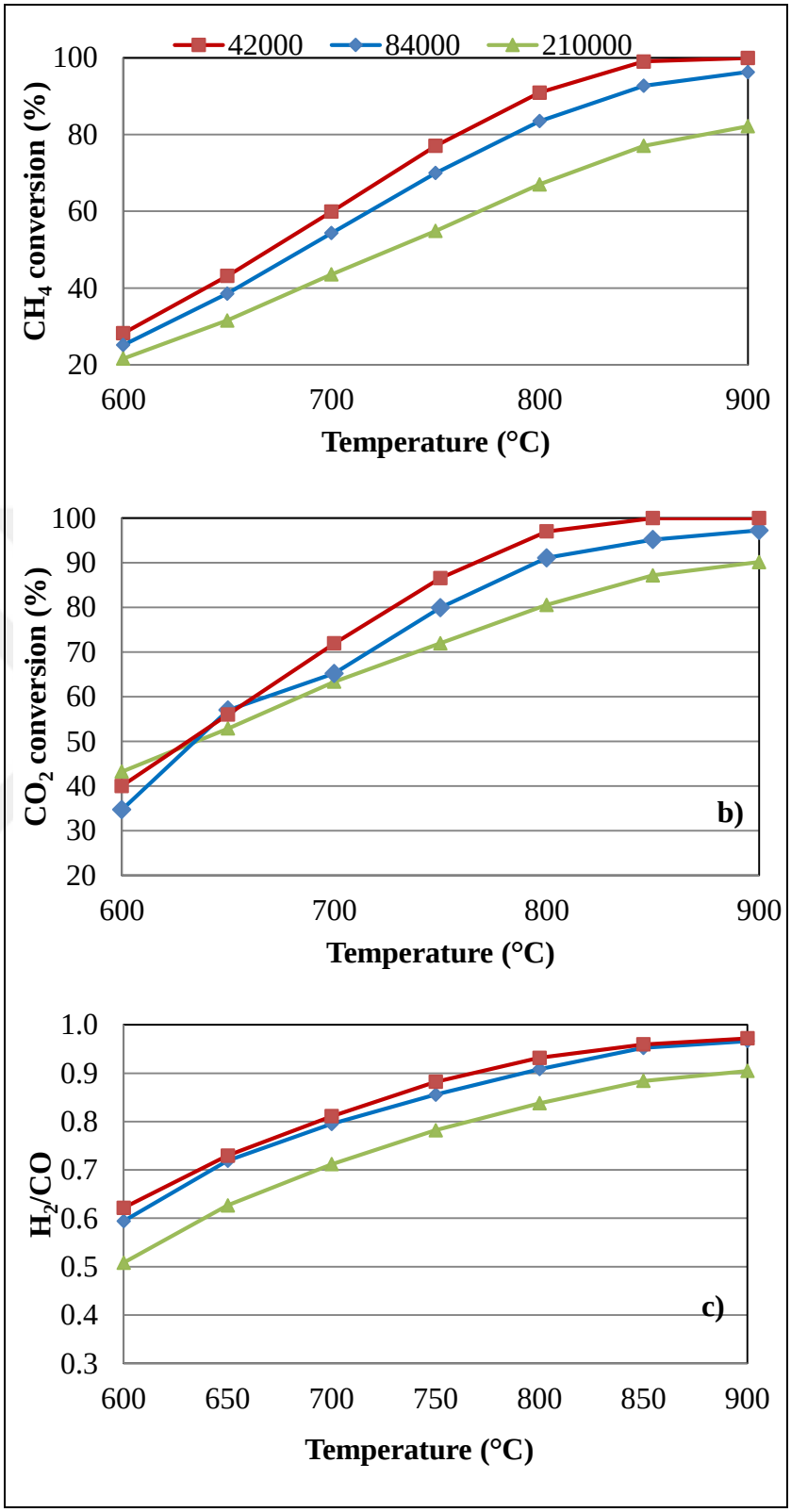

Figure 4.32. The effect of various GHSV ($ml g_{cat}^{-1} h^{-1}$) on the catalytic performance of NiCo impregnated MgO nanorods: a) CH_4 conversion, b) CO_2 conversion, c) H_2/CO ratio.

Therefore, it can be said that low catalyst amount such as 20 mg directly have an effect on the catalytic performance of NiCo impregnated MgO nanorods due to the inadequate contact time. Moreover, its lower dependency on temperature may be related to more coke deposition over the low amount of catalyst at lower temperatures; the catalyst may lose its catalytic activity faster since the active sites are more easily blocked by the coke.

4.5.5. Effect of Co Addition to Ni-based MgO

The sequential or co-impregnation of Co metals into Ni-based catalysts have been widely studied by various researchers since it may improve the catalytic activity through some beneficial effects of Co such as increasing CO_2 adsorption capacity or metal dispersion etc (Gao *et al*., 2017). On the other hand, in some studies, no contribution on the catalytic active was found, and it was even believed to deteriorate the catalyst activation enhancing the coke formation in some case (Ay and Üner, 2015). The role of Co seems to change from case to case depending on various factors such as the type of the support, metal size, amount or preparation methods. Therefore, the effect of Co co-addition to Ni metal over MgO nanorod structured on the catalytic performance was also examined at various temperatures over 50 mg of catalyst loading. The results can be seen in Figure 4.33.

The addition of 2wt.% of Co metal to 8wt.%Ni metals over nanorod structures slightly increased the catalytic activity up to 800 °C. After this temperature, it seemed to have no effect on the catalytic performance. As the results, the presence of Co has improved the CH_4 conversion into H_2 production, thus the product yield more. This may be due to the fact that Co really could enhance the catalyst resistance to coke compared to pure Ni-based catalyst. A time on stream study at 750 °C were also conducted for 8 h to understand the role Co on the catalytic performance of Ni-based MgO nanorod catalyst.

The results as in Figure 4.34 showed that both catalyst was quite stable during these hours, and both CH_4 and CO_2 conversions significantly higher in the presence of additional 2 wt.% of Co metal. Besides to enhanced coke resistance, Co addition may also improve CO_2 adsorption and thus the conversion as well.

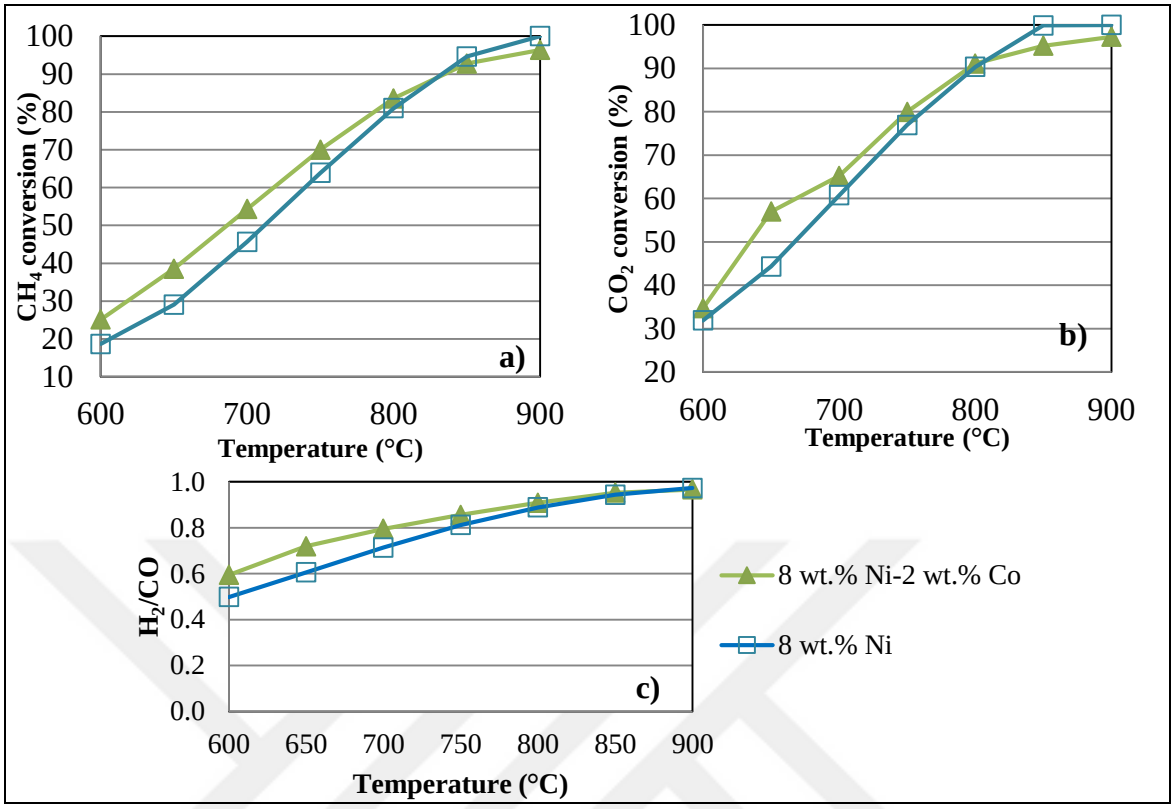

Figure 4.33. The catalytic performances of 8wt.%Ni-2wt.%Co and 8wt.%Ni impregnated MgO nanorods: a) CH_4 conversion, b) CO_2 conversion, c) H_2/CO ratio.

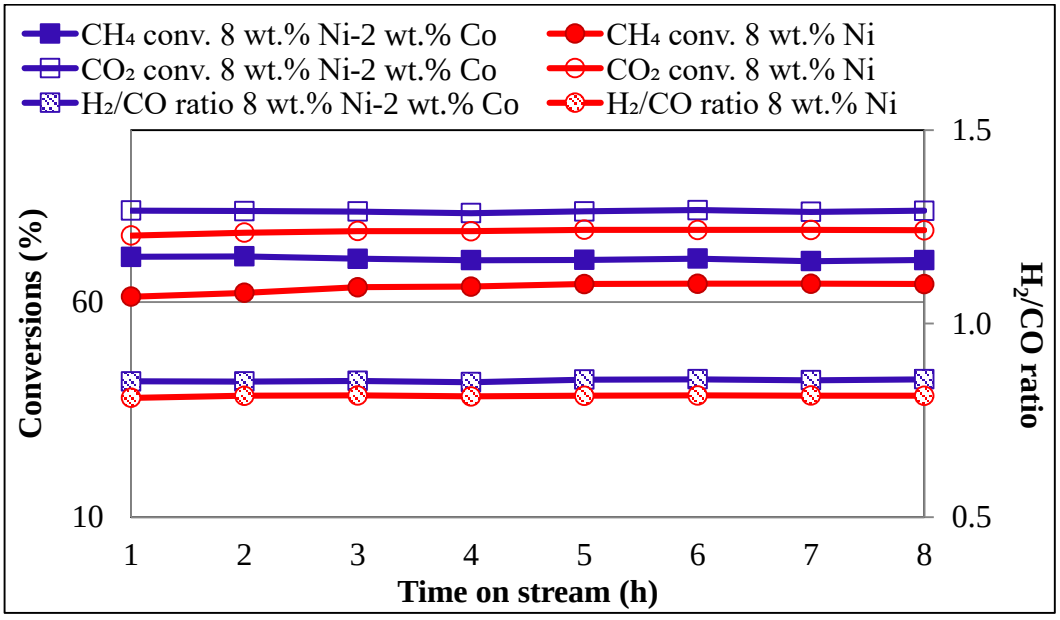

Figure 4.34. Catalytic performance of 8wt.%Ni -2 wt.% Co and 8wt.%Ni impregnated MgO nanorods during 8 h time on stream test.

In the absence of Co, both CH_4 and CO_2 conversions slightly increased with time. Since the product ratio remained the same, the products yields were analyzed separately. As seen in Figure 4.35, the product yields decreased with time in the absence of 2wt.%Co. Therefore, these increased conversions with lower products may be the reason of increased unwanted side reactions.

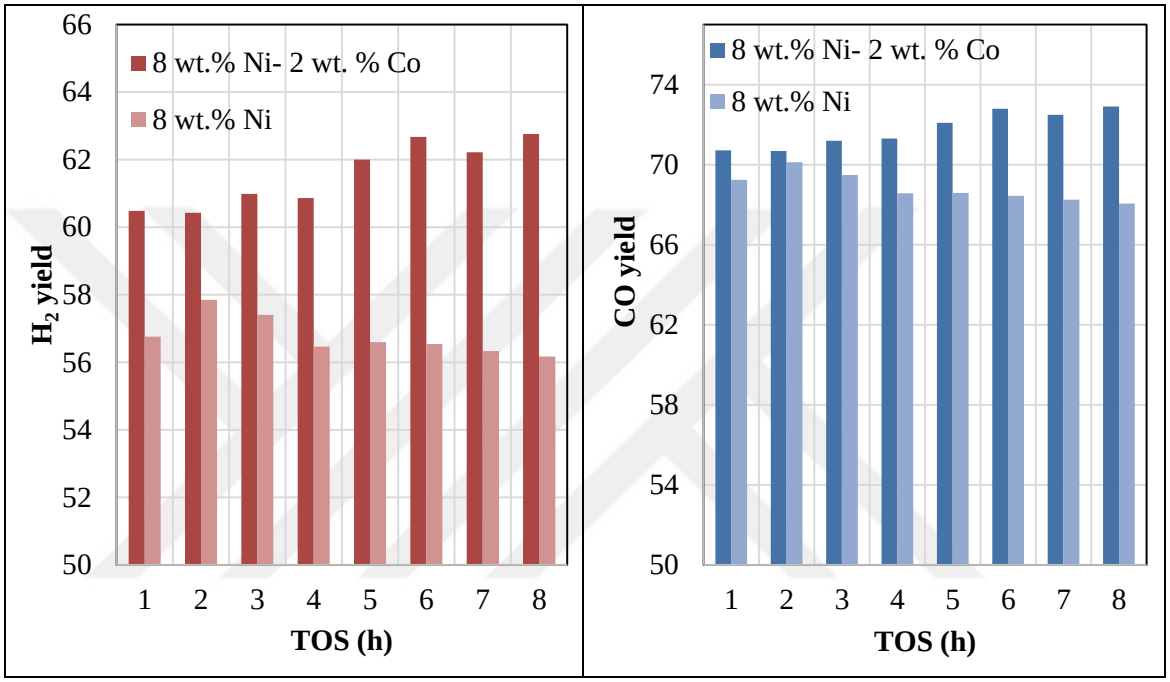

Figure 4.35. H_2 and CO product yieds of 8wt.%Ni-2wt.%Co and 8wt.%Ni impregnated MgO nanorods during 8 h time on stream test.

4.5.6. Characterization of Spent Ni-based MgO Nanorods

SEM chracterization (Figure 4.3) was conducted over 8wt.%Ni-2wt.%Co impregnated MgO nanorod catalysts spent at 600 °C with a 84,000 $mlg_{cat}^{-1}h^{-1}$ GHSV in order to investigate the catalyst morphology after the reaction. The SEM results in various magnifications are seen in Figure 4.36a-d. As it was clearly seen in Figure 4.36b, the catalyst structure like nano sheets as in fresh catalyst seemed to be preserved during reaction. In addition, the figure showed no carbon formation over these nano sheets. SEM chracterization of nanorod catalysts spent at 750 °C under 8 h TOS can also be seen in Figure B.1.

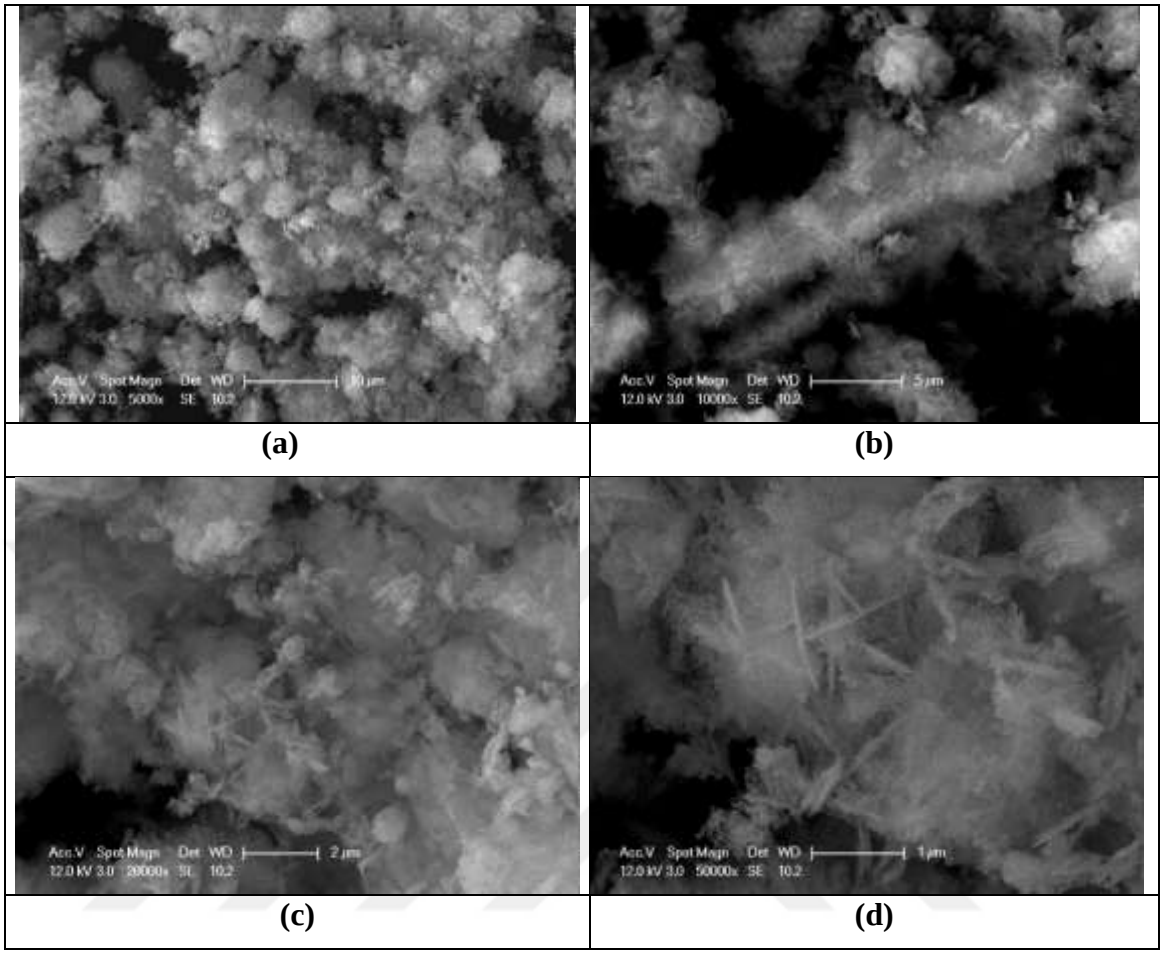

Figure 4.36. SEM images of spent Ni-based nanorod catalyst at 600 °C in various magnification: (a) 5000x, (b) 10000x, (c) 20000x, (d) 50000x.

4.5.7. Catalytic Performance Analysis of Ni-based MgO Nanorods over Monolithic Structures

As already mentioned in Section 4.3, the utilization of the monolithic structures in the industrial CDRM process can be beneficial since they have several virtues as to particulate systems such as high surface area, but better heat transfers and low pressure drop. Therefore, MgO nano structured materials was aimed to combine with the monolithic base mainly for the sake of obtaining an advanced surface area of the catalysts with low pressure drop. For this purpose, various coating procedure of MgO nanorods over cordierite type monoliths has been firstly synthesized as in the Table 3.5.

Among these catalysts, trial 1 and 2, in which the growth of the nanorods was wanted to be formed over the monolithic surfaces during the reaction process in the autoclave, could not be achieved successfully. The weighed of the dried samples in both trial showed very low amount of coating; the inefficient coating was even observable with naked eye. Therefore, these samples did not be coated by active metals for further studies. The poor coating of monoliths may be due to the weak adhesion of the reaction solution with cordierite surfaces. Also, some of the MgO nanorods, containing either Ni-Co metal solution or not, were accumulated the wall of the autoclave during reaction probably stemming from the evaporating and condensing process of the solution. On the other hands, the catalytic performances of monoliths containing MgO nanorod synthesized other ways (as explained in experimental section) monolithic catalysts were able to be tested. The results are as in Figure 4.36.

For comparison, the catalytic activity of the same amount of Ni-Co impregnated over MgO nanorods used in Section 4.5.2 and Ni-Co impregnated over MgO wash-coated monolith in Section 4.3.1 were also shown in the Figure 4.37. The same amount of Ni-Co/MgO wash-coated monolith were showed the highest catalytic activity in terms of CH_4 and CO_2 conversions till 800 °C. After this temperature, all catalysts resulted in the similar catalytic conversions. The catalytic activity of nanorod coated monolithic structures in the form of Ni-Co impregnated over calcined MgO coated monolith nearly led to the same conversions as in the form of Ni-Co impregnated over MgO coated than calcined monolith (SEM images of fresh Ni-based over nanorod coated monolith is in Figure B.2). This result showed that the preparation procedure of MgO nanorods over monoliths did not play any key role on the catalytic conversions at various temperatures varied from 600 °C to 800 °C. However, the catalytic activity was increased at almost all temperatures as to the one obtained by Ni-Co impregnated over MgO nanorods used in section 4.5.2. This improvement may be stemmed from the structure of monoliths since it may give way to better contact of the reactants with catalyst or the other enhanced properties of the monoliths such as more effective heat transfer; as similar results were obtained in Section 4.3 for Ni-Co/MgO wash-coated monolithic.

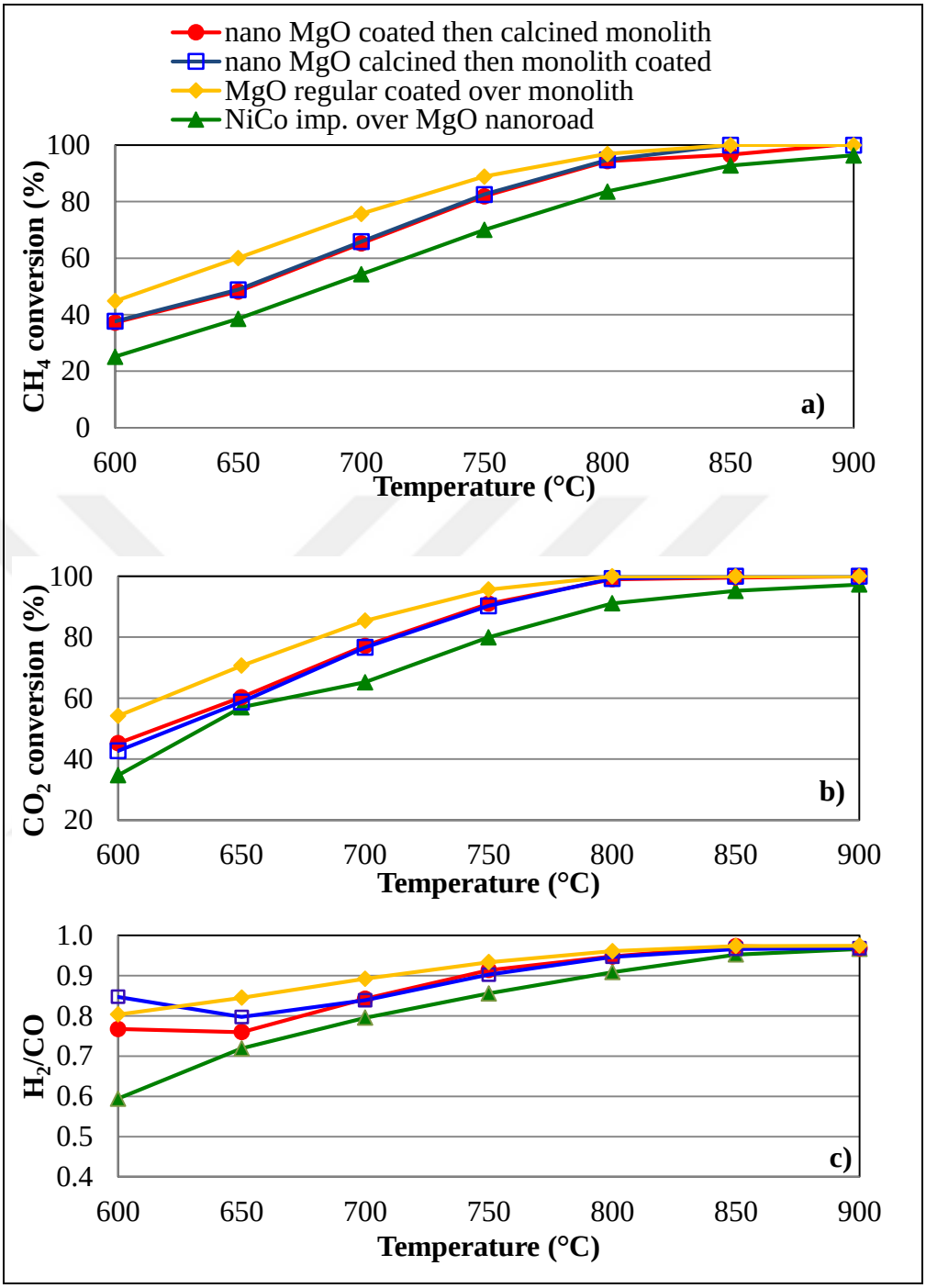

Figure 4.37. Performance test of various MgO coated monolithic structures: a) CH_4 conversion, b) CO_2 conversion, c) H_2/CO ratio.

On the other hand, regardless of the preparation procedure of Mg, the catalytic activity of Ni-Co impregnated over MgO nanorod coated monoliths was lower than that obtained over Ni-Co impregnated over MgO wash-coated monolith. This was an unexpected result since smaller size of the catalyst providing higher surface area has been known to have a

positive effect on the catalytic performance. MgO particulate used in Section 4.3 might diffuse better through the monolith channels than MgO nanorods. Indeed, coating with MgO nanorod was harder in catalyst preparation process than coating with MgO particulate.

In terms of syngas ratio (H_2/CO), monolithic structures still gave way to better product distribution. Ni-Co impregnated over MgO nanorods resulted significantly lower H_2/CO ratio at 600 °C comparing to other samples while the one obtained in Ni-Co impregnated over calcined MgO nanorod coated monolith was the highest. This case may show that RWGS side reaction may be more active over Ni-Co impregnated over MgO nanorods catalyst at this temperature since its spent SEM images in Section 4.5.6 did not show any kind of carbon formation.

In addition, the reduction procedure, which tends to influence the catalytic activity of the catalysts, may be inadequate for the Ni-Co impregnated over MgO nanorod samples The contact time of the H_2 with the catalyst surface may be better in the monolithic structures leading to better reduction.

4.6. Thermodynamic Consistency Analysis of the Experimental Results

A thermodynamic equilibrium product analysis for carbon dioxide reforming of methane with the assumption of carbon formation was computed by HSC Chemistry 6.0 software using the minimization for Gibbs free energy technique in order to determine the consistency of our experimental results with the thermodynamic limits. Nikoo and Amin (2011) have performed a similar thermodynamic calculation considering all feasible reactions in the presence of CO_2 and CH_4 and resulted in various products such as CO_2, CH_4, H_2, CO, C_2H_4, C_2H_6, H_2O, DME and methanol. However, C_2H_4, C_2H_6, methanol (MeOH) and dimetylether (DME) products were only trace amounts (like 10^{-4}, 10^{-6}, 10^{-8} and 10^{-18} moles respectively); therefore, they were disregarded in our calculations. However, pure solid graphite carbon was taken into account in chemical and phase equilibrium as gas species similar to other group's performance on this issue (Nikoo and Amin, 2011; Sun *et al*, 2011).

Figure 4.38 shows the thermodynamic analysis of CRDM in the presence of CH_4 (42.35%), CO_2 (42.35%) and N_2 (14.30%) feed compositions at various temperatures from 0 °C to 1000 °C and at 1 atm resulted H_2, CO, H_2O and C products in kmol. Carbon formation decreases with the increasing temperature and after 900 °C it is vanished. In addition, in this temperature range, H_2 and CO reaches maximum value while CH_4 and CO_2 amounts become zero. In other words, below at 900 °C, H_2/CO ratio is seemed to greater than 1 due to carbon formation (Pakhare *et al*, 2014).

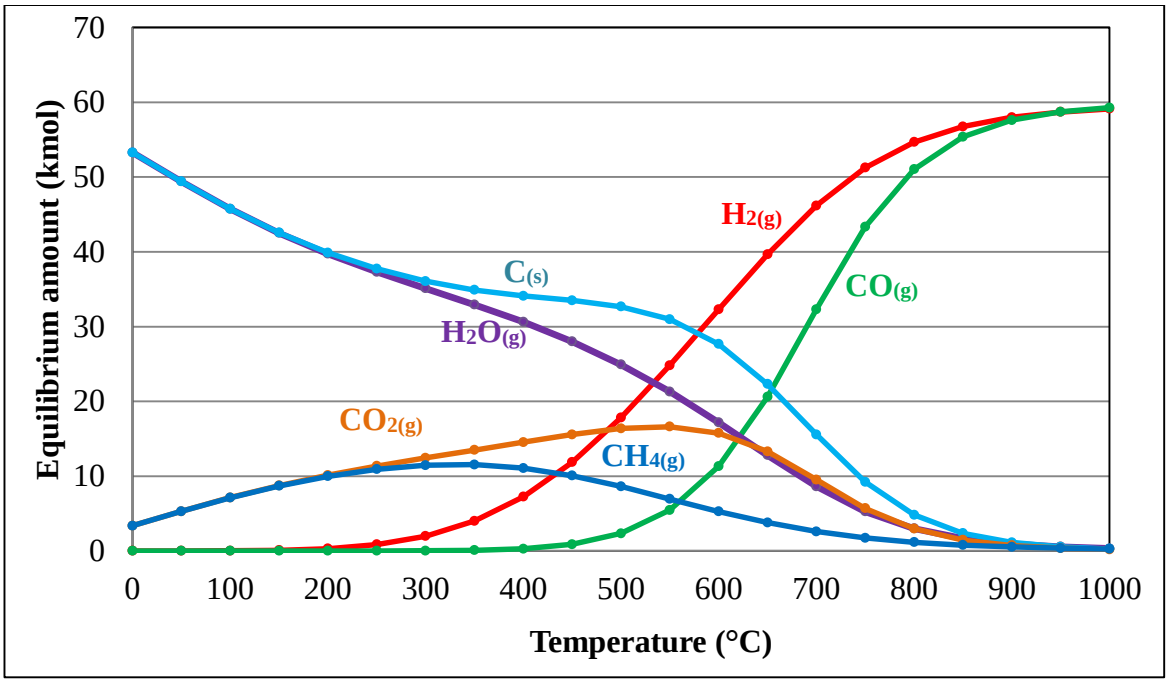

Figure 4.38. Thermodynamic equilibrium analysis for CDRM by HSC Chemistry 6.0.

In order to compare the numerical results obtained in the experimental and thermodynamic analysis, the highest catalytic activity results achieved over 100 mg 8wt.%Ni-2wt.%Co/MgO coated monolithic catalyst in Section 4.3.1 were used at various temperature form 600 °C to 900 °C under 70 ml/min feed flow.

As seen in Figure 4.39, CH_4 conversion and H_2/CO ratio of monolithic sample was lower than the thermodynamic results while the CO_2 conversion was over the thermodynamic limits, which is physically impossible. However, in literature, the higher or lower CH_4 and CO_2 conversions than the thermodynamic limits have been observed due to

the problems in quantifying the carbon deposition (Nikoo and Amin, 2011). For instance, similar to our results, at temperature 700 °C Nikoo and Amin (2011) has declared such lower thermodynamic CO_2 conversions (66.3%) in comparison with the experimental ones (91.7%) of Jablonski *et al.* (2005) while CH_4 conversion were higher in the thermodynamic result (91.5%) than the experimental one (72.4%). There was also a huge difference with the experimental and thermodynamic values of H_2/CO ratio below 700 °C; then, they were reached to the same value of approximately one with increasing temperature (Nikoo and Amin, 2011).

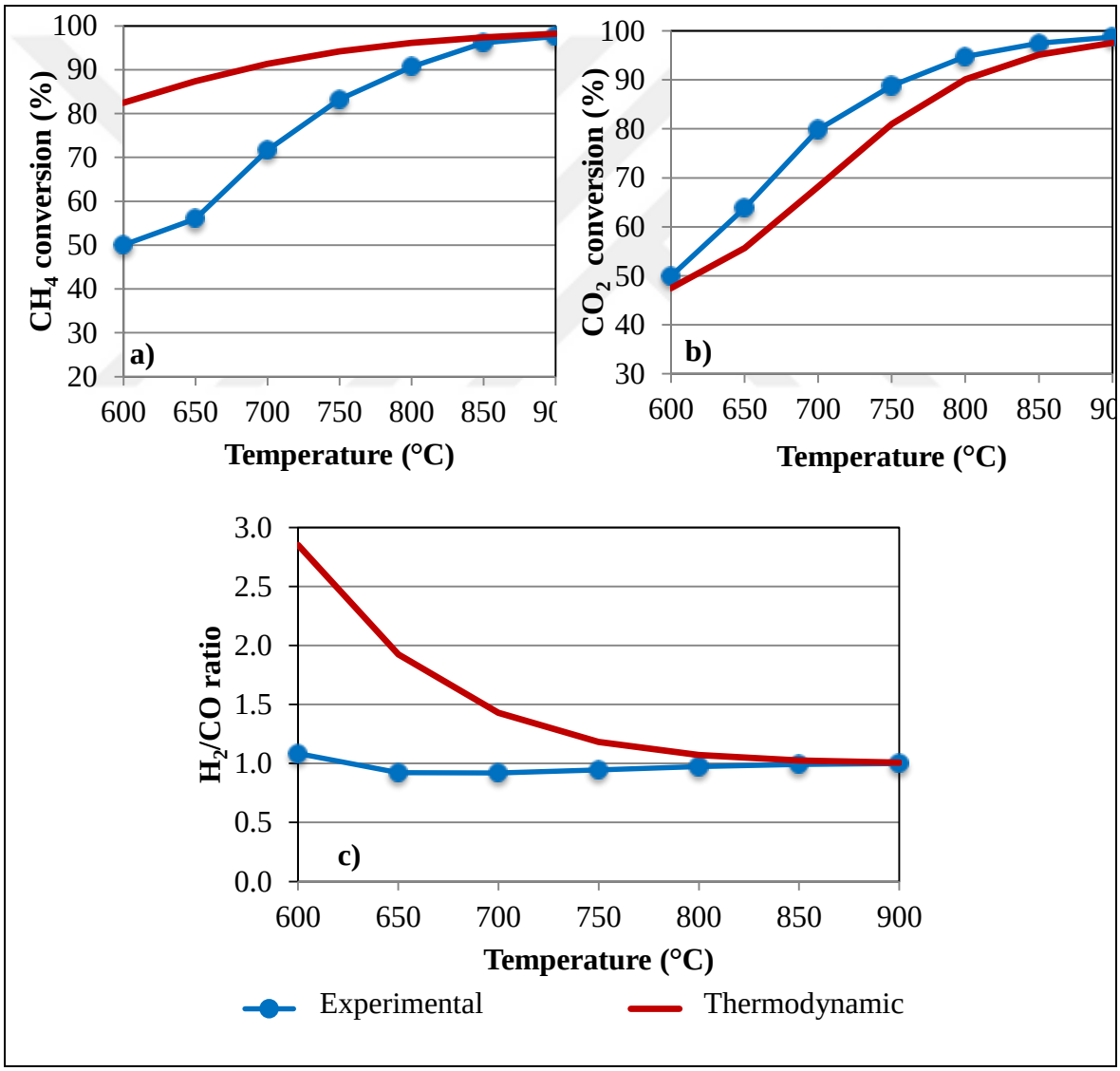

Figure 4.39. The experimental results of Ni-Co/MgO cordierite monolithic catalyst and thermodynamic results: (a) CH_4 equilibrium conversion (%), (b) CO_2 equilibrium conversion (%), (c) H_2/CO ratio.

In our case, the carbon balance for this catalyst was about 90-95% at low temperatures while it was close to 100% at higher temperatures. Moreover, both thermodynamic and experimental CH_4 and CO_2 conversions reached to approximately 100% when the temperature increased to 900 ˚C.

The thermodynamic product distribution in various feed ratio of CH_4/CO_2 such as ratio from 0.5 to 1.5 were also evaluated as in Figure 4.40. CH_4 conversion decreased with increasing amount of methane from 0.5 to 1.5 in the feed, while the CO_2 conversion increased since carbon dioxide is the limiting reactant in all these cases. In the experimental results of 8wt.%Ni-2wt.%Co/MgO monolithic at various CH_4/CO_2 ratios such as 0.5, 1 and 1.5 (Figure 4.7a-b), the catalytic activity trend of CH_4 and CO_2 conversions for each CH_4/CO_2 ratio were quite similar to the one obtained in the thermodynamic analysis (Figure 4.40a-b). However, there were some differences in the trends of experimental H_2/CO syngas ratio (Figure 4.7c) as to thermodynamic ones (Figure 4.40c). Although lowest H_2/CO ratio was obtained in the presence of 0.5 CH_4/CO_2 ratio in both analysis, the experimental value was nearly the same in the presence of 1 and 1.5 CH_4/CO_2 ratio while thermodynamic ratio was higher with 1.5 CH_4/CO_2 ratio. However, in all cases experimental product ratio was lower than the thermodynamic ratio.

In addition, effect of various feed flow rates such as 30 ml/min, 50 ml/min and 70 ml/min on the thermodynamic analysis of CDRM has been studied. The results can be seen in Figure 4.41. The change in the feed flow rate did not influence the thermodynamic activity at all. Finally, the effect of oxygen addition (from 0% to 3%) to the feed on the thermodynamic carbon formation was evaluated on at various temperatures from 600 °C to 900 °C. The results are as in Figure 4.42.

As it was seen in Figure 4.42, as the temperature increased the coke formation decreased as expected, and this decrease is more dramatic in the presence of oxygen. For example, coke deposition fully suppresses at 850 ˚C in the presence of 2-3% oxygen while it diminished at 900 ˚C when the oxygen content of the feed was 1%; there was still coke deposition at 900 ˚C if no oxygen added to the feed. The addition of 3% O_2 to the feed decreased the carbon deposition amount from 9.23 kmol to 5.85 kmol at 750 °C.

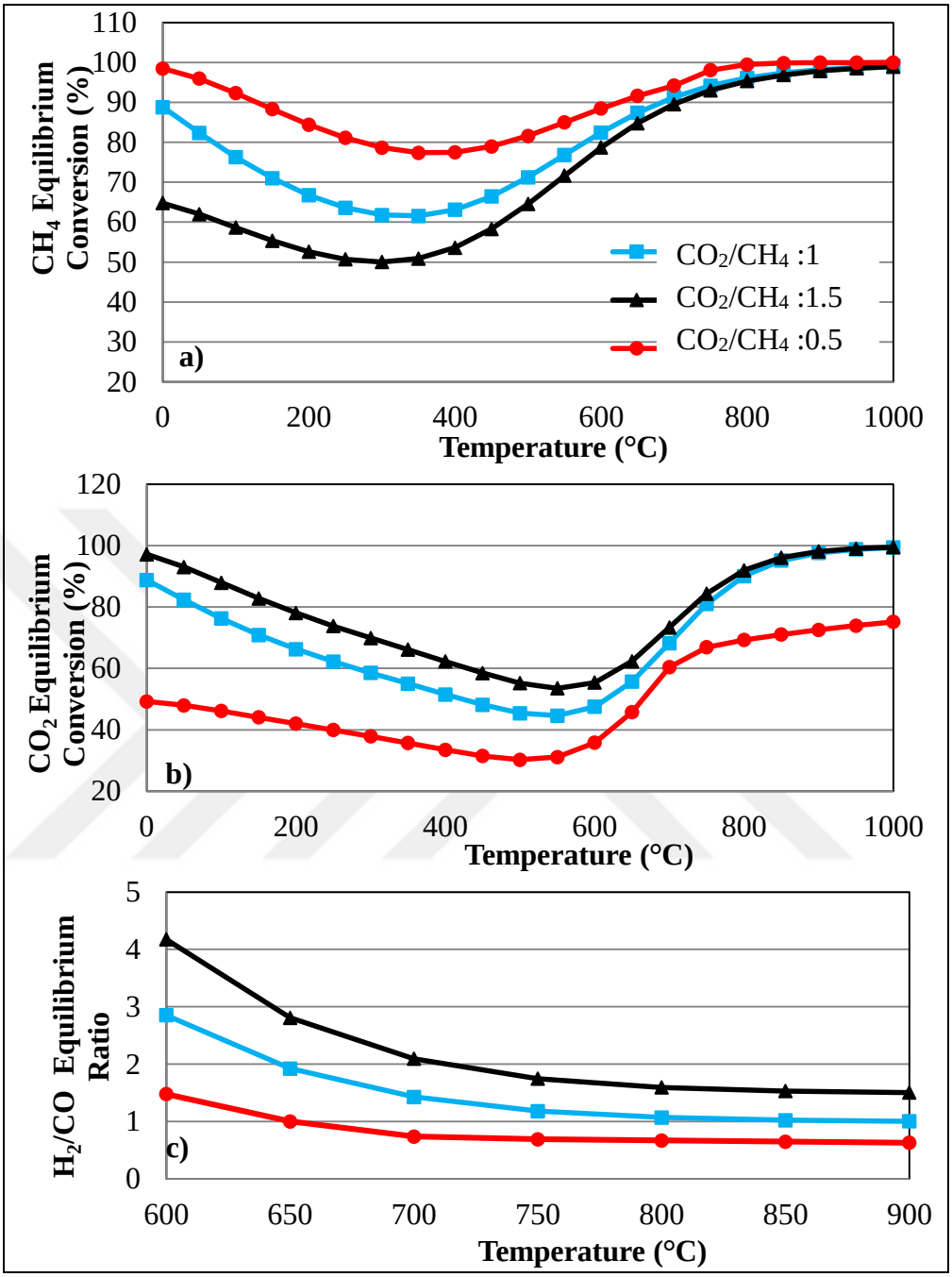

Figure 4.40. Thermodynamic results of CDRM at various feed ratio of CH_4/CO_2: (a) CH_4 equilibrium conversion (%), (b) CO_2 equilibrium conversion (%), (c) H_2/CO ratio.

Thus, it can be said that almost all experimental results that we obtained are consistent with the thermodynamic analysis. The only exception is that the thermodynamic CO_2 conversion was found to be lower than actual value in some cases apparently due to the fact that the carbon deposition in actual experiments could not be fully accounted.

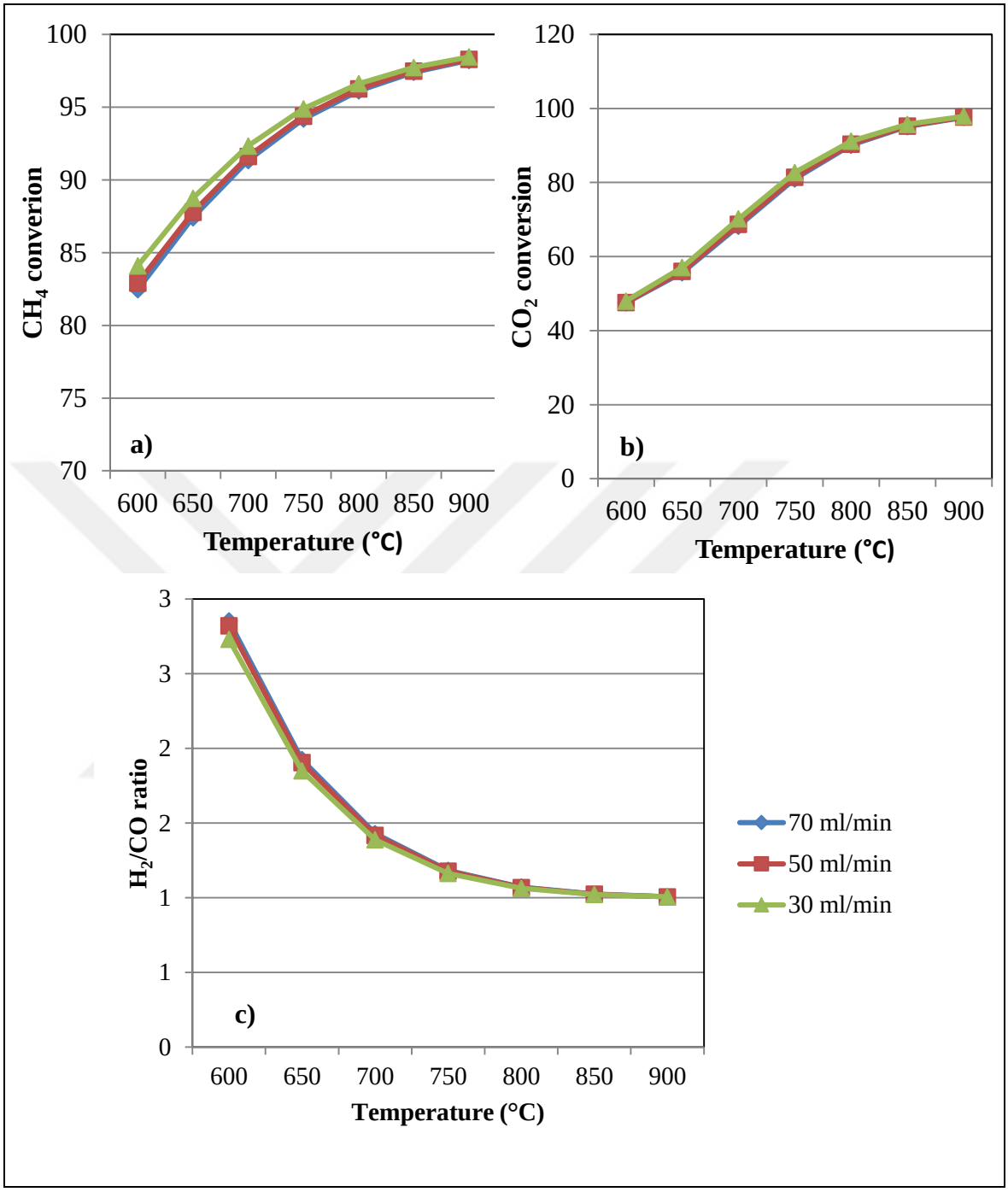

Figure 4.41. Thermodynamic results of CDRM at various feed flow rates: (a) CH_4 equilibrium conversion (%), (b) CO_2 equilibrium conversion (%), (c) H_2/CO ratio.

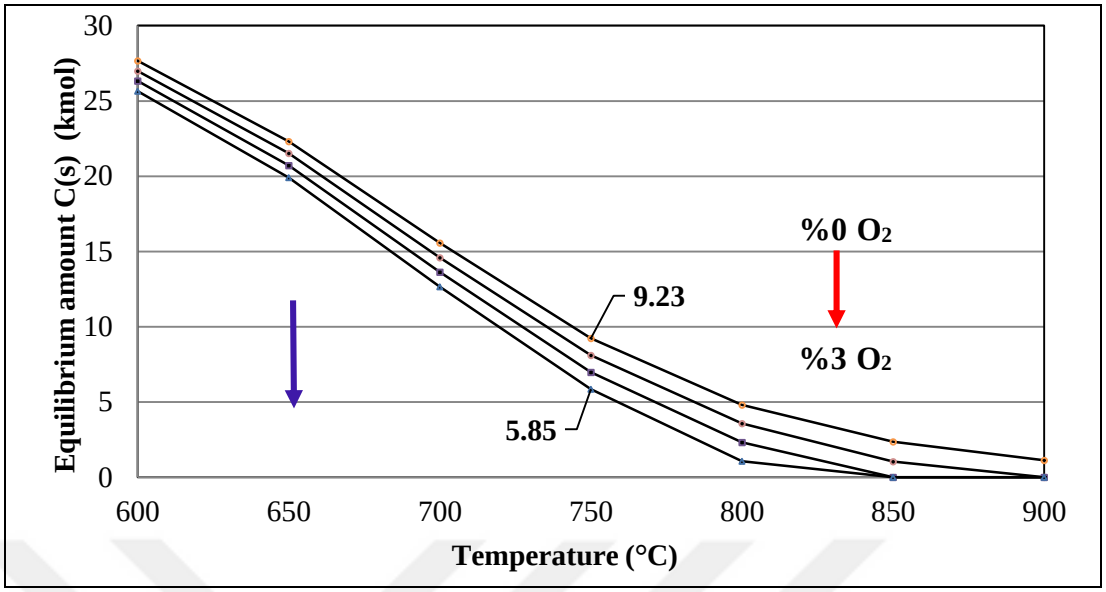

Figure 4.42. Effect of oxygen addition to the feed on the thermodynamic carbon formation.

5. CONCLUSION

5.1. Conclusions

The main objective of this study was to improve the economic feasibility of CDRM process by reducing the reaction temperature and/or pressure drop with high H_2 and CO product yield with a good stability. For this purpose, the photocatalytic assistance in CDRM over various photocatalysts such as Ni-based TiO_2 and ZnO was evaluated first with the hope to decrease reaction temperature. Then the studies were proceeded with the catalytic evaluation of Ni-based catalyst over various structured materials like monolith, nanowire or nanorod to improve activity and stability as well as reducing the pressure drop.

In the works involving photocatalyst assisted CDRM,8wt.%Ni-2wt.%Co over various semiconductor supports such as TiO_2 and ZnO as well as MgO with sensitizers like cis, bis ((isothiocyanato) bis (2,2-bipyridyl-4,4-dicarboxylato) ruthenium (II)) dye and $CH_3NH_3PbI_xCl_{3-x}$ perovskite were tested at various temperatures and lamp sources. The main conclusions can be summarized as following:

- Ni-based catalysts over TiO_2 and ZnO as well as MgO did not show any kind of catalytic conversions to H_2 and CO product at lower than 300 °C.
- Both TiO_2 and ZnO were not be able to work as photocatalysts at a temperature range from room to 500 °C either in the presence of visible or UV ligh sources for CDRM process.
- 8 h irridation time over photocatalysts did not make any contirbution for the reaction under contiouns flow of CO_2 and CH_4 gases.
- Neither dye addition nor $CH_3NH_3PbI_xCl_{3-x}$ perovskite structure improved the photocatalytic property of TiO_2.

In the second part of the study, 8wt.%Ni-2wt.%Co over monolithic structures coated with MgO, CeO_2 and SiO_2 were catalytically tested at temperatures from 600 °C to 900 °C,

and then the effect of monolithic structure in CDRM were investigated in more details. The following conclusions can be drawn from this part of the study:

- 8wt.%Ni-2wt.%Co metals over MgO coated cordierite monolith performed better than the coated mullite monolith and particulate catalysts.
- The wash-coated SiO_2 and CeO_2 cordierite monoliths were resulted lower catalytic activity than the wash-coated MgO cordierite monoliths.
- 8wt.%Ni-2wt.%Co metals over MgO coated cordierite monolith can effectively work under various GHSV such as 18000, 30000, 42000 $mlg_{cat}^{-1}h^{-1}$ with nearly the same catalytic activity.
- The closest H_2/CO ratio to unity was obtained in the presence of 1 and 1.5 of reactant CH_4/CO_2 ratio.
- SEM-EDX results showed that Ni and Co active metals were well dispersed over MgO wash-coated cordierite monoliths with 7.69 wt.% and 1.88 wt.%, respectively. These amounts were decreased after the reaction; high coke formation was observed over the catalysts.
- The presence of 3% O_2 in the feed had significantly reduced the coke formation over 8wt.%Ni-2wt%Co metals over MgO coated cordierite at 750 ℃ the without changing the catalytic activity at all.
- As to the XRD studies, the crystalline phases of 8wt.%Ni-2wt.%Co metals over MgO coated monoliths was not changed in the presence of 3% O_2 to the feed; moreover, performing XPS scans for Ni 2p and Co 2p was possible over these samples while the coke over the samples used in the absence of O_2 could not be carried out for the active metals.
- 8wt.%Ni-2wt%Co metals over MgO coated cordierite monoliths were highly stable during 48 hours in the presence of 3% O_2 at 750 °C under 42000 $mlg_{cat}^{-1}h^{-1}$ GHSV with a CH_4/CO_2 feed ratio of 1.

In the third part of the study, the performance test of $Ni_xCo_{3-x}O_4$ nanowire structures (x=0, 0.5 and 1) was evaluated at temperatures from 600 ℃ to 900 ℃ under various operating conditions. The major findings are as follows:

- The amount of urea, the concentration of the active metal solutions and the mixing type had key roles in the synthesis of $Ni_xCo_{3-x}O_4$ nanowire structures.
- The reduction procedure of $Ni_xCo_{3-x}O_4$ nanowire structures affected the catalytic performance; the better product distribution was obtained when the catalyst was reduced at 600 °C under 30 ml/min H_2 for 1 h.
- Among various $Ni_xCo_{3-x}O_4$ nanowire structures (x=0, 0.5 and 1), $Ni_2Co_1O_4$ showed highest CH_4 and CO_2 conversions, while $Ni_{0.5}Co_{2.5}O_4$ led to higher H_2/CO ratio.
- The catalytic performance of $Ni_{0.5}Co_{2.5}O_4$ nanowire structure at various feed flows such as 15, 30, 50 and 70 ml/min with a CH_4/CO_2 ratio of 1 at 750 °C showed that the catalytic activity of catalyst was sensitive to the change of flow rate under the same conditions.
- The time on stream tests for 8 hours showed that both reduced and unreduced $Ni_{0.5}Co_{2.5}O_4$ and $Ni_2Co_1O_4$ nanowire catalysts were not stable at 750 °C even if 3% of O_2 to the feed and/or 1 wt.% Pd was added to the catalysts.
- SEM characterization showed that $Ni_{0.5}Co_{2.5}O_4$ nanowire samples kept their wire structures after the reduction and the CDRM reaction in the presence of O_2 at 600 °C while, in the absence of O_2, they mostly lost their structure and resulted in high amount of coke formation.
- The XRD pattern of $Ni_{0.5}Co_{2.5}O_4$ nanowire was changed significantly after the reduction and reaction processes comparing to the freshly synthesized catalyst.

In the fourth part of the study, the catalytic performance of 8wt.%Ni-2wt.%Co over MgO nanorod and 8wt.%Ni-2wt.%Co over MgO nanorod coated monolith structures were investigated at various operating conditions. The main conclusions are as follows:

- As to SEM analysis, the preparation method of the MgO nanorod as well as the method of addition of active metals over MgO nanorod have an influence on the surface morphology of the catalysts. The impregnation of the Ni and Co active metals seemed to be better dispersed over MgO nanorods.
- XRD analysis of fresh and reduced samples of 8wt.%Ni-2wt.%Co impregnated MgO nanorods showed the presence of metal Ni and Co after reduction procedure. XPS scans for Ni2p and Co2p showed similar phases in both situations.

- The calcination procedure of MgO, in the presence of air flow or not, did not affect the catalytic performance of 8wt.%Ni-2wt.%Co impregnated MgO nanorods.
- The procedure for the addition of active metals over MgO nanorod had an effect on the catalytic performance. Ni-Co impregnated over MgO nanorod showed similar and reproducible catalytic activity to the one with Ni-Co impregnated on particulate MgO; however, the results obtained over the co-prepared Ni-Co-MgO nanostructured catalysts was not reproducible probably due to un-uniform distribution of active metals in MgO.
- As the GHSV of the feed flow was increased, the catalytic conversions of 8wt.%Ni-2wt.%Co impregnated MgO nanorods were decreased due to the decrease in the contact time of reactants with catalyst surface.
- The addition of 2wt.%Co to 8wt.%Ni impregnated MgO nanorods slightly increased the catalytic conversions as well as the product ratio (CO/H_2) at almost all temperature range from 600 °C to 900 °C.
- SEM results of spent 8wt.%Ni-2wt.%Co impregnated MgO nanorod catalysts at 600 °C with 84,000 $ml g_{cat}^{-1} h^{-1}$ GHSV did not lead any coke deposition.
- The change of coating procedure of MgO nanorod over cordierite monolith as nano MgO first coated and then calcined or calcined MgO was directly coated over monolith did not change the performance significantly. However; in both cases, the catalytic activity of monolithic catalyst was higher than the direct use of Ni-Co impregnated MgO nanorod; but lower than Ni-Co impregnated over particulate MgO coated monolithic structure.

5.2. Recommendation

Considering the results obtained in this study, the following recommendations may be beneficial for the future work:

- In order to improve the photocatalytic assistance in CDRM, the ways of increasing the light sensitivity of current photocatalysts and exposure time for the light were needed to be improved.

- CDRM kinetic studies over 8wt.%Ni-2wt.%Co metals over MgO coated cordierite monoliths in the presence and absence of the oxygen can be performed in order to understand the effect of low oxygen better.
- In order to increase the stability of the $Ni_xCo_{3-x}O_4$ nanowire structures for CDRM process, the other ways of growing lower amount of $Ni_xCo_{3-x}O_4$ nanowire over monolithic structure should be developed since the amount of Ni and Co used have significant impact on the CDRM catalytic stability.
- Since the monolithic form of the Ni-Co impregnated MgO nanorod structures were promising, the alternative ways of the coating or growing of MgO nanorods over monoliths can be investigated. Other materials such as mullite type monoliths or some binding chemicals can be used in order to obtain better coating or growth of MgO nanorods.
- More characterizations techniques can be conducted for further understanding of synthesized $Ni_xCo_{3-x}O_4$ nanowire and MgO nanorods structures. For instance, BET surface area analysis for the evaluation of the nanostructure morphology in CDRM, SEM-EDX mapping tests for investigation the Ni and Co active metal dispersion over $Ni_xCo_{3-x}O_4$ nanowire structures and MgO nanorods, ICP (inductively coupled plasma) analysis for finding metal loadings in all cases or TEM tests for the particulate size analysis can be performed.
- CDRM kinetic experiments of $Ni_xCo_{3-x}O_4$ nanowire structures as well as Ni-Co impregnated of MgO nanorods can be performed to understand the reaction mechanism over these structures. Morover, conducting a FTIR-DRIFT analysis can be used to figure out the reaction mechanism.
- Performing a thermodynamic analysis prior to each type of experimental studies can be helpful to discover the effect of operating conditions on the catalyst performances and to design the reaction system.

REFERENCES

Abdollahifar, M., M. Haghighi and A. A. Babaluo, 2014, "Syngas production via dry reforming of methane over Ni/Al_2O_3–MgO nanocatalyst synthesized using ultrasound energy", *Journal of Industrial and Engineering Chemistry,* Vol. 20, pp. 1845–1851.

Abdollahifar, M., M. Haghighi, A. A. Babaluo and S. K. Talkhoncheh, 2016, "Sono-synthesis and characterization of bimetallic Ni–Co/Al–MgO nanocatalyst: Effects of metal content on catalytic properties and activity for hydrogen production via CO_2 reforming of CH_4", *Ultrasonics Sonochemistry,* Vol.31, pp. 173–83.

Aiello, R., J. E. Fiscus, H. C. Loye and M. D. Amiridis, 2000, "Hydrogen production via the direct cracking of methane over Ni/SiO_2: Catalyst deactivation and regeneration", *Applied Catalysis A: General,* Vol. 192, pp. 227–234.

Al-Fatesh, A., 2015, "Suppression of carbon formation in CH_4–CO_2 reforming by addition of Sr into bimetallic Ni–Co/γ-Al_2O_3 catalyst", *Journal of King Saud University – Engineering Sciences,* Vol. 27, pp. 101–107.

Al-Hazmi, F., F. Alnowaiser, A. A. Al-Ghamdi, A. A. Al-Ghamdi, M. M. Aly, R. M. Al-Tuwirqi and F. El-Tantawy, 2012, "A new large – scale synthesis of magnesium oxide nanowires: Structural and antibacterial properties", *Superlattices Microstructure,* Vol. 52, pp. 200–209.

Amin, R., B. Liu, Z. B. Huang and Y. C. Zhao, 2016, "Hydrogen and syngas production via CO_2 dry reforming of methane over Mg/La promoted Co-Ni/MSU-S catalyst", *International Journal of Hydrogen Energy,* Vol. 41, pp. 807–819.

Anpo, M., 2013, "Photocatalytic reduction of CO_2 with H_2O on highly dispersed Ti-oxide catalysts as a model of artificial photosynthesis", *Journal of CO_2 Utilization,* Vol. 1, pp. 8–17.

Arifin, K., E. H. Majlan, W. R. W. Daud and M. B. Kassim, 2012, "Bimetallic complexes in artificial photosynthesis for hydrogen production: A review", *International Journal of Hydrogen Energy*, Vol. 37, pp. 3066–3087.

Asencios, Y. J. O., J. D. A. Bellido and E. M. Assaf, 2011, "Synthesis of NiO–MgO–ZrO catalysts and their performance in reforming of model biogas", *Applied Catalysis A: General*, Vol. 397, pp. 138–144.

Assabumrungrat, S., S. Charoenseri, N. Laosiripojana, W. Kiatkittipong and P. Praserthdam, 2009, "Effect of oxygen addition on catalytic performance of Ni/SiO_2.MgO toward carbon dioxide reforming of methane under periodic operation", *International Journal of Hydrogen Energy*, Vol. 34, pp. 6211– 6220.

Ay, H., and D. Üner, 2015, "Dry reforming of methane over CeO_2 supported Ni, Co and Ni–Co catalysts", *Applied Catalysis B: Environmental*, Vol. 179, pp. 128–138.

Baudouin, D., U. Rodemerck, F. Krumeich, A. Mallmann, K. Szeto, H. Ménard, L. Veyre, J-P. Candy, P. B. Webb, C. Thieuleux and C. Copéret, 2013, "Particle size effect in the low temperature reforming of methane by carbon dioxide on silica-supported Ni nanoparticles", *Journal of Catalysis*, Vol. 297, pp. 27–34.

Benrabaa, R., H. Boukhlouf, A. Lofberg, A. Rubbens, R. Vannier, E. Bordes-Richard and A. Barama, 2012, "Nickel ferrite spinel as catalyst precursor in the dry reforming of methane: Synthesis, characterization and catalytic properties", *Journal of Natural Gas Chemistry*, Vol. 21, pp. 595–604.

Bian, Z., I. Y. Suryawinata, and S. Kawi, 2016, "Highly carbon resistant multicore-shell catalyst derived from Ni-Mgphyllosilicate nanotubes@silica for dry reforming of methane", *Applied Catalysis B: Environmental*, Vol. 195, pp. 1–8.

Budiman, A. W., S.-H. Song, T.-S. Chang, C.-H. Shin and M.-J. Choi, 2012, "Dry reforming of methane over cobalt catalysts: A literature review of catalyst development", *Catalysis Surveys from Asia,* Vol. 16, pp.183–197.

Bradford, M. C. J. and M. A. Vannice, 1996, "Catalytic reforming of methane with carbon dioxide over nickel catalysts I. Catalyst characterization and activity", *Applied Catalysis A: General,* Vol. 142, pp. 73–96.

Byrappa, K. and T. Adschiri, 2007, "Hydrothermal technology for nanotechnology", *Progress in Crystal Growth and Characterization of Materials,* Vol. 53, 117–166.

Chang, S., Z. Zaınal, K. Tan, N. A. Yusof, W. M. D. W. Yusoff and S. R. S. Prabaharan, 2012, "Surface morphology and crystallinity of metal oxides in nickel-cobalt binary system", *Sains Malaysiana,* Vol. 41, pp. 465-470.

Chen, L., Q. Zhu and R. Wu, 2011, "Effect of Co-Ni ratio on the activity and stability of Co-Ni bimetallic aerogel catalyst for methane oxy-CO_2 reforming", *International Journal of Hydrogen Energy,* Vol. 36, pp. 2128–2136.

Chen, W., W. Sheng, F. Cao and Y. Lu, 2012, "Microfibrous entrapment of Ni/Al_2O_3 for dry reforming of methane: Heat/mass transfer enhancement towards carbon resistance and conversion promotion", *International Journal of Hydrogen Energy,* Vol. 37, pp. 18021–18030.

Chen, Z., S. Wang, W. Liu, X. Gao, D. Gao, M. Wang and S. Wang, 2016, "Morphology-dependent performance of Co_3O_4 via facile and controllable synthesis for methane combustion", *Applied Catalysis A: General,* Vol. 525, pp. 94–102.

Chen, S., W. Song, H. Lin, S. Wang, S. Biswas, M. Mollahosseini, C. Kuo, P. Gao and S. L. Suib, 2016b, "Manganese oxide nanoarray-based monolithic catalysts: Tunable morphology and high efficiency for CO oxidation", *ACS Applied Materials and Interfaces,* Vol. 8, pp 7834–7842.

Chen, Z., S. Wang, Y. Ding, L. Zhang, L. Lv, M. Wang and S. Wang, 2017, "Pd catalysts supported on Co_3O_4 with the specified morphologies in CO and CH_4 oxidation", *Applied Catalysis A: General,* Vol. 532, pp. 95–104.

Ciambelli, P., V. Palma and E. Palo, 2010, "Comparison of ceramic honeycomb monolith and foam as Ni catalyst carrier for methane autothermal reforming", *Catalysis Today*, Vol. 155, pp. 92–100.

Corthals, S., T. Witvrouwen, P. Jacobs and B. Sels, 2011, "Development of dry reforming catalysts at elevated pressure: D-optimal vs. full factorial design", *Catalysis Today*, Vol. 159, pp. 12–24.

Di Cosimo, J. I., V. K. Diez**,** C. Ferretti and C. R. Apesteguia, 2014, "Basic catalysis on MgO: Generation, characterization and catalytic properties of active sites", The *Royal Society of Chemistry*, Vol. 26, pp. 1–28.

Damyanova, S., B. Pawelec**,** K. Arishtirova and J. L. G. Fierro, 2012, "Ni-based catalysts for reforming of methane with CO_2", *International Journal of Hydrogen Energy*, Vol. 37, pp. 15966–15975.

Danilova, M. M., Z. A. Fedorova, V. A. Kuzmin, V. I. Zaikovskii, A. V. Porsin and T. A. Krieger, 2015, "Combined steam and carbon dioxide reforming of methane over porous nickel based catalysts*", Catalysis Science and Technology*, Vol. 5, pp. 2761-2768.

Delavari, S. and N. A. S. Amin, 2016a, "Photocatalytic conversion of CO_2 and CH_4 over immobilized titania nanoparticles coated on mesh: Optimization and kinetic study", *Applied Energy*, Vol. 162, pp. 1171-1185.

Delavari, S. and N. A. S. Amin , 2016b, "Photocatalytic conversion and kinetic study of CO_2 and CH_4 over nitrogen-doped titania nanotube arrays", Journal of Cleaner Production, Vol. 111, pp. 143-154.

Deutschmann, O., R. Schwiedernoch, L. I. Maier and D. Chatterjee, 2001, "Natural gas conversion in monolithic catalysts: Interaction of chemical reactions and transport phenomena", *Studies in Surface Science and Catalysis*, Vol. 136, pp. 251–258.

Dimitrijevic, N. M., B. K. Vijayan, O. G. Poluektov, T. Rajh, K. A. Gray, H. He and P. Zapol, 2011, "Role of water and carbonates in photocatalytic transformation of CO_2 to CH_4 on titania", *Journal of the American Chemical Society*, Vol. 133, pp. 3964–3971.

Doherty, M. D., D. C. Grills, J. T. Muckerman, D. E. Polyansky, E. Fujita, 2010, "Toward more efficient photochemical CO_2 reduction: Use of CO_2 or photogenerated hydrides", *Coordination Chemistry Reviews*, Vol. 254, pp. 2472–2482.

Dou, J. and H. C. Zeng, 2014, "Integrated networks of mesoporous silica nanowires and their bifunctional catalysis−sorption application for oxidative desulfurization", *ACS Catalysis*, Vol. 4, pp. 566−576.

Du, X., D. Zhang, L. Shi, R. Gao and J. Zhang, 2013, "Coke- and sintering-resistant monolithic catalysts derived from in situ supported hydrotalcite-like films on Al wires for dry reforming of methane", *Nanoscale*, Vol. 5, pp. 2659–2663.

Du, S., W. Tang, Y. Guo, A. Binder, E. A. Kyriakidou, T. J. Toops, S. Wang, Z. Ren, S. Hoang and P. X. Gao, 2017, "Understanding low temperature oxidation activity of nanoarray-based monolithic catalysts: from performance observation to structural and chemical insights", *Emission Control Science and Technology*, Vol. 3, pp. 1-19.

Estephane, J., S. Aouad, S. Hany, B. E. Khoury, C. Gennequin, H. E. Zakhem, J. E. Nakat, A. Aboukais and E. A. Aad, 2015, "CO_2 reforming of methane over Ni-Co/ZSM5 catalysts. Aging and carbon deposition study", *International Journal of Hydrogen Energy*, Vol. 40, pp. 9201–9208.

Fan, M., A. Z. Abdullah and S. Bhatia, 2010, "Utilization of greenhouse gases through carbon dioxide reforming of methane over Ni–Co/MgO–ZrO_2: Preparation, characterization and activity studies", *Applied Catalysis B: Environmental*, Vol. 100, pp. 365–377.

Fan, A. M., Zuhairi and A. S Bhatia, 2011, "Hydrogen production from carbon dioxide reforming of methane over Ni–Co/MgO–ZrO_2 catalyst: Process optimization", *International Journal of Hydrogen Energy*, Vol. 36, pp. 4875-4886.

Finn, C., S. Schnittger, L. J. Yellowlees and J. B. Love, 2012, "Molecular approaches to the electrochemical reduction of carbon dioxide", *Chemical Communications*, Vol. 48, pp. 1392–1399.

Frontera, P., A. Macario, A. Aloise, P. L. Antonucci, G. Giordano and J. B. Nagy, 2013, "Effect of support surface on methane dry-reforming catalyst preparation", *Catalysis Today*, Vol. 218, pp. 18–29.

Frusteri, F., F. Arena, G. Calogero, T. Torre and A. Parmaliana, 2001, "Potassium-enchanced stability of Ni/MgO catalysts in the dry reforming of methane", *Catalysis Communications*, Vol. 2, 49–56.

Gaillard, M., M. Virginie and A. Y. Khodakov, 2017, "New molybdenum-based catalysts for dry reforming of methane in presence of sulfur: A promising way for biogas valorization", *Catalysis Today*, Vol. 289, pp. 143–150.

Gawande, M. B., R. Zboril, V. Malgras and Y. Yamauchi, 2015, "Integrated nanocatalysts: a unique class of heterogeneous catalysts", *Journal of Materials Chemistry A*, 2015, Vol. 3, pp. 8241–8245.

Gao, X., K. Hidajat and S. Kawi, 2016, "Facile synthesis of Ni/SiO_2 catalyst by sequential hydrogen/air treatment: A superior anti-coking catalyst for dry reforming of methane", *Journal of CO_2 Utilization*, Vol. 15, pp. 146–153.

Gao, X., Z. Tan, K. Hidajat and S. Kawi, 2017, "Highly reactive Ni-Co/SiO_2 bimetallic catalyst via complexation with oleylamine/oleic acid organic pair for dry reforming of methane", *Catalysis Today*, Vol. 281, pp. 250–258.

Gandhi, S. P. and S. Patel, 2015, "Dry reforming of methane over supported nickel catalysts promoted by zirconia, ceria and magnesia", *International Journal of Advanced Research in Engineering and Technology*, Vol. 6, pp. 131–146.

Giroux, T., S. Hwang, Y. Liu, W. Ruettinger and L. Shore, 2005, "Monolithic structures as alternatives to particulate catalysts for the reforming of hydrocarbons for hydrogen generation", *Applied Catalysis B: Environmental*, Vol. 56, pp. 95–110.

Guan, G., T. Kida, T. Harada, M. Isayama and A. Yoshida, 2003, "Photoreduction of carbon dioxide with water over $K_2Ti_6O_{13}$ photocatalyst combined with Cu/ZnO catalyst under concentrated sunlight", *Applied Catalysis A: General*, Vol. 249, pp. 11–18.

Guo, Y., Z. Ren, W. Xiao, C. Liua, H. Sharma, H. Gao, A. Mhadeshwar and P. X. Gao, 2013, "Robust 3-D configurated metal oxide nano-array based monolithic catalysts with ultrahigh materials usage efficiency and catalytic performance tunability", *Nano Energy*, Vol. 2, pp. 873–881.

Han, J. W., C. Kim, J. S. Park and H. Lee, 2014, "Highly coke-resistant Ni nanoparticle catalysts with minimal sintering in dry reforming of methane", *Chemistry and Sustainability*, Vol. 7, pp. 451–456.

Han, S. J., Y. Bang, H. J. Kwon, H. C. Lee, V. Hiremath, I. K. Song and J. G. Seo, 2014, "Elevated temperature CO_2 capture on nano-structured $MgO–Al_2O_3$ aerogel: Effect of Mg/Al molar ratio", *Chemical Engineering Journal*, Vol. 242, pp. 357–363.

Han, B., W. Wei, L. Chang, P. Cheng and Y. H. Hu, 2016, "Efficient visible light photocatalytic CO_2 reforming of CH_4", *American Chemical Society*, Vol. 6, pp. 494–497.

Han, J. W., J. S. Park, M. S. Choi and H. Lee, 2017, "Uncoupling the size and support effects of Ni catalysts for dry reforming of methane", *Applied Catalysis B: Environmental*, Vol. 203, pp. 625–632.

Handoko, A. D., K. Li and J. Tang, 2013, "Recent progress in artificial photosynthesis: CO_2 photoreduction to valuable chemicals in a heterogeneous system", *Current Opinion in Chemical Engineering*, Vol. 2, pp. 200–206.

Heck, R. M., S. Gulati and R. J. Farrauto, 2001, "The application of monoliths for gas phase catalytic reactions", *Chemical Engineering Journal*, Vol. 82, pp. 149–156.

Horváth, É., K. Baán, E. Varga, A. Oszkó, Á. Vágó, M. Töro and A. Erdohelyi, 2017, "Dry reforming of CH_4 on Co/Al_2O_3 catalysts reduced at different temperatures", *Catalysis Today*, Vol. 281, pp. 233–240.

Huo, J., J. Jing and W. Li, 2014, "Reduction time effect on structure and performance of Ni-Co/MgO catalyst for carbon dioxide reforming of methane", *International Journal of Hydrogen Energy*, Vol. 39, pp. 21015-21023.

Jiang, Y., L. Zhang, H. Zhan, C. Zhang and S. Liu, 2016, "Hierarchical $Ni_{0.54}Co_{0.46}O_2$ nanowire and nanosheet arrays grown on carbon fiber cloth for high-performance supercapacitors", *Journal of Power Sources*, Vol. 329, pp. 473–483.

Kaydouh, M. N., N. E. Hassan, A. Davidson, S. Casale, H. E. Zakhem and P. Massiani, 2016, "Highly active and stable Ni/SBA-15 catalysts prepared by a "two solvents" method for dry reforming of methane", *Microporous Mesoporous Materials*, Vol. 220, pp. 99–109.

Ke, Q., C. Tang, Z-C. Yang, M. Zheng, L. Mao, H. Liu and J. Wang, 2015, "3D nanostructure of carbon nanotubes decorated Co_3O_4 nanowire arrays for high performance supercapacitor electrode", *Electrochimica Acta*, Vol. 163, pp. 9–15.

Khajenoori, M., M. Rezaei and F. Meshkani, 2015, "Dry reforming over CeO-promoted Ni/MgO nano-catalyst: Effect of Ni loading and CH_4/CO_2 molar ratio". *Journal of Industrial and Engineering Chemistry*, Vol. 21, pp. 717–722.

Kiesgen de Richter, R., T. Ming and S. Caillol, 2013, "Fighting global warming by photocatalytic reduction of CO_2 using giant photocatalytic reactors", *Renewable and Sustainable Energy Reviews*, Vol. 19, pp. 82–106.

Kohn, M. P., M. J. Castaldi and R. J. Farrauto, 2010, "Auto-thermal and dry reforming of landfill gas over a $Rh/\gamma\text{-}Al_2O_3$ monolith catalyst", *Applied Catalysis B: Environmental*, Vol. 94, pp. 125–133.

Lavoie, J. M., 2014, "Review on dry reforming of methane, a potentially more environmentally-friendly approach to the increasing natural gas exploitation", *Frontiers in Chemistry*, Vol. 2, pp. 811–817.

Laszlo, B., K. Baán, E. Varga, A. Oszkó, A. Erdohelyi, Z. Konya and J. Kiss, 2016, "Photo-induced reactions in the CO_2-methane system on titanate nanotubes modified with Au and Rh nanoparticles", *Applied Catalysis B: Environmental*, Vol. 199, pp. 473–484.

Lia, K., X. Ana, K. H. Parka, M. Khraishehb and J. Tanga, 2014, "A critical review of CO_2 photoconversion: Catalysts and reactors", *Catalysis Today*, Vol. 224, pp. 3–12.

Li, L., L. Zhang, Y. Zhang and J. Li, 2015, "Effect of Ni loadings on the catalytic properties of Ni/MgO (111) catalyst for the reforming of methane with carbon dioxide", *Journal of Fuel Chemistry and Technology*, Vol. 43, pp. 315-322.

Li, D., M. Lu, S. Xu, C. Chen, Y. Zhan and L. Jiang, 2017, "Preparation of supported Co catalysts from Co-Mg-Al layered double hydroxides for carbon dioxide reforming of methane, *International Journal of Hydrogen Energy*, Vol. 42, pp. 5063-5071.

Liang, Y. T., B. K. Vijayan, K. A. Gray and M. C. Hersam, 2011, "Minimizing graphene defects enhances titania nanocomposite-based photocatalytic reduction of CO_2 for improved solar fuel production", *Nano Letters.*, Vol. 11, pp. 2865–2870.

Lichtfouse, E., J. Schwarzbauer and D. Robert, *Hydrogen Production and Remediation of Carbon and Pollutants* , Springer, Switzerland, 2015.

Liu, H., S. Li, S. Zhang, J. Wang, G. Zhou and L. Chen, 2008, "Catalytic performance of novel Ni catalysts supported on SiC monolithic foam in carbon dioxide reforming of methane to synthesis gas", *Catalysis Communications,* Vol. 9, pp. 51–54.

Liu, D., W. N. E. Cheo, Y. W. Y. Lim, A. Borgna, R. Lau and Y. Yang, 2010, "A comparative study on catalyst deactivation of nickel and cobalt incorporated MCM-41 catalysts modified by platinum in methane reforming with carbon dioxide", *Catalysis Today,* Vol. 154, pp. 229–236.

Long, H., Y. Xu, X. Zhang, S. Hu, S. Shang, Y. Yin and X. Dai, 2013, "Ni-Co/Mg-Al catalyst derived from hydrotalcite-like compound prepared by plasma for dry reforming of methane", *Journal of Energy Chemistry,* Vol. 22, pp. 733–739.

Luisetto, I., S. Tuti and E. D. Bartolomeo, 2012, "Co and Ni supported on CeO_2 as selective bimetallic catalyst for dry reforming of methane", *International Journal of Hydrogen Energy,* Vol. 37, pp. 15992–15999.

Luisetto, I., C. Sarno, D. D. Felicis, F. Basoli, C. Battocchio, S. Tuti, S. Licoccia and E. D. Bartolomeo, 2017, "Ni supported on γ-Al_2O_3 promoted by Ru for the dry reforming of methane in packed and monolithic reactors", *Fuel Processing Technology,* Vol. 158, pp. 130–140.

Mahmodi, G., S. Sharifnia, F. Rahimpour and S. N. Hosseini, 2013, "Photocatalytic conversion of CO_2 and CH_4 using ZnO coatedmesh: Effect of Operational parameters and optimization", *Solar Energy Materials and Solar Cells,* Vol. 111, pp. 31–40.

Marban, G., I. Lopez, T. Valdes-Solıs and A. B. Fuertes, 2008, "Highly active structured catalyst made up of mesoporous Co_3O_4 nanowires supported on a metal wire mesh for the preferential oxidation of CO", *International Journal of Hydrogen Energy,* Vol. 33, pp. 6687–6695.

Matei-Rutkovska, F., G. Postole, C. G. Rotaru, M. Florea, V. I. Parvulescu and P. Gelin, 2016, “Synthesis of ceria nanopowders by microwaveassisted hydrothermal method for dry reforming of methane”, *International Journal of Hydrogen Energy*, Vol. 14, pp. 2512–2525.

Merajin, M. T., S. S. N. Hosseini and N. Yazdanpour, 2013, “Photocatalytic conversion of greenhouse gases (CO_2 and CH_4) to high value products using TiO_2 nanoparticles supported on stainless steel webnet”, *Journal of the Taiwan Institute of Chemical Engineers*, Vol. 44, pp. 239-246.

Meshkani, F., M. Rezaei and M. Andache, 2014, “Investigation of the catalytic performance of Ni/MgO catalysts in partial oxidation, dry reforming and combined reforming of methane”, *Journal of Industrial and Engineering Chemistry*, Vol. 20, pp. 1251–1260.

Miguel, N., J. Manzanedo and P. L. Arias, 2012, “Active and stable Ni-MgO catalyst coated on a metal monolith for methane steam reforming under low steam-to-carbon ratios”, *Chemical Engineering Technologies*, Vol. 35, pp. 2195–2203.

Monroy, T. G., L. C. Abella, S. M. Gallardo and H. Hinode, 2012, “ZrO_2-promoted Ni/MgO catalyst for methane dry reforming”, *Journal of Material Science and Engineering A*, Vol. 2, pp. 544–549.

NASA, 2017, “Global climate change”, https://climate.nasa.gov/, accessed at September 2017.

Nikoo, M. K. and N. A. S. Amin, 2011, “Thermodynamic analysis of carbon dioxide reforming of methane in view of solid carbon formation”, *Fuel Processing Technology*, Vol. 92, pp. 678–691.

Nishimura, A., G. Mitsui, K. Nakamura, M. Hirota and E. Hu, 2012, “CO_2 reforming characteristics under visible light response of Cr- or Ag-doped TiO_2 prepared by sol-

gel and dip-coating process", *International Journal of Photoenergy,* Vol. 2012, pp. 1-12.

O'Connor, A. M. and J. R. H. Ross, 1998, "The effect of O_2 addition on the carbon dioxide reforming of methane over Pt/ZrO_2 catalysts", *Catalysis Today*, Vol. 46, pp. 203–210.

Olivier, J. G. J., G. Janssens-Maenhout, M. Muntean and J. A. H. W. Peters, "Trends in Global CO_2 Emissions", *PBL Netherlands Environmental Assessment Agency Report*, The Hague, 2016.

Oyama, S. T., P. Hacarlioglu, Y. Gu and D. Lee, 2012, "Dry reforming of methane has no future for hydrogen production: Comparison with steam reforming at high pressure in standard and membrane reactors", *International Journal of Hydrogen Energy,* Vol. 37, pp. 10444–10450.

Özyönüm, G. and R. Yildirim, 2016, "Water gas shift activity of Au-Re catalyst over microstructured cordierite monolith wash-coated by ceria", *International Journal of Hydrogen Energy*, Vol. 41, pp. 5513–5521.

Pakhare, D. and J. Spivey, 2014, "A review of dry (CO) reforming of methane over noble metal catalysts", *Chemical Society Reviews,* Vol. 47, pp. 7813–7837.

Phongaksorn, M., S. Tungkamani, N. Dharmasaroja, T. Sornchamni, R. Chuvaree, N. Kanjanabat and N. Siri-Nguan, 2015, "Elucidation of the influence of Ni-Co catalytic properties on dry methane reforming performance", *Chemical Engineering Transactions,* Vol. 43, pp. 925–930.

Philippopoulos, C. J. and M. D. Nikolaki, 2010, "Photocatalytic processes on the oxidation of organic compounds in water", *New Trends in Technologies,* Vol. 9, pp. 89–107.

Promaros, E., S. Assabumrungrat, N. Laosiripojana, P. Praserthdam, T. Tagawa and S. Goto, 2007, "Carbon dioxide reforming of methane under periodic operation", *Korean Journal of Chemical Engineering,* Vol. 24, pp. 44–50.

Ray, K., S. Sengupta and G. Deo, 2017, "Reforming and cracking of CH_4 over Al_2O_3 supported Ni, Ni-Fe and Ni-Co catalysts", *Fuel Processing Technology,* Vol. 156, pp. 195–203.

Reddy, G. K., S. Loridant, A. Takahashi, P. Delichère and B. M. Reddy, 2010, "Reforming of methane with carbon dioxide over $Pt/ZrO_2/SiO_2$ catalysts -Effect of zirconia to silica ratio", *Applied Catalysis A: General,* Vol. 389, pp. 92–100.

Ren, Z., Y. Guo, Z. Zhang, C. Liu and P. X. Gao, 2013, "Nonprecious catalytic honeycombs structured with three dimensional hierarchical Co_3O_4 nano-arrays for high performance nitric oxide oxidation*", Journal of Materials Chemistry A,* Vol. 1, pp. 9897–9905.

Ren, Z., V. Botu, S. Wang, Y. Meng, W. Song, Y. Guo, R. Ramprasad, S. L. Suib and P. X. Gao, 2014, "Monolithically integrated spinel $M_xCo_{3-x}O_4$ (M=Co, Ni, Zn) nanoarray catalysts: Scalable synthesis and cation manipulation for tunable low-temperature CH_4 and CO oxidation", *Angewandte Chemie International Edition,* Vol. 53, 7223 – 7227.

Ren, Z., Z. Wub, W. Song, W. Xiao, Y. Guo, J. Ding, S. L. Suib and P. X. Gao, 2016, "Low temperature propane oxidation over Co_3O_4 based nano-array catalysts: Ni dopant effect, reaction mechanism and structural stability", *Applied Catalysis B: Environmental*, Vol. 180, pp. 150–160.

Zhang, R. J., G. F. Xia, M. F. Li, Y. Wu, H. Nie and Li D. D., 2015, "Effect of support on the performance of Ni-based catalyst in methane dry reforming", *Journal of Fuel Chemistry and Technology,* Vol. 43, pp. 1359-13565.

Ryu, J. H., K. Y. Lee, H. La, H. J. Kim, J. I. Yang and H. Jung, 2007, "Ni catalyst wash-coated on metal monolith with enhanced heat-transfer capability for steam reforming", *Journal of Power Sources*, Vol. 171, pp. 499–505.

San-José-Alonso, D., J. Juan-Juan, M. J. Illan-Gomez and M. C. Roman-Martinez, 2009, "Ni, Co and bimetallic Ni–Co catalysts for the dry reforming of methane", *Applied Catalysis A: General*, Vol. 371, pp. 54–59.

San-José-Alonso, D., M. J. Illan-Gomez and M. C. Roman-Martinez, 2013, "Low metal content Co and Ni alumina supported catalysts for the CO_2 reforming of methane", *International Journal of Hydrogen Energy*, Vol. 38, pp. 2230–2239.

Sengupta, S. and G. Deo, 2015, "Modifying alumina with CaO or MgO in supported Ni and Ni–Co Catalysts and its effect on dry reforming of CH_4", *Journal of CO_2 Utilization*, Vol. 10, pp. 67–77.

Serrano-Lotina, A. and L. Daza, 2013, "Influence of the operating parameters over dry reforming of methane to syngas", *International Journal of Hydrogen Energy*, Vol. 39, pp. 4089 – 4094.

Serrano-Lotina, A. and L. Daza, 2014, "Long-term stability test of Ni-based catalyst in carbon dioxide reforming of methane", *Applied Catalysis A: General*, Vol. 474, pp. 107–113.

Shang, Z., S. Li, L. Li, G. Liu and X. Liang, 2017, "Highly active and stable alumina supported nickel nanoparticle catalysts for dry reforming of methane", *Applied Catalysis B: Environmental*, Vol. 201, pp. 302–309.

Shi, D., Y. Feng and S. Zhong, 2004, "Photocatalytic conversion of CH_4 and CO_2 to oxygenated compounds over Cu/CdS-TiO_2/SiO_2 catalyst", *Catalysis Today*, Vol. 98, pp. 505–509.

Soloviev, S. O., A. Y. Kapran, S. N. Orlyk and E. V. Gubareni, 2011, "Carbon dioxide reforming of methane on monolithic Ni/Al_2O_3-based catalysts", *Journal of Natural Gas Chemistry,* Vol. 20, pp. 184–190.

Son, I. H., S. J. Lee, I. Y. Song, W. Jeon, I. Jung and D. W. Jeong, 2014a, "Study on coke formation over Ni/γ-Al_2O_3, Co-Ni/γ-Al_2O_3, and Mg-Co-Ni/γ-Al_2O_3 catalysts for carbon dioxide reforming of methane", *Fuel*, Vol. 136, pp. 194–200.

Son, I. H., S. J. Lee and H. S. Roh, 2014b, "Hydrogen production from carbon dioxide reforming of methane over highly active and stable MgO promoted Co-Ni/γ-Al_2O_3 catalyst", *International Journal of Hydrogen Energy*, Vol. 39, pp. 3762–3770.

Sun, Y., T. Ritchie, S. S. Hla, S. McEvoy, W. Stein and J. H. Edwards, 2011, "Thermodynamic analysis of mixed and dry reforming of methane for solar thermal applications", *Journal of Natural Gas Chemistry*, Vol. 20, pp. 568–576.

Takanabe, K., K. Nagaoka, K. Nariai and K. Aika, 2005, "Titania-supported cobalt and nickel bimetallic catalysts for carbon dioxide reforming of methane", *Journal of Catalysis,* Vol. 232, pp. 268–275.

Tao, F. F., J. Shan, L. Nguyen, Z. Wang, S. Zhang, L. Zhang, Z. Wu, W. Huang and S. Zeng, 2015, "Understanding complete oxidation of methane on spinel oxides at a molecular level", *Nature Communications*, Vol. 6, pp. 7798–8798.

Teramura, K., T. Tanaka, H. Ishikawa, Y. Kohno and T. Funabiki, 2004, "Photocatalytic Reduction of CO_2 to CO in the Presence of H_2 or CH_4 as a Reductant over MgO", *Journal of Physical Chemistry B,* Vol. 108, pp. 346–354.

Titus, J., T. Roussière, G. Wasserschaff, S. Schunk, A. Milanov, E. Schwab and G. Wagner, 2016, "Dry reforming of methane with carbon dioxide over NiO–MgO–ZrO_2", *Catalysis Today,* Vol. 270, pp. 68–75.

Tomishige, K., M. Nurunnabi, K. Maruyama and K. Kunimori, 2004, "Effect of oxygen addition to steam and dry reforming of methane on bed temperature profile over Pt and Ni catalysts", *Fuel Processing Technology*, Vol. 85, pp. 1103–1120.

Usubharatana, P., D. McMartin, A. Veawab and P. Tontiwachwuthikul, 2006, "Photocatalytic process for CO_2 emission reduction from industrial flue gas streams", *Industrial and Engineering Chemistry Research,* Vol. 45, pp. 2558–2568.

Walker, D. M., S. L. Pettit, J. T. Wolan and J. N. Kuhn, 2012, "Synthesis gas production to desired hydrogen to carbon monoxide ratios by tri-reforming of methane using Ni–MgO–(Ce,Zr)O2 catalysts", *Applied Catalysis A: General*, Vol. 445– 446, pp. 61–68.

Wang, H. Y. and E. Ruckenstein, 2001, "CO_2 reforming of CH_4 over Co/MgO solid solution catalysts — effect of calcination temperature and Co loading", *Applied Catalysis A: General*, Vol. 209, pp. 207–215.

Wang, Y. H., H. M. Liu and B. Q. Xu, 2009, "Durable Ni/MgO catalysts for CO_2 reforming of methane: Activity and metal–support interaction", *Journal of Molecular Catalysis A: Chemical,* Vol. 299, pp. 44–52.

Wang, K., X. Li, S. Ji, B. Huang and C. Li, 2008, "Preparation of Ni-based metal monolithic catalysts and a study of their performance in methane reforming with CO_2", *ChemSusChem,* Vol. 1, pp. 527–533.

Wang, C., N. Sun, N. Zhao, W. Wei and Y. Zhao, 2017, "Template-free preparation of bimetallic mesoporous Ni-Co-CaO-ZrO_2 catalysts and their synergetic effect in dry reforming of methane", *Catalysis Today,* Vol. 281, pp. 268–275.

Windisch, F. C., K. F Ferris, G. J. Exarhos and S. K. Sharma, 2002, "Conducting spinel oxide films with infrared transparency", *Thin Solid Films,* Vol. 420-421, pp. 89–99.

Wu, H., V. L. Parola, G. Pantaleo, F. Puleo, A. M. Venezia and L. F. Liotta, 2013, "Ni-based catalysts for low temperature methane steam reforming: Recent results on Ni-Au and comparison with other bi-metallic systems", *Catalysts,* Vol. 3, pp. 563–583.

Qiu, M., Y. Li., T. Wang, Q. Zhang, C. Wang and X. Zhang, 2012, "Upgrading biomass fuel gas by reforming over Ni–MgO/γ-Al_2O_3 cordierite monolithic catalysts in the lab-scale reactor and pilot-scale multi-tube reformer", *Applied Energy,* Vol. 90, pp. 3–10.

Xu, B., J. Wei, H. Wang, K. Sun and Q. Zhu, 2001, "Nano-MgO: novel preparation and application as support of Ni catalyst for CO_2 reforming of methane", *Catalysis Today,* Vol. 68, pp. 217–225.

Xu, Y., H. Long, Qiang Weia, X. Zhanga, S. Shanga, X. Dai and Y. Yin, 2013, "Study of stability of Ni/MgO/γ-Al_2O_3 catalyst prepared by plasma for CO_2 reforming of CH_4", *Catalysis Today,* Vol. 211, pp. 114– 119.

Vasileiadis, S. and Z. Ziaka-Vasileiadou, 2004, "Biomass reforming process for integrated solid oxide-fuel cell power generation", *Chemical Engineering Science,* Vol. 59, pp. 4853 – 4859.

Villegas, L., F. Masset and N. Guilhaume, 2007, "Wet impregnation of alumina-washcoated monoliths: Effect of the drying procedure on Ni distribution and on autothermal reforming activity", *Applied Catalysis A: General,* Vol. 320, pp. 43–55.

Yao, L., J. Zu, X. Peng, D. Tong and C. Hu, 2013, "Comparative study on the promotion effect of Mn and Zr on the stability of Ni/SiO_2 catalyst for CO_2 reforming of methane", *International Journal of Hydrogen Energy,* Vol. 38, pp. 72688–7279.

Yuliati, L., H. Itoh and H. Yoshida, "Photocatalytic methane coupling and methane dry reforming over gallium oxide", *Proceedings of International Symposium on Eco Topia Science,* ISETS07, 2007.

Yuliati, L. and H. Yoshida, 2008, "Photocatalytic conversion of methane", *Chemical Society Reviews,* Vol. 37, pp. 1592–1602.

Yuliati, L., T. Hattori, H. Itoh and H. Yoshida, 2008, "Photocatalytic nonoxidative coupling of methane on gallium oxide and silica-supported gallium oxide", *Journal of Catalysis,* Vol. 257, pp. 396–402.

Zhang, T. and M. D. Amiridis, 1998, "Hydrogen production via the direct cracking of methane over silica-supported nickel catalysts", *Applied Catalysis A: General,* Vol. 167, pp. 161–172.

Zhang, J., H. Wang and A. K. Dalai, 2008, "Effects of metal content on activity and stability of Ni-Co bimetallic catalysts for CO_2 reforming of CH_4", *Applied Catalysis A: General,* Vol. 339, pp. 121–129.

Zhang, L., L. Li, Y. Zhang, Y. Zhao and J. Li, 2014, "Nickel catalysts supported on MgO with different specific surface area for carbon dioxide reforming of methane", *Journal of Energy Chemistry,* Vol. 23, pp. 66–72.

Zhang, F., N, Wang, L. Yang, M. Li and L. Huang, 2014, "Ni-Co bimetallic MgO-based catalysts for hydrogen production via steam reforming of acetic acid from bio-oil", *International Journal of Hydrogen Energy*, Vol. 39, pp. 18688-18694.

Zhang, L., Q. Zhang, Y. Liu and Y. Zhang, 2016, "Dry reforming of methane over Ni/MgO-Al_2O_3 catalysts prepared by two-step hydrothermal method", *Applied Surface Science,* Vol. 389, pp. 25–33.

Zhang, N., Y. Ding, J. Zhang, B. Fu, X. Zhang, X. Zheng and Y. Fang, 2017, "Construction of MnO_2 nanowires@$Ni_{1-x}Co_xO_y$ nanoflake core-shell heterostructure for high performance supercapacitor", *Journal of Alloys and Compounds,* Vol. 694, pp. 1302–1308.

APPENDIX A: SEM-EDX CHARACTERIZATION RESULTS FOR SPENT Ni-Co/MgO COATED MONOLITH CATALYSTS

SEM-EDX elemental analysis was also conducted over spent 8wt.%Ni-2wt.%Co/MgO monolith catalyst in the absence and presence of 3% O_2 addition as mentioned in Section 4.3.6. The results for the spent catalyst in the absence of oxygen were in Figure A.1 while the spent one in the presence of 3% O_2 addition was in Figure A.2.

The average value of each mapped element by EDX analysis taken in 2000x was also shown in Table A.1 and Table A.2 respectively for both cases.

Table A.1. The average value of EDX analysis spent Ni-Co/MgO monolith catalyst in the absence of oxygen taken in 2000x.

Element	Avg. Wt.%	Avg. At%
C K	41.30	57.16
O K	18.40	19.235
Mg K	13.31	9.115
Al K	9.27	5.75
Si K	11.13	6.64
Ca K	0.62	0.26
Co K	1.31	0.37
Ni K	4.67	1.33
Total	100.00	100.00

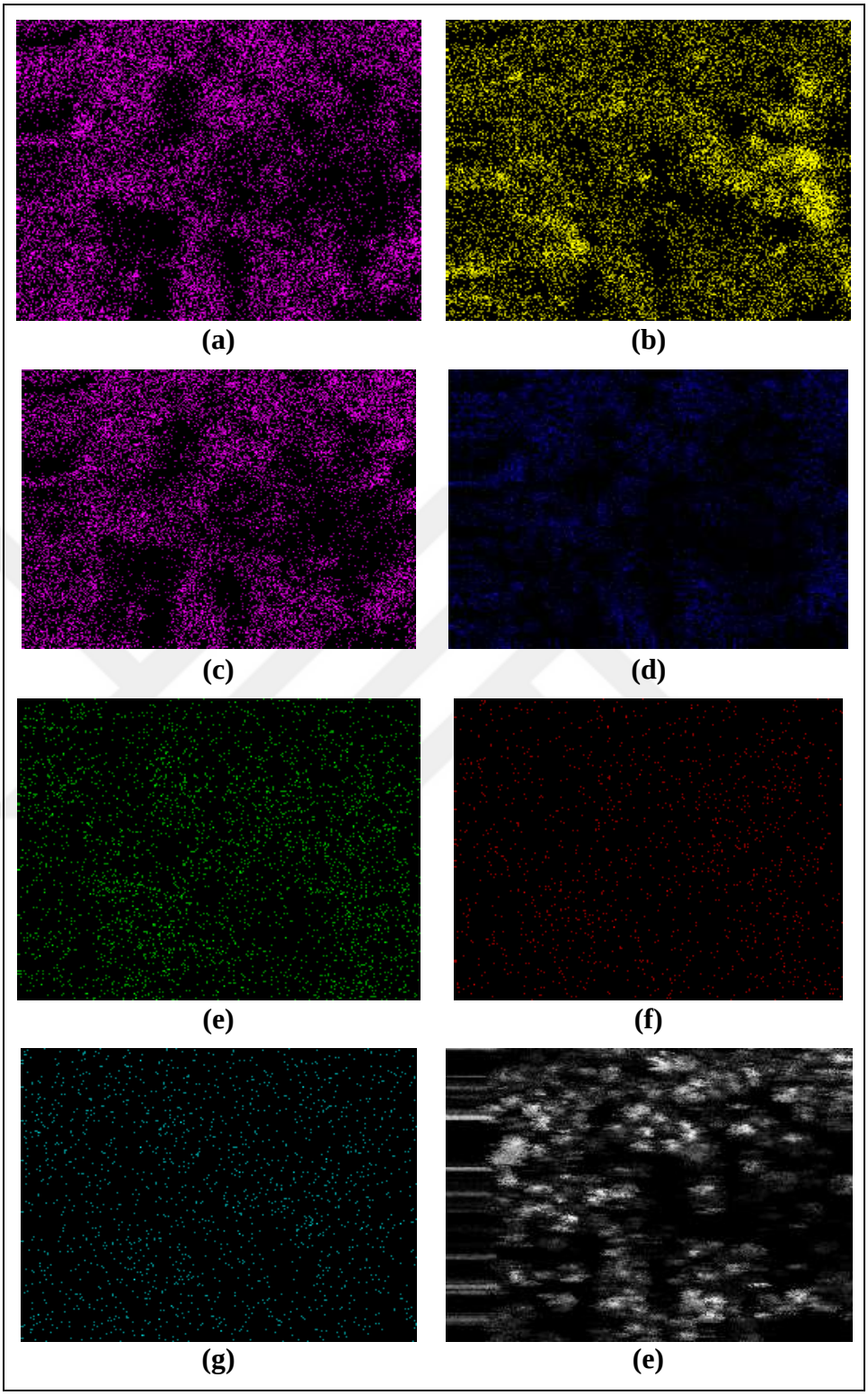

Figure A.1. EDX elemental mapping of spent Ni-Co/MgO monolith catalyst in the absence of oxygen (a) Si, (b) Mg, (c) Al, (d) O, (e) Ni, (f) Co, (g) Ca and (e) image in 2000x.

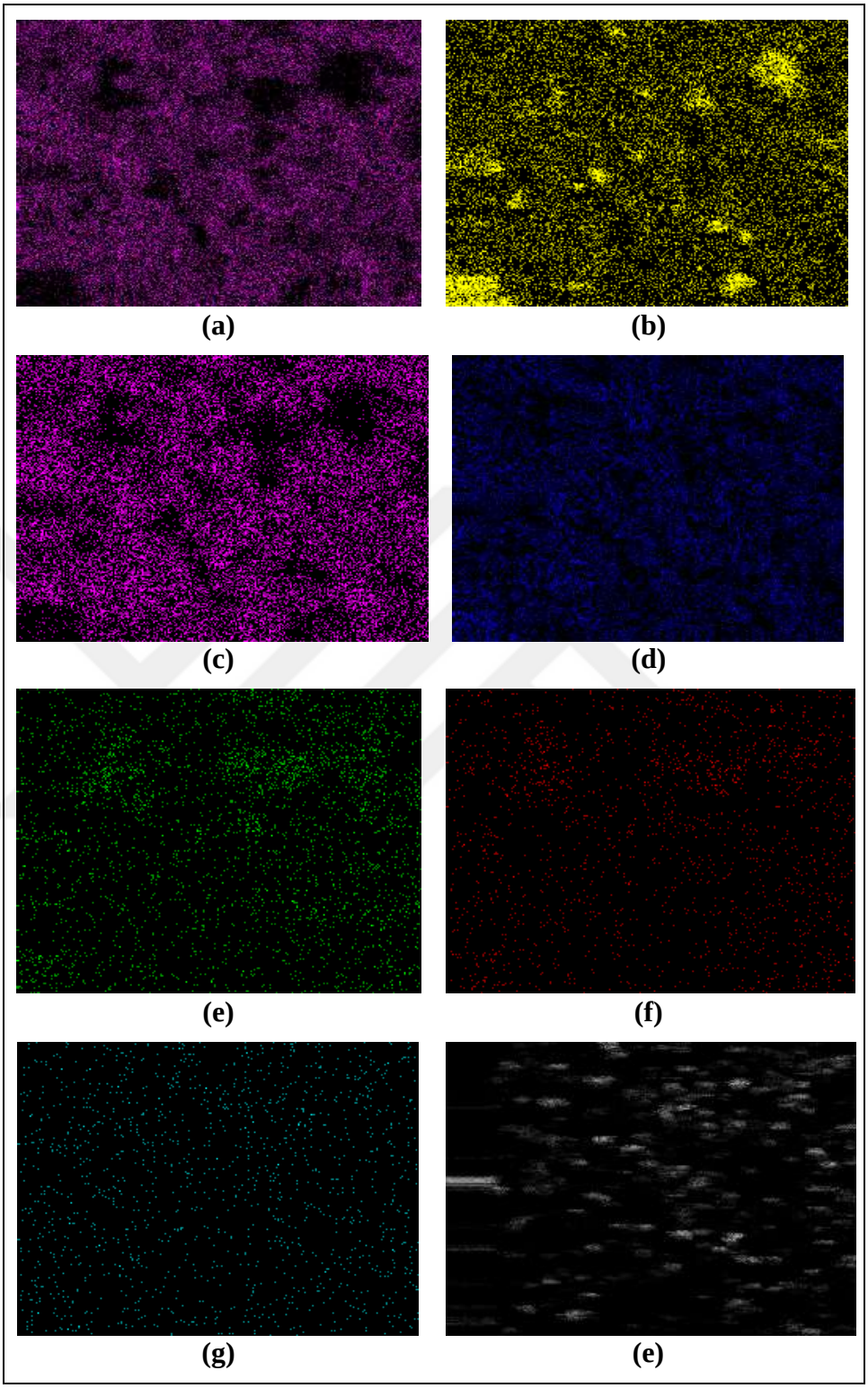

Figure A.2. EDX elemental mapping of spent Ni-Co/MgO monolith catalyst in the presence of 3% O_2 addition: (a) Si, (b) Mg, (c) Al, (d) O, (e) Ni, (f) Co, (g) Ca and (e) image in 2000x.

Table A.2. The average value of EDX analysis of spent Ni-Co/MgO monolith catalyst in the presence of 3% O_2 addition taken in 2000x.

Element	**Avg. Wt.%**	**Avg. At%**
C K	13.30	22.23
O K	30.90	38.82
Mg K	9.99	8.26
Al K	16.82	12.53
Si K	21.97	15.73
Ca K	0.26	0.13
Co K	1.48	0.50
Ni K	5.30	1.82
Total	100.00	100.00

APPENDIX B: SEM CHARACTERIZATION RESULTS FOR FRESH AND SPENT Ni-BASED NANOROD CATALYTS

SEM analysis was also performed over 8wt.%Ni-2wt.%Co impregnated MgO nanorod catalysts spent at 750 °C with a 84,000 $mlg_{cat}^{-1}h^{-1}$ for 8 h in order to investigate the catalyst morphology after 8 h TOS test and fresh 8wt.%Ni-2wt.%Co impregnated over MgO coated than calcined monolith catalyst to observe examine the nanorod morphology over monolithic structure. The results for the spent Ni-based impregnated MgO nanorod catalyst can be seen in Figure B.1 while fresh Ni-based impregnated MgO coated monoliths are in Figure B.2.

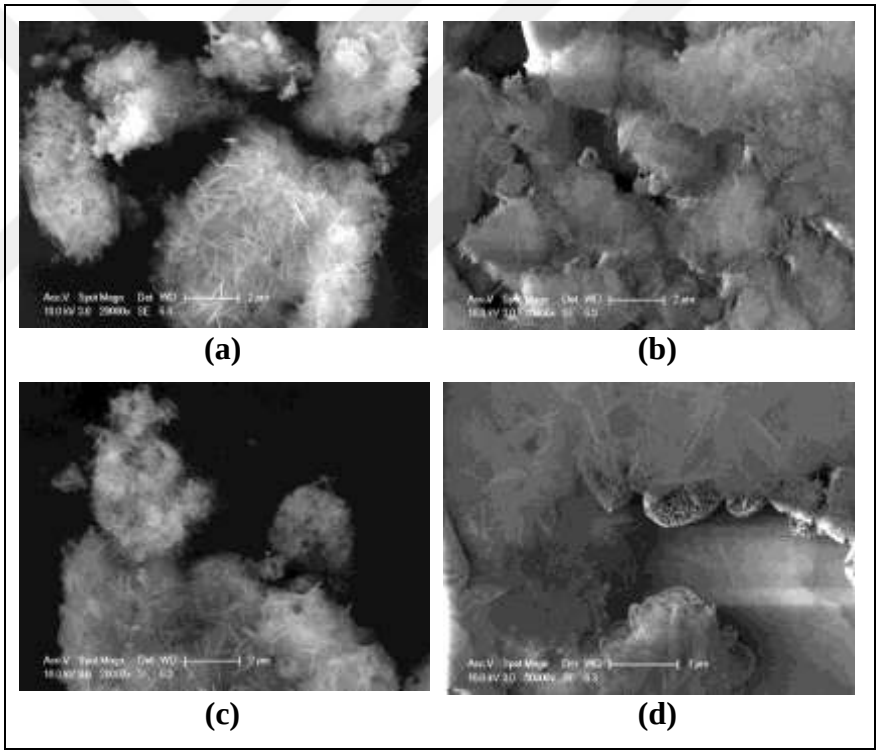

Figure B.1. SEM images of spent Ni-based nanorod catalyst at 750 for 8h in various magnification: (a-c) 20000, (d) 50000.

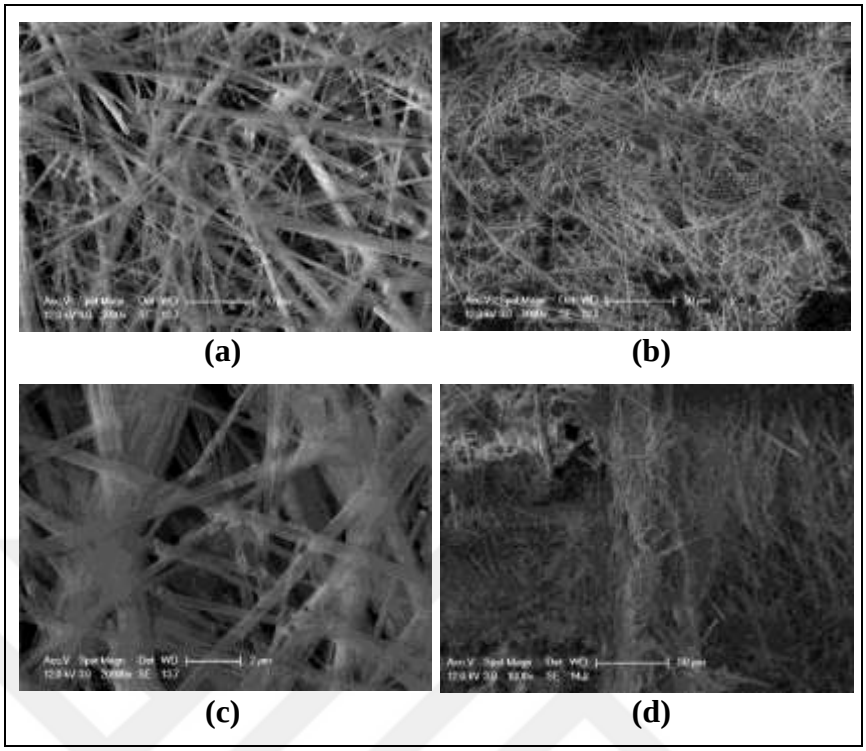

Figure B.2. SEM images of fresh Ni-based nanorod monolithic catalyst in various magnification; inside: (a) 500x, (b) 1000x, (c) 20000x and lateral: (d) 1000x.